

SPECTRAL, SPATIAL, AND TEMPORAL VARIATIONS  
OBSERVED FOR OUTER ZONE ELECTRONS FROM  
10 TO 100 keV WITH SATELLITE INJUN 3

by

Theodore A. Fritz

A thesis submitted in partial fulfillment of the  
requirements for the degree of Doctor of Philosophy  
in the Department of Physics and Astronomy  
in the Graduate College of  
The University of Iowa

August, 1967

Thesis supervisor: Professor J. A. Van Allen

## ACKNOWLEDGMENTS

The author wishes to express his appreciation to Dr. James A. Van Allen for his many helpful suggestions and comments throughout the development of the present study and for providing the necessary research program which made this thesis possible. The author has benefited from discussions with Dr. D. A. Gurnett, Messrs. K. L. Ackerson, and J. D. Craven about various aspects of the present study.

Extensive use has been made in this study of data obtained with several Injun 3 detectors which were constructed by Dr. L. A. Frank, Messrs. D. E. Stilwell, C. D. Laughlin, J. D. Craven, H. K. Hills, and J. Gardner.

Special thanks are extended to Mr. Cary Wong for his assistance with much of the plotting and data reduction and to Miss Ann Schmeichel and Miss Lavona Williams for the typing involved in the preparation of this manuscript.

This work was performed in part under Office of Naval Research grant Nonr 1509 (06) and in part under National Aeronautics and Space Administration grant NsG 233-62 while the author was a research fellow of the National Aeronautics and Space Administration.

## ABSTRACT

Spectral, spatial, and temporal variations of outer zone electrons with energies from 10 keV to 100 keV observed with Injun 3 are presented. Electrons with  $E_e \geq 40$  keV were constantly observed precipitating into the atmosphere for all latitudes,  $\Lambda \geq 45^\circ$ . At latitudes below the high latitude boundary, the flux of  $\geq 40$  keV electrons in the loss cone was observed to always be  $\sim 10^{-2}$  that of the locally mirroring flux. There was usually a spike of precipitating  $\geq 40$  keV electrons observed at the high latitude boundary and the flux of  $\geq 40$  keV electrons was usually observed to approach isotropy over the upper hemisphere at the position of the satellite at this boundary. Large intensities of electrons with energies not much greater than 40 keV were observed precipitating into the atmosphere for  $\Lambda \geq 65^\circ$  during magnetically quiet periods and the position of the high latitude outer zone boundary (intensity cutoff) was observed to vary by  $\Delta \Lambda \sim 7^\circ$  while no magnetic activity was occurring. The latitude where the ratio of the trapped to the precipitated  $\geq 40$  keV particle fluxes breaks from  $10^{-2}$  toward one is introduced as a more meaningful concept of the high latitude limit to durably trapped  $\geq 40$  keV electrons than the usual intensity cutoff.

Strong observational support was found for the model of Taylor and Hones [1965] which adiabatically accelerates and then precipitates solar wind electrons in the auroral zone during magnetically active periods. The existence of a two-stream instability mechanism reported by Stix [1964] and discussed by Evans [1967] which can act during the intense  $\geq 10$  keV precipitation events was also given observational support. Evidence is presented for the existence of another mechanism which acts in the region of the satellite (200 km to 1000 km) almost constantly, directionally accelerates electrons with  $E_e < 40$  keV toward the atmosphere, and produces isotropic electron pitch angle distributions over the upper hemisphere at the position of the satellite predominantly at low altitudes right on top of the atmosphere for the region of the outer zone  $\Lambda \geq 65^\circ$ .

## TABLE OF CONTENTS

	Page
I. INTRODUCTION . . . . .	1
A. Historical Background. . . . .	1
B. Description of the Study . . . . .	4
II. DESCRIPTION OF EXPERIMENT. . . . .	6
A. The Satellite, Injun 3 . . . . .	6
B. The Geiger Tubes . . . . .	7
C. Differential Magnetic Spectrometer . . . . .	8
D. Electron Multiplier. . . . .	9
E. The 3914 Å Auroral Photometer. . . . .	10
F. Inflight Operation and Calibration Checks. . . . .	11
III. DESCRIPTION OF RELEVANT PARAMETERS . . . . .	18
A. The Spectral Parameter, $\gamma$ . . . . .	18
B. The Disturbance or "Dumping Parameter, $\phi$ . . . . .	21
C. The Latitude Parameters, $\Lambda$ and $L$ . . . . .	22
D. The Geomagnetic Activity Parameters $K_p$ , $A_p$ , and Dst. . . . .	22
E. The Local Time Parameter, MLT. . . . .	23

# TABLE OF CONTENTS (CONT'D.)

	Page
IV. CHARACTERISTICS OF ELECTRONS IN THE "QUIET" OR UNDISTURBED OUTER ZONE . . . . .	25
V. SOME DISTURBED OUTER ZONE CHARACTERISTICS . . . . .	32
A. Periods of Low Geomagnetic Activity . . . . .	32
B. Periods of Moderate Geomagnetic Activity. . . . .	43
C. Periods of Large Geomagnetic Activity . . . . .	57
VI. THE "AVERAGE" OUTER ZONE. . . . .	67
A. Statistical Study of the Outer Zone Trapping Region . . . . .	67
1. The Spectral Parameter, $\gamma$ , vs L . . . . .	71
2. The Spectral Parameter, $\gamma$ , vs B . . . . .	74
3. The Spectral Parameter, $\gamma$ , vs Local Time. . . . .	77
4. The Spectral Parameter, $\gamma$ , vs $A_p$ and $K_p$ . . . . .	77
5. The Spectral Parameter, $\gamma$ , vs $j_{\perp}(E_e \geq 40 \text{ keV})$ . . . . .	78
6. The Spectral Parameter, $\gamma$ , vs the Intensity of Precipitating Electrons. . . . .	80
7. The Dumping Parameter, $\phi$ , vs L. . . . .	83
8. The Dumping Parameter, $\phi$ , vs B. . . . .	86
B. Statistical Study of Intense Auroral Zone Particle Activity . . . . .	90

# TABLE OF CONTENTS (CONT'D.)

	Page
1. The Spectral Parameter, $\gamma$ , vs Invariant Latitude, $\Lambda$ . . . . .	93
2. The Spectral Parameter, $\gamma$ , vs Magnetic Local Time. . . . .	93
3. The Spectral Parameter, $\gamma$ , vs $j(E_e \geq 10 \text{ keV})$ . . .	95
4. The Spectral Parameter, $\gamma$ , vs the Dumping Parameter, $\phi$ . . . . .	96
5. The Spectral Parameter, $\gamma$ , vs $K_p$ . . . . .	96
VII. SUMMARY OF PRINCIPAL FINDINGS . . . . .	98
A. Precipitation of Electrons Into the Atmosphere. . . .	98
B. High Latitude Outer Zone Boundary . . . . .	99
C. Observed Particle Variations. . . . .	101
VIII. DISCUSSION. . . . .	108
A. The Pitch Angle Diffusion Mechanism of Kennel and Petschek [1966a]. . . . .	109
B. The Magnetospheric Model of Taylor and Hones [1965] .	117
C. The Two Stream Plasma Instability Mechanism of Stix [1964] . . . . .	126
Appendix I. MAGNETIC ORIENTATION OF INJUN 3. . . . .	131
Appendix II. THE RESPONSE OF DETECTOR 5 . . . . .	139
REFERENCES. . . . .	146
FIGURE CAPTIONS . . . . .	152
FIGURES 1-38. . . . .	157

## I. INTRODUCTION

### A. Historical Background

The discovery of the radiation zones occurred early in 1958 using data from Geiger tubes flown on the first two U. S. satellites, Explorers 1 and 3 [Van Allen, Ludwig, Ray, and McIlwain, 1958] and with the launch of Explorer 4 the detailed investigation of the types of particles, their energy spectra, their spatial distribution, and their time variations began. It was with Explorer 4 that Van Allen, McIlwain, and Ludwig [1959] found a relative minimum in the count rates along the line of force at approximately  $50^\circ$  geomagnetic latitude. It was this relative minimum that became the dividing line between what has become known as the classical "inner" and "outer" Van Allen radiation zones. The Explorer 4 results indicated that the inner zone contained radiation of a much more penetrating nature than the outer zone.

The deep-space probe Pioneer 3 carried two Geiger counters, one of which was of the same type as that on Explorer 4, out and then back through the radiation zones. These data extended the relative minimum between the inner and outer zone almost to the



geomagnetic equator and confirmed the results of Explorer 4 about the composition of the two zones [Van Allen and Frank, 1959].

It has been stated by Farley [1963] that the results of Pioneer 3 brought to an end the discovery of the gross features of the radiation zones. These gross features were outlined principally through the work of Van Allen and his associates and remain today a valid description of the radiation zones.

A period of several years followed in which there was disagreement among the experimenters with regard to the intensities and the energy spectrum of electrons in the outer zone. Most of the discrepancies and disagreements were due to the non-ideal nature of the early detectors that were flown, since it was not known whether the counting rates of these detectors were the result of higher energy penetrating particles or bremsstrahlung produced by a large flux of lower energy particles. Matters were further complicated due to the fact that many experimenters tried to link the particles of the radiation zones with those precipitated into visible aurorae which McIlwain [1960] and others had measured with rocket-borne detectors and had shown to have a very steep spectrum rising toward low energies.

With the launching of the Injun I and Explorer 12 satellites, the long period of controversy over the electron energy spectrum was brought to a close. This was largely the result of a well-designed differential magnetic spectrometer flown on each satellite. In January, 1962, O'Brien, Van Allen, Laughlin, and Frank [1962] published flux estimates using data from Explorer 12 for electrons in the outer zone near the equatorial plane. The intensities of electrons with energies greater than 40 keV were given as  $10^8$  particles/cm<sup>2</sup> sec; the intensities of those with energies in the range  $1.6 \text{ MeV} \leq E_e \leq 5 \text{ MeV}$  were given as  $2 \times 10^5$  particles/cm<sup>2</sup> sec; and the intensities of those with energies above 5 MeV were found to be less than  $10^3$  particles/cm<sup>2</sup> sec. These measurements have been found to be substantially correct by subsequent experimenters in this field. If one assumes a power law for the integral electron energy spectrum,  $n(>E) = kE^{-\gamma}$ , then  $\gamma$  is approximately 1.5 for these fluxes.

In the present paper a study of the spectral, spatial, and temporal variations of outer zone electrons in the energy range from 10 keV to 100 keV is made using the low altitude, high latitude satellite Injun 3.

In the text the results of the more recent measurements of outer zone electrons published in the literature will be discussed along with the results of the present paper.

#### B. Description of the Study

The present paper is divided into eight chapters. In Chapter II a description of the satellite and the detectors used in the study is given and in Chapter III a description of the various parameters used in organizing the study is presented. The study itself is in three parts which constitute Chapters IV through VI. In Chapter IV, the outer zone electron characteristics which are present during quiet or undisturbed periods are presented, and in Chapter V some characteristics of outer zone electrons are presented during various degrees of magnetic activity indicating the conditions in the disturbed outer zone. In Chapter VI, statistical studies are presented using various portions of the Injun 3 data. These studies are designed to support and extend the observations and conclusions drawn in the previous two chapters and present the characteristics of the "average" outer zone. In Chapter VII the observations and conclusions drawn from the three parts of the study are condensed and discussed in

terms of an overall picture and in Chapter VIII they are examined to determine how they pertain to existing models and presently proposed particle acceleration or controlling mechanisms.

## II. DESCRIPTION OF EXPERIMENT

### A. The Satellite, Injun 3

Satellite Injun 3 was launched on 13 December 1962 into an orbit with apogee altitude 2785 km, perigee altitude 237 km, orbital inclination  $70.4^\circ$ , and period 116 minutes [O'Brien, Laughlin, and Gurnett, 1964]. The satellite was magnetically oriented by the use of a permanent magnet, and detector look-angle orientations on the satellite were referenced to this magnetic axis by the angle  $\theta$ . When the satellite was properly aligned, the  $\theta = 0^\circ$  axis was parallel to the geomagnetic B vector and was directed down into the atmosphere in the northern hemisphere. The orientation of the satellite was measured with two Schonstedt flux gate magnetometers mounted with their axes parallel to  $\theta = 90^\circ$  and  $\theta = 130^\circ$ , respectively. After alignment was obtained, the orientation system of the satellite maintained alignment to the extent that the rms deviation from alignment was less than  $5^\circ$  under almost all conditions for the ten month active lifetime of the satellite [see Appendix I]. A description of the Injun 3 satellite was given by O'Brien, Laughlin, and Gurnett [1964]. In the present study data were used from the following detectors.

### B. The Geiger Tubes

Detector 1 was a thin-windowed directional 213-type Geiger tube with an angular field of view of about  $26^\circ$  diameter centered at the  $\theta = 90^\circ$  position. It had a window thickness of  $1.2 \text{ mg cm}^{-2}$  of mica, an energy threshold for electrons of approximately 40 keV, and a geometric factor of about  $0.6 \times 10^{-2} \text{ cm}^2 \text{ ster}$  [Craven, 1966; Frank, Van Allen, and Craven, 1964]. The  $\theta = 90^\circ$  direction was normal to the geomagnetic  $\vec{B}$  vector when the satellite was aligned and Detector 1 responded to particles which were mirroring near the position of the satellite and which were therefore trapped. Detector 5 had a window thickness similar to that of Detector 1 but had an angular field of about  $86^\circ$  diameter centered on the  $\theta = 180^\circ$  axis, and had a geometric factor of about  $5.0 \times 10^{-2} \text{ cm}^2 \text{ ster}$ . In this position Detector 5 looked up the geomagnetic  $\vec{B}$  vector and sampled particles which were being precipitated into the atmosphere. Because a number of the findings of the present study depend on the response of Detector 5, a thorough study of possible contamination is carried out in Appendix II. These two detectors were developed by L. A. Frank, H. K. Hills, and J. D. Craven. Their energy passbands are presented in Figure 1. The Detector 1 passband was taken from Craven [1966] and the Detector 5 passband was constructed from the quoted geometric factor and the assumption that the window thickness was identical to that of Detector 1.

### C. Differential Magnetic Spectrometer

The differential spectrometer, developed by C. D. Laughlin, contained three 213-type Geiger tubes encased in a lead cylinder  $3.5 \text{ gm/cm}^2$  thick. The 213 Geiger tube has a thin window of mica,  $1.2 \text{ mg/cm}^2$  thick, and two of these tubes (labelled SpL and SpH for Spectrometer Low and Spectrometer High, respectively) had magnets positioned in front of them which deflected electrons with energy,  $E_e$ , through approximately  $90^\circ$  such that  $40 \text{ keV} \leq E_e \leq 50 \text{ keV}$  for SpL and  $80 \text{ keV} \leq E_e \leq 100 \text{ keV}$  for SpH. The third Geiger tube (labelled SpB for Spectrometer Background) was a similar omnidirectionally shielded one which was used to eliminate the contribution of bremsstrahlung and penetrating radiation from the counting rates of SpL and SpH.

The differential spectrometer was a unique and self-sufficient experiment in that it depended on no other detector for the proper interpretation of its data. It was able to sample the particle flux for trapped electrons in two distinct small energy intervals and permitted the determination without ambiguity of the slope of the electron energy spectrum in this energy range.

The defining apertures for the SpL and SpH detectors in the Injun 3 differential spectrometer gave these detectors

unidirectional geometric factors,  $g$ , of  $1.6 \times 10^{-4} \text{ cm}^2 \text{ steradian}$  and  $2.5 \times 10^{-4} \text{ cm}^2 \text{ steradian}$ , respectively [C. D. Laughlin, private communication]. The omnidirectional geometric factor,  $G$ , for each tube was determined in flight with cosmic ray background and was normalized to the known omnidirectional geometric factor of 302-type Geiger tube also flown on Injun 3. The values were  $G_{\text{SpL}} = 0.20 \pm 0.02 \text{ cm}^2$ ,  $G_{\text{SpH}} = 0.09 \pm 0.01 \text{ cm}^2$ ,  $G_{\text{SpB}} = 0.24 \pm 0.02 \text{ cm}^2$ . (The uncertainties in the values of  $G$  do not include any uncertainty for the value of  $G_{302}$ .) The energy passbands for SpL and SpH are given in Figure 1.

The angular fields of view for SpL and SpH were about  $12^\circ$  in diameter centered on the  $\theta = 90^\circ$  axis. Since the particles were magnetically analyzed, the viewing cones were not centered on the geometric axis of each aperture system but were displaced about  $5^\circ$ , being "cross-eyed", i.e., toward one another. The effective axes were in the plane perpendicular to the geomagnetic  $\vec{B}$  vector. Hence, the non-parallelism of the axes was ignored since the flux was presumed aximuthally symmetric around  $\vec{B}$ .

#### D. Electron Multiplier

The electron multiplier on Injun 3, developed by D. E. Stilwell, used a 19-stage Ascop type 541 series photomultiplier



tube operated at 2500 volts. Incident particles, striking the sensitive area of the first dynode directly, produced electrons by a secondary emission process. These secondaries were then drawn on to successive dynodes in the normal photomultiplier cascade scheme. The anode current was fed to a simple neon-glow tube relaxation oscillator whose output frequency was a function of the current drawn from the circuit input. In this manner an analog to digital conversion of the anode current, which was proportional to the incident particle number flux, was accomplished. The aperture of the electron multiplier was covered by a thin nickel foil ( $86 \mu\text{g}/\text{cm}^2$ ) which imposed an energy threshold of approximately 10 keV for electrons. The multiplier was positioned in the  $\theta = 130^\circ$  position and therefore sampled particles whose local pitch angle was  $\sim 50^\circ$ . The spectral response passband for the multiplier is given in Figure 1. For a discussion and verification of this passband and the inflight performance of the multiplier, see Fritz and Gurnett [1965].

#### E. The 3914 Å Auroral Photometer

The 3914 Å auroral photometer consisted of an Ascop-type 541A photometer operated at 2500 volts, a single  $\sim 3$ -inch focal length lens and an interference filter 2 inches in diameter. The

anode current was fed to a simple neon-glow tube relaxation oscillator whose output frequency was a function of the current drawn from the circuit input. In this manner an analog to digital conversion of the anode current was accomplished [O'Brien, Laughlin, and Gurnett, 1964]. The photometer was mounted in the  $\theta = 0^\circ$  direction and had an angular field of view of about  $10^\circ$ . The filter was centered at  $3933 \text{ \AA}$  and was  $81 \text{ \AA}$  wide at the half peak transmission points. For a more complete discussion of this detector, see O'Brien and Taylor [1964].

#### F. Inflight Operation and Calibration Checks

Because of the large array of detectors on Injun 3, the inflight performance of these detectors could be checked against preflight calibrations to an extent relatively unusual in satellite studies.

The operation of the differential spectrometer was studied in detail over the 8 month period following launch. The maximum observed detector responses for SpL, SpH, and SpB were tabulated over this period along with the responses of these detectors to cosmic ray background. The results of this tabulation are presented in Table 1 and Figure 2. As observed in Figure 2, the responses of these detectors to cosmic ray background (over the

polar caps of the earth) remained unchanged throughout the active life of the satellite. Neither of the three detectors encountered particle fluxes capable of driving them to their maximum preflight calibrated rates so the rates presented in Table 1 are sets of responses taken when the three detectors were responding primarily to penetrating radiation at rates near the maximum observed inflight rates.

The operation of the SpL and SpB detectors was satisfactory over the entire period. The SpH detector experienced a large change in its maximum observable counting rate while its response to cosmic rays remained unchanged through this period. This malfunction was examined in detail. The detector showed a progressive deterioration in the maximum observed rate reaching a minimum in June and then recovering somewhat in July and August. The satellite's battery voltage showed a very similar profile over the same time period. In summary, the malfunction of SpH affected the maximum rate of the detector, left the very low rates unaffected, and was associated with the satellite's battery voltage. The most plausible explanation of the behavior of SpH was that the tube was operating near the edge of its voltage plateau region [see Laughlin, 1960]; and when the Geiger tubes started to respond

to intense particle fluxes, they drew an appreciable fraction of the current needed by a voltage regulator circuit to maintain the necessary voltage applied to the tubes. When the satellite supply voltage was lowered, the voltage regulator circuit was unable to compensate when the tubes were responding at a high rate and the resulting voltage applied to the tubes was decreased. This caused the SpH detector to operate off the voltage plateau region. This region did not extend to as low a voltage as the SpL and SpB detector voltage plateau regions. This type of malfunction would have affected the operation of the detector only when the detector was counting near its maximum rate. As the counting rates of the SpL and SpB detectors decreased, the SpH counting rate should have remained nearly constant and returned to normal behavior when the SpL and SpB rates became low enough. This point was investigated using data taken on June 20, 1963 (which was during the worst period of the malfunction). Data were selected when the SpH and SpB were responding primarily to penetrating radiation. The results are tabulated in Table 2. It will be noticed that as the SpB rate decreased by more than two orders of magnitude, the SpH rate remained constant to within a factor of two.

It is the opinion of the author that the SpH detector can be considered trustworthy for low counting rates through this entire period. In the present paper, however, all data from the spectrometer recorded after 20 May 1963 were excluded from the study (with the exception of data at  $L = 2.0$  which were not used after 1 May 1963).

As a check on the pre-flight calibration of the Geiger tubes, this author generated a number of calibrations from inflight data. The spectral pass band of Detector 1 was determined using the differential spectrometer to find the electron energy spectrum and then testing numerically integrated passbands to find the best fit. This passband agrees very well with that published by Craven [1966]. (Figure 1).

A complete characteristic curve of true rate  $R$  versus apparent rate  $r$  for Detector 1 was generated using the responses of spectrometer which was operating over the linear part of its  $R$  vs  $r$  characteristic. This curve is in good agreement with one produced from the preflight calibrations [J. D. Craven, private communications]. A partial  $R$  vs  $r$  curve was generated for Detector 5 using the responses of the spectrometer when both detectors looked at identical particle fluxes. This happened early in the

life of the satellite when it was tumbling and the axis of the these detectors would occasionally lie at equal angles to the geomagnetic  $\vec{E}$  vector. The response of Detector 5 at an apparent rate greater than 8,000 c/s yielded a true rate which was uncertain to two orders of magnitude due to disagreement between the preflight and inflight R vs r characteristics. Hence, Detector 5 was clearly saturated in that region of its R vs r characteristic.

Since both Detector 1 and Detector 5 saturated when responding to the intense inner zone fluxes, their maximum observed rates throughout the lifetime of the satellite gave a check on the detector's operation. These rates were found to have remained essentially constant for both detectors during the entire period.

Table 1

Month	Maximum Observed Rates			Ratio of Maximum Rates		Ratio of Omnidirectional Geometric Factors from Cosmic Ray Background	
	SpL	SpH	SpB	SpL/SpB	SpH/SpB	$G_{SpL}/G_{SpB}$	$G_{SpH}/G_{SpB}$
December	2995	1504	2478	1.21	0.61	$.88 \pm .10$	$.39 \pm .06$
January	3020	1482	2509	1.20	0.59	$.85 \pm .06$	$.40 \pm .04$
February	2872	1027	2472	1.16	0.42	$.84 \pm .09$	$.28 \pm .05$
March	2914	732	2473	1.18	0.30	$.75 \pm .06$	$.45 \pm .04$
April	2850	480	2460	1.16	0.19	$.87 \pm .15$	$.46 \pm .10$
May ( 1-15)	2897	213	2473	1.17	0.086	$.87 \pm .09$	$.44 \pm .06$
(15-31)	2861	99	2461	1.16	0.040	$.78 \pm .07$	$.37 \pm .04$
June( 1-15)	2992	18	2474	1.21	0.007	$.80 \pm .09$	$.37 \pm .04$
(15-30)	2761	35	2418	1.14	0.015	$.87 \pm .09$	$.40 \pm .06$
July( 1-15)	2989	50	2423	1.23	0.021	$.85 \pm .10$	$.37 \pm .05$
(15-31)	2421	117	2012	1.20	0.058	$.77 \pm .08$	$.38 \pm .05$

Table 2

SELECTED DETECTOR RESPONSES DUE PRIMARILY  
TO PENETRATING RADIATION IN THE INNER ZONE  
ON 20 JUNE 1963

Observation	SpB Response	SpH Response	Ratio
	counts/second	counts/second	
1	2462	24.6	.0100
2	1539	21.3	.0138
3	702	18.5	.0263
4	505	17.2	.0341
5	406	17.8	.0439
6	285	15.1	.0586
7	185	15.0	.0813
8	129	14.3	.110
9	77.6	13.3	.171
10	36	12.4	.348
11	22.8	12.1	.530
Responses due to cosmic ray back- ground	0.650	0.275	.423



### III. DESCRIPTION OF RELEVANT PARAMETERS

In undertaking this study a set of parameters was introduced to organize the problems under investigation. The data transmission system on Injun 3 operated for seventeen minutes after reception of a properly coded command from a receiving station below the satellite. Each of the detectors on the satellite had its own twelve bit accumulator which was sampled once every one-fourth second for the data used in this study (with the exception of the 3914 Å auroral photometer which was sampled once every two seconds) [O'Brien, Laughlin, and Gurnett, 1964]. The orbital parameters of the satellite including the L, B coordinates of McIlwain [1961] were assigned to each one-fourth second (frame) of data, using the ephemeris supplied by the Goddard Space Flight Center. For most of the data presented in this study, the data were summed over consecutive eight second intervals due to a lack of sufficient counting statistics on a frame by frame (one-fourth second) basis.

#### A. The Spectral Parameter, $\gamma$

Using the responses of the SpL and SpH detectors corrected for background, a two parameter spectral model of the electron

energy spectrum could be completely determined . In studies of geomagnetically trapped radiation, the intensity or flux is usually plotted on log-log paper because of the large temporal and/or spatial variations which are observed. On such a plot of the intensity vs particle energy a power law spectrum.

$$dN = K E^{-\gamma} dE$$

plots as a straight line which has a slope equal to the exponent,  $\gamma$ . It is this spectral parameter,  $\gamma$ , that has been chosen to organize the electron energy spectral information from the differential spectrometer. Although this parameter,  $\gamma$ , represents the exponent in the power law spectral model, it is emphasized that its interpretation be only as a measure of the slope of the spectrum in the energy range from 40 keV to 100 keV and not as a parameter describing the entire energy spectrum.

Evaluation of the spectral parameter,  $\gamma$ , for the differential spectrometer was done by initially assuming a given numerical value for  $\gamma$  and integrating numerically over the response curves for SpL and SpH given in Figure 1 by using the integral,

$$R_i = K \int_0^{\infty} g_i(E) E^{-\gamma} dE$$

where

$R_i$  = the response of either SpL or SpH in counts per second corrected for background

$g_i(E)$  = the effective passband geometric factor in  $\text{cm}^2$  steradian of either detector

$K$  = a constant with units of electrons per  $\text{cm}^2$  per second per steradian per keV multiplied by keV to the  $\gamma$  power (i.e.,  $N_0 E_0^\gamma$ )

The ratio of the responses of the two detectors

$$\frac{R_{\text{SpL}}}{R_{\text{SpH}}} = \frac{K \int_0^\infty g_{\text{SpL}}(E) E^{-\gamma} dE}{K \int_0^\infty g_{\text{SpH}}(E) E^{-\gamma} dE}$$

is independent of the constant  $K$  and uniquely determines the slope parameter,  $\gamma$ . By varying the value of  $\gamma$  used in the numerical integration just described, the ratio  $R_{\text{SpL}}/R_{\text{SpH}}$  was calculated and graphed as a function of  $\gamma$ . An analytic expression for the graphed function,  $\gamma = 1.20 + 3.10 \log_{10} (R_{\text{SpL}}/R_{\text{SpH}})$  was found to give  $\gamma$  accurately over the range of ratios from 0.1 to 200.

In a similar manner, it was possible to determine a spectral parameter,  $\gamma$ , using the response functions of the electron multiplier and Detector 1 given in Figure 1 to describe the

electron energy spectrum between 10 keV and 40 keV. The calculation of this parameter was based on two assumptions. The first was that the responses of both detectors were due almost entirely to electrons and the second was that the flux of electrons in the energy range from 10 keV to 40 keV was isotropic over the upper hemisphere at the position of the satellite. Due to the small sensitivity of the electron multiplier and the necessarily large electron fluxes needed to make the electron multiplier respond, the nature of the events causing the multiplier to respond usually satisfied the above two conditions. This will be demonstrated in Chapters V and VI.

#### B. The disturbance or "Dumping Parameter, $\phi$

A dumping parameter,  $\phi$ , was calculated by dividing the flux of particles measured with Detector 5 by the flux of particles measured with Detector 1. The parameter,  $\phi$ , was therefore the ratio of the flux of electrons with  $E_e \geq 40$  keV being precipitated into the atmosphere to the flux of electrons with  $E_e \geq 40$  keV mirroring near the position of the satellite. As the amount of "dumping" increased, the parameter,  $\phi$ , approached the value of one in agreement with the observation of O'Brien [1964] and of Parthasarathy, Berkey, and Venkatesan [1966] that

the precipitation process is such that the angular distribution of electrons tends to approach isotropy over the upper hemisphere at the altitude of the satellite.

In Section F of Chapter II, it was noted that when Detector 5 was responding at a rate in excess of 8,000 c/s, the detector was saturated. Under these conditions, the value of the parameter  $\phi$  was set equal to one for plotting. In the statistical studies of Chapter VI no value of the parameter  $\phi$  was calculated under these circumstances.

#### C. The Latitude Parameters, $\Lambda$ and L

In the present study, the invariant latitude,  $\Lambda$  [O'Brien, 1962] and the L coordinate of McIlwain [1961] are used interchangeably. Both coordinates have been useful in the study of trapped radiation and are related to one another by the relationship,  $L \cos^2 \Lambda = 1$ . Although L is usually thought of as labeling a particular magnetic shell (L being the equatorial radius expressed in earth radii of a particular shell in a dipole-equivalent field), one can think of it as a latitude parameter increasing from the geomagnetic equator to each of the geomagnetic poles.

#### D. The Geomagnetic Activity Parameters, $K_p$ , $A_p$ , and Dst

The geomagnetic activity parameters,  $K_p$  and  $A_p$ , used in the present study are published routinely by Lincoln

in the Journal of Geophysical Research. The geomagnetic planetary 3-hour indices  $K_p$  and the Average Field Amplitude index,  $A_p$ , in units of two gamma ( $2 \times 10^{-5}$  gauss) are prepared routinely at the Geophysikalisches Institut of the University of Gottingen, Free Republic of Germany.

The Dst values used in the present study were computed by Sugiura and Hendricks of the Goddard Space Flight Center using the equation

$$Dst = \frac{1}{n} \sum_{i=1}^n (\Delta H_i - S_{qi}) \sec \lambda_i$$

where  $\lambda$  is the magnetic latitude,  $\Delta H$  is the deviation of the horizontal geomagnetic field component from the average quiet time field and  $S_q$  is the average daily variation at the magnetic observatories. For the time period used here, data were used from eight stations situated around the world such that  $10^\circ < \lambda_i < 45^\circ$ . Dst is considered to be a measure of the surface field produced by a storm-time ring current [Akasofu, 1966].

#### E. The Local Time Parameter, MLT

Because the motion and behavior of the particles under study in this paper are governed by the geomagnetic field, magnetic

local time (MLT) is used here instead of the usual geographic local time. Magnetic local time is defined as the angle between the planes which are defined by the geomagnetic dipole axis and the earth-sun line and by the geomagnetic dipole axis and the earth center-satellite line. MLT takes into account both the daily and the seasonal variations in the orientation of the geomagnetic dipole axis with respect to the earth-sun line. For the orbit of Injun 3, MLT differed by as much as  $\pm 2.3$  hours from the corresponding geographic local time at the high latitudes. At lower latitudes the two local times were always more nearly equal. [For further remarks on magnetic local time, see Appendix I, Fritz and Gurnett (1965)].

#### IV. CHARACTERISTICS OF ELECTRONS IN THE "QUIET" OR UNDISTURBED OUTER ZONE

All data recorded from Injun 3 for the detectors discussed in Chapter II were plotted for each traversal of the outer zone made by the satellite during its 10 month active lifetime. These plots were generated automatically by the University of Iowa IBM 7044 computer and plotted on Calcomp Digital Incremental plotters.

With the data organized in this manner the plots were examined on geomagnetically quiet days determined from the 3 hour  $K_p$  indices and standard magnetograms taken at stations near the position of the satellite. Figure 3 is presented as a characteristic undisturbed pass. The  $K_p$  index was  $1_0$  and the daily  $A_p$  index was 5 for the period of this pass. The intensity of electrons with  $E_e \approx 40$  keV and with  $E_e \approx 90$  keV mirroring at the position of the satellite decreased with increasing latitude from  $\Lambda = 45^\circ$  reaching a minimum at  $\Lambda = 55^\circ$  to  $60^\circ$  after which these intensities increased somewhat before falling off with varying degrees of sharpness at the high latitude outer zone termination. The minimum or "slot" at  $\Lambda \approx 55^\circ$  to  $60^\circ$  was sometimes very noticeable for  $\geq 40$  keV trapped electrons but in most cases the ratio



between the maximum and minimum fluxes for  $\Lambda > 55^\circ$  was less than a factor of 10. These characteristics are in good agreement with the median intensity profile as a function of latitude presented by Armstrong [1965a]. The electron energy spectrum between 40 keV and 100 keV had a tendency to soften with increasing latitude above  $\Lambda = 60^\circ$  ( $L = 4.0$ ), but it was significantly softer in the "slot" ( $L \approx 3.5$ ) than at adjacent latitudes. The softer spectrum at  $L \approx 3.5$  was evidenced by a greater relative depression of the 100 keV electron intensity in the slot than that of the 40 keV fluxes.

The intensity of electrons with  $E_e \geq 10$  keV and pitch angle  $\alpha \approx 50^\circ$  for these undisturbed conditions was always less than the threshold counting rates of the Injun 3 electron multiplier, ( $2.0 \times 10^6$  electrons/cm<sup>2</sup> sec. ster). Using the results reported by Armstrong [1965b] that the angular distribution of  $\geq 40$  keV electrons in the outer zone was not strongly peaked at  $\alpha = 90^\circ$  (e.g., if  $j(\alpha) = \sin^n \alpha$  then  $1 \leq n \leq 2$ ) the fact that  $j(E_e \geq 10 \text{ keV}) < 2.0 \times 10^6 \text{ cm}^2 \text{ sec. ster.}$  throughout the outer zone was interpreted to indicate that the electron energy spectral slope between 10 keV and 40 keV did not increase sharply but was approximately equal to or less than the spectral slope between

40 keV and 100 keV. In Figure 3 note that the spectral slope parameter,  $\gamma$ , determined between 40 keV and 100 keV at  $\Lambda = 65^\circ$  was  $\gamma = 2.8 \pm 0.4$  whereas an upper limit for the slope parameter,  $\gamma$ , determined between 10 keV and 40 keV in the manner described above was  $\gamma < 2.7$  (see Chapter III for the details on the determination of  $\gamma$ ).

The intensity of  $\geq 40$  keV electrons moving with pitch angles at the position of the satellite such that they would mirror below an altitude of 100 km and be lost to the atmosphere before being reflected was found to vary with increasing latitude in an almost identical manner as the  $> 40$  keV electrons intensities mirroring at the position of the satellite. When Detector 5 was responding primarily to precipitated electrons (this was true when  $B \gtrsim 0.28$  gauss - see Appendix II) the dumping parameter,  $\phi$ , which was equal to the ratio of  $j(E_e > 40 \text{ keV}, \alpha < 43^\circ)$  to  $j(E_e > 40 \text{ keV}, \alpha = 90^\circ)$  was nearly constant as a function of increasing latitude and approximately equal to  $10^{-2}$  for latitudes below the high latitude outer zone termination. At the high latitude boundary, the intensity of  $> 40$  keV electrons being precipitated into the atmosphere usually increased sharply. Many of these spikes of precipitated electrons

reached and maintained isotropy over the upper hemisphere at the position of the satellite on and beyond the boundary. The dumping parameter  $\phi$ , therefore increased sharply from  $10^{-2}$  to approximately 1 for these spikes of precipitated electrons.

A search was made to determine whether these spikes of precipitated electrons occurred at all local times during undisturbed periods. Examples from this investigation are presented in Figure 4. It is observed that these spikes occurred in all sectors of magnetic local time and that the general features discussed above of  $> 40$  keV dumped and trapped electron intensity profiles as a function of latitude were also present in all magnetic local time sectors. It will be noted that Detector 5 is responding primarily to dumped electrons (see Appendix II) for all passes except Rev 1626 where contamination by trapped particles was present. The dashed portions of the curves for the dumping parameter,  $\phi$ , indicate periods when Detector 5 was responding at a rate less than 10 counts/second but sufficiently above background so that a value of  $\phi$  could be determined.

The high latitude spike of  $> 40$  keV precipitated electrons was not observed in all undisturbed passes. In Figure 5, three examples are presented for which no high latitude spike was

observed. In only one of the examples was the satellite at values of  $B$  where Detector 5 was responding primarily to precipitating electrons. In this example (Revolution 1981) the dumping parameter,  $\phi$ , was again independent of latitude and equal to approximately  $10^{-2}$ . The conditions of geomagnetic activity for the passes of Figures 3-5 are presented in Figure 6.

Detector 1 and Detector 5 being open end Geiger tubes were sensitive to soft solar X-rays (efficiency =  $10^{-2}$  to  $10^{-1}$  over the range of 4 to 12 Å) [Van Allen, Frank, Maehlum, and Acton, 1965; Wende, 1966]. For this reason solar aspect sensors were included in the Injun 3 payload with comparable fields of view to Detector 1 and Detector 5 in order to detect the presence of the sun in the detector viewing cone [O'Brien, Laughlin, and Gurnett, 1964]. Because the diameter of the viewing cone of Detector 1 was small ( $26^\circ$ ), a response to solar X-rays was usually easy to distinguish by a counting rate peak coincident with a response of the companion solar aspect sensor. An example of this behavior is shown in Rev 1700 of Figure 5 for Detector 1.

The impression gained in the present study was that the ratio of the precipitated to the trapped electron fluxes (the  $\phi$  parameter) was independent of latitude up to the high latitude

outer zone boundary. Frank, Van Allen, and Craven [1964] performed a statistical study of the diurnal variations of geomagnetically trapped and precipitated electrons using the same two Injun 3 detectors used here. They found that the contours of constant counting rate for each detector plotted as a function of latitude viewed from the pole were very similar for local times on the night side ( $1700 \text{ hours} \leq LT \leq 0900 \text{ hours}$ ), but they found that an apparent maximum of the intensities of precipitated electrons (Detector 5) occurred at approximately local noon ( $\approx 0900$  to  $1300$ ) at  $4 \leq L \leq 10$ , without an accompanying maximum in the intensities of trapped electrons (Detector 1).

The counting rate contours of Frank, Van Allen, and Craven for local night ( $1700 < LT < 0900$ ) are consistent with the fact that the dumping parameter,  $\phi$ , appeared to remain independent of latitude up to the high latitude outer zone boundary. However, the apparent maximum found near local noon is inconsistent with the present result. All passes with local times near local noon were examined in detail. It was found that almost without exception when the satellite was near local noon, the solar aspect corresponding to Detector 5 viewed the sun. An example of such a pass taken during an undisturbed period is presented in Figure 5 (Rev 1708). Because the diameter of the viewing cone of

Detector 5 was large ( $86^\circ$ ), there was never a characteristic peak observed as in the case of Detector 1 (see Rev 1700, Figure 5) when the detectors viewed the sun, but on many of the passes contamination of the Detector 5 response by soft solar X-rays was evident (e.g., Rev 1708).

If the apparent maximum found by Frank, et al. was due to solar X-rays, the only modification to their conclusions would be that the diurnal variation of the precipitated electrons must be similar to the large diurnal variation noted for trapped electrons, and this would then be in agreement with the present results. McDiarmid and Burrows [1964] reported a similar diurnal study for trapped and precipitated  $\geq 40$  keV electrons using a detector with a much smaller opening angle ( $\sim 4.5^\circ$ ). They found that the shape of the distributions of the average intensity for both  $\geq 40$  keV trapped and  $\geq 40$  keV precipitated electrons were very similar as a function of local time ( $60^\circ \leq \Lambda \leq 68^\circ$ ). Their results agree with those of the present paper and indicate that the large maximum found by Frank, et al. on the day side was probably due to contamination by solar X-rays.

## V. SOME DISTURBED OUTER ZONE CHARACTERISTICS

In examining the body of Injun 3 data, it was not always possible to find the quiet or undisturbed outer zone electron characteristics even during periods when there was little or no magnetic activity taking place. In this chapter some characteristics of outer zone electrons are discussed in connection with the degree of magnetic activity occurring at the same time. This chapter is divided into three sections in which electron characteristics are discussed during low, moderate, and very active magnetic conditions.

### A. Periods of Low Geomagnetic Activity

The example presented in Figure 3 of the characteristics of undisturbed outer zone electrons was taken on January 1, 1963. On that day the  $K_p$  index was never greater than 2<sub>0</sub> and the daily  $A_p$  index was 5. On the following day the  $K_p$  index was never greater than 1<sub>0</sub>, the  $A_p$  index was 1, and the day was designated one of the five quiet days in magnetic activity for the month of January. We will now examine the behavior of the outer zone electrons during this two day period of low magnetic activity.

Passes through the outer zone taken two hours before and two hours after Rev 240 (presented in Figure 3) are presented in Figure 7. It will be noted that Rev 239 exhibited all the characteristics of an undisturbed pass discussed in Chapter IV. However, on the next pass (Rev 241) after these two undisturbed passes, the undisturbed character disappeared. The profiles for  $j_{\perp}$  ( $40 \text{ keV} \leq E_e \leq 50 \text{ keV}$ ),  $j$  ( $E_e \geq 40 \text{ keV}$ ) trapped,  $j$  ( $E_e \geq 40 \text{ keV}$ ) dumped, the spectral parameter,  $\gamma$ , and the dumping parameter,  $\phi$ , were all modified but the profile of  $j_{\perp}$  ( $80 \text{ keV} \leq E_e \leq 100 \text{ keV}$ ) remained unchanged. It will be noted in Rev 241 that the satellite encountered spikes of precipitated  $\geq 40 \text{ keV}$  electrons which corresponded to either regions or periods of large amounts of precipitation. These spikes of precipitation increased the flux of  $\geq 40 \text{ keV}$  electrons mirroring at the position of the satellite noticeably. The precipitating electrons measured by Detector 5 probably had an energy equal to  $\approx 40 \text{ keV}$  since the value of  $j_{\perp}$  ( $40 \text{ keV} \leq E_e \leq 50 \text{ keV}$ ) increased to approximately the value of  $j_{\perp}$  ( $E_e \geq 40 \text{ keV}$ ) while the value of  $j_{\perp}$  ( $80 \text{ keV} \leq E_e \leq 100 \text{ keV}$ ) remained unchanged during the precipitation spikes. During the precipitation portion of the pass, the spectral parameter,  $\gamma$  increased more sharply with latitude and reached a maximum value of



$\gamma = 5.7 \pm 0.4$  coincident with one of the precipitation spikes at  $\Lambda \approx 68^\circ$  after which it decreased in value as the high latitude outer zone boundary was approached. The dumping parameter,  $\phi$ , reflected the same character as the precipitation spikes and at one point reached one (isotropy over the upper hemisphere at the position of the satellite) but in general was somewhat less than one.

The next two passes recorded by Injun 3 in passing through this region are presented in Figure 8. Rev 243 occurred approximately 4 hours after Rev 241 (Figure 7). It will be noted that a very large amount of precipitation was again found on this pass but this time there appeared to be only a single spike with the dumping parameter,  $\phi$ , increasing sharply from a value of  $\approx 10^{-2}$  to  $\approx 1$  in only two degrees of latitude. The flux of  $\geq 40$  keV electrons remained essentially isotropic for the duration of the enhanced precipitation portion of the pass with  $j(E_e \geq 10 \text{ keV})$  increasing to a value above the threshold of the electron multiplier. During this enhanced precipitation the spectral parameter again increased sharply and reached a maximum value of  $\gamma = 6.6 \pm 0.6$ . It will be noted that this increase was due to a large increase in the value of  $j_{\perp}$  ( $40 \text{ keV} \leq E_e \leq 50 \text{ keV}$ ) while the latitude profile of  $j_{\perp}$  ( $80 \text{ keV} \leq E_e \leq 100 \text{ keV}$ ) remained unchanged during the

precipitation process. This indicated again that the energy of the precipitating electrons measured by Detector 5 was not much greater than 40 keV. However, at lower latitudes, it will be noted that the spectral parameter  $\gamma$  had a value of  $\gamma = 0.1 \pm 0.5$  at  $\Lambda \approx 61^\circ$  indicating a surprisingly hard spectrum for this region.

It was not possible to determine an accurate value of  $j$  ( $E_e \geq 10$  keV) during the precipitation portion of the pass due to noisy telemetry at that point. However, it was possible to place the value of  $j$  ( $E_e \geq 10$  keV) between  $4.5 \times 10^6$  and  $3 \times 10^7$  electrons/cm<sup>2</sup> sec. ster. These values indicate that the spectral parameter,  $\gamma$ , for the slope of the electron energy spectrum between 10 keV and 40 keV was between  $\gamma = 2.9$  and  $\gamma = 4.2$ . Both of these values are smaller than the maximum value of  $\gamma$  observed for the range from 40 keV to 100 keV indicating that the spectrum did not continue to rise more steeply toward the lower energies. If an exponential type spectral form is fitted to the data at 10 keV and 40 keV, an average energy between 7 and 12 keV is found.

With the exception of the enhanced precipitation portion of the pass, Rev 243 displayed most of the typical undisturbed

characteristics discussed in Chapter IV. The dumping parameter,  $\phi$ , was independent of latitude and equal to  $\approx 10^{-2}$  for all latitudes below the precipitation spike. The spectral parameter,  $\gamma$ , exhibited a broad peak around  $\Lambda = 58^\circ$  where each of the latitude profiles,  $j_{\perp}(E_e \geq 40 \text{ keV})$ ,  $j(E_e \geq 40 \text{ keV})$  dumped,  $j_{\perp}(40 \text{ keV} \leq E_e \leq 50 \text{ keV})$ , and  $j_{\perp}(80 \text{ keV} \leq E_e \leq 100 \text{ keV})$  indicated the presence of a slot.

The next pass (Rev 244 of Figure 8) taken approximately two hours later indicated that the values of  $j_{\perp}(E_e \geq 40 \text{ keV})$ ,  $j(E_e \geq 40 \text{ keV})$  dumped, and  $j_{\perp}(40 \text{ keV} \leq E_e \leq 50 \text{ keV})$  in the region where the precipitation had been observed on Rev 243 had all decreased with the value of  $j(E_e \geq 40 \text{ keV})$  dumped decreasing by two orders of magnitude. Rev 244 exhibited the appearance of a return or decay toward the undisturbed outer zone electron characteristics. The next two passes through this region occurred fourteen and sixteen hours respectively after Rev 244. The first of these two passes, Rev 252, exhibited the characteristics of an undisturbed pass and is presented in Figure 9. The second pass, Rev 253, also presented in Figure 9, was very similar to the pass taken 24 hours prior to it, Rev 241 (Figure 7). Similar precipitation spikes were observed and the value of the dumping parameter never reached one similar to the spikes observed for Rev 241.

The next pass, Rev 255, through this region recorded by Injun 3 is presented in Figure 10. It occurred approximately twenty-four hours after Rev 243 (Figure 8), and was very similar in form to Rev 243. In Rev 255 the flux of  $\geq 40$  keV electrons reached and maintained isotropy near and on the outer zone boundary as in the case of Rev 243 but there was much more low latitude precipitation in Rev 255 and  $j$  ( $E_e \geq 10$  keV) remained less than  $2.0 \times 10^6$  electrons/cm<sup>2</sup> sec. ster. The very noticeable softening of the spectrum between 40 keV and 100 keV which took place at  $\Lambda \approx 65^\circ$  was coincident with a sharp increase in the intensity of precipitating electrons indicating again that the energy of the precipitating electrons was not much greater than 40 keV. Most of the discussion of the characteristics of Rev 243 can be applied in a similar manner to Rev 255.

The passes, Rev 239-255, presented thus far were all recorded over North America and most were recorded by the College, Alaska tracking station. In Figure 10, a pass through the outer zone is presented which was recorded in the southern hemisphere over Woomera, Australia. This pass was taken between Rev 243 and Rev 244 of Figure 8. It will be noted that Rev 243 in Figure 10 exhibited most of the undisturbed pass characteristics. It

should be kept in mind that Detector 5 "looked" down toward the atmosphere in the southern hemisphere and its response in this pass was due to particles which had mirrored below the satellite and were moving toward the equatorial plane. In general, however, the undisturbed pass profile characteristics can be observed in Rev 243 of Figure 10.

The undisturbed nature of Rev 243 in Figure 10 indicated that the disturbed conditions observed in Rev 241-244 were either (1) very confined in longitude or local time since the magnetic local times for the two passes labelled Rev 243 differed by only  $\approx 3$  hours, or (2) restricted in such a way that conjugate point disturbances did not occur. It is not possible to distinguish between the two possibilities using only the Injun 3 data.

Therefore, we have observed that during periods of low geomagnetic activity, large increases in the values of  $j_{\perp}$  ( $E_e \geq 40$  keV),  $j$  ( $E_e \geq 40$  keV) dumped, and  $j_{\perp}$  ( $40$  keV  $\leq E_e \leq 50$  keV) from their respective undisturbed values occurred, with the intensity of precipitating electrons changing by as much as two orders of magnitude. The maximum energy of the precipitated electrons was not much greater than 40 keV and this gave rise to a very noticeable softening of the trapped electron

energy spectrum between 40 keV and 100 keV associated with these precipitation events. The precipitation events were not able to increase the value of  $j_{\perp}$  ( $80 \text{ keV} \leq E_e \leq 100 \text{ keV}$ ) indicating an absence of precipitating electrons with energies in that range.

A closer check was made on the variations observed in Figures 7-10 of the dumping parameter,  $\phi$ , and the spectral parameter,  $\gamma$ , in relation to the degree of magnetic activity occurring. The temporal variations of the particle intensities could not be readily compared due to the presence of non-real time variations [e.g.,  $B$  - dependences of the fluxes (Armstrong, 1965a)]. For the present, the assumption that  $\gamma$  and  $\phi$  were not strong functions of  $B$  (the range of  $B$ ,  $\Delta B \approx .060$  gauss for these passes) was made. This assumption will be discussed in Chapter VI. The variations of the spectral parameter,  $\gamma$ , and the dumping parameter,  $\phi$ , as a function of time for the two day period, 1-2 January 1963, are presented in Figure 11 for five different latitudes. The variations of various magnetic field measurements which were applicable to these latitudes are also presented in Figure 11.

For  $\Lambda = 50^\circ$ , there was essentially no variation in either the value of the spectral parameter,  $\gamma$ , or the dumping parameter  $\phi$ , and for  $\Lambda = 55^\circ$  the values of both parameters showed larger

variations but these variations exhibited no clear pattern. (A large B dependence  $\gamma$  was found for the region,  $\Lambda \approx 55^\circ$ , in Chapter VI, but it was not sufficient to explain the variations found here. Note that the minimum value of  $\gamma$  for  $\Lambda = 55^\circ$  was found at  $B = 0.325$  gauss whereas values of  $\gamma$  determined two hours before at  $B = 0.308$  gauss and four hours later at  $B = 0.359$  gauss were both substantially larger.) These variations are attributed to changes in the apparent position of the "slot" as a function of latitude from pass to pass.

At  $\Lambda = 60^\circ$ , the spectral parameter and the dumping parameter exhibited some moderate variation with time while the magnetometer at Sitka, Alaska (magnetic latitude,  $\lambda_m = 60.0^\circ$ ) indicated no activity whatsoever. For  $\Lambda \geq 65^\circ$ , temporal variations were more prominent.

In Figure 11 for  $\Lambda = 65^\circ$  and  $\Lambda = 68^\circ$ , it will be noted that the increases in the dumping parameter were usually accompanied by an increase in the spectral parameter and by small fluctuations in the magnetometer data taken on the ground near the satellite at College, Alaska ( $\lambda_m = 64.6^\circ$ ) and Pt. Barrow, Alaska ( $\lambda_m = 68.5^\circ$ ). The fluctuations in the magnetometer readings can be regarded as very small since a normal geomagnetic storm can produce fluctuations of 1000 gammas or more at these two stations.

Therefore, the conclusion reached from this pass sequence was that large intensities of electrons with  $E_e \lesssim 40$  keV could be precipitated into the atmosphere without an appreciable amount of magnetic activity occurring, even in the vicinity of the satellite.

Another type of variation in the outer zone electron characteristics that was observed to occur during periods of low magnetic activity was the variation of the position of the high latitude outer zone boundary. In Figure 12, four passes recorded by Injun 3 in passing through the high latitude outer zone boundary near the midnight meridian on June 22, 1963 are presented. During the period of these passes the Kp index was 1+ or less and for the eighteen preceding hours and the following 48 hours the Kp index was never greater than 2-. Both June 22 and June 23 were each one of the five magnetically quiet days of the month. Magnetograms recorded at Sitka, Alaska ( $\lambda_m = 60^\circ$ ), College, Alaska ( $\lambda_m = 65^\circ$ ), and Barrow, Alaska ( $\lambda_m = 68^\circ$ ) during the period of the passes in Figure 12 indicated that no magnetic activity was occurring at any of these stations. However, during this period the boundary was first observed at  $\Lambda \approx 74^\circ$  on Rev 2378 which was taken during a large precipitation event similar to those examined



previously in Rev 243 (Figure 8) and Rev 255 (Figure 10). Two hours later on Rev 2379 the precipitation was not as intense and the boundary was observed at  $\Lambda \approx 71^\circ$ . On the following pass, Rev 2380, the large precipitation had disappeared and the boundary had collapsed to  $\Lambda \approx 67^\circ$ . The following pass, Rev 2381, found the boundary had moved outward again to  $\Lambda \approx 70^\circ$ .

In this sequence of four passes the apparent outer zone boundary for  $\geq 40$  keV electrons was observed to change in position from  $74^\circ$  to  $67^\circ$ , a change of  $\Delta \Lambda = 7^\circ$ , in four hours during a period of low geomagnetic activity. It will also be noted in each of the four passes that the point at which the dumping parameter,  $\phi$ , started to increase sharply was approximately  $65^\circ$  for each pass. (Note also that the dumping parameter,  $\phi$ , well inside the boundary was still approximately equal to although slightly larger than  $10^{-2}$  for these four passes and the response of Detector 5 was probably due in part to trapped particles.)

Previous measurements of the position of the outer zone boundary have attempted to correlate changes in the position with the various magnetic activity parameters [Maehlum and O'Brien, 1963; Williams and Ness, 1966; Williams, 1966; and Rao, 1967]. Williams [1966] found a change  $\Delta \Lambda = 7^\circ$  in a shift of the  $\geq 280$  keV

electron boundary from  $67^\circ$  to  $60^\circ$  associated with the April 18, 1965 magnetic storm which had a maximum Dst depression of  $\approx 140 \gamma$ . Rao [1967] examined the position of the  $\geq 40$  keV electron outer zone boundary for the same April 18, 1965 storm and found there was a "catastrophic" inward movement of the boundary to  $\Lambda = 65^\circ$  and an overall change of  $\Delta \Lambda \leq 8^\circ$  in position associated with the storm.

It is noted from the results of the present study that such a change can occur without an accompanying geomagnetic storm, even during periods of low magnetic activity.

#### B. Periods of Moderate Geomagnetic Activity

There were between fifteen and twenty magnetic events during the lifetime of Injun 3 in which the Kp index was 25 or larger or for which Dst executed a large sudden decrease of  $50 \gamma$  or more (Figure 6). One of the smaller of these events, occurring during the period from April 2, 1963 to April 11, 1963, was examined in detail. The event was reasonably isolated in time being preceded by approximately 20 days of relatively quiet conditions and followed by four relatively quiet days, two of which were designated two of the ten magnetically quiet days in

April. The maximum values of the  $A_p$  index and the  $K_p$  sums index were 32 and 33 respectively, both occurring on April 5, 1963, but Dst reached a maximum depression of only - 27  $\gamma$  (Figure 6).

During this period, data were recorded from Injun 3 by the Woomera, Australia tracking station as the satellite retraced the same trajectory near the midnight meridian through a L, B, MLT coordinate system on each of ten consecutive days. Such a trajectory effectively eliminated all known non-real time variations of the particle intensities at a given invariant latitude for our discussion here.

For this sequence of passes Detector 5 was responding to reflected particles (i.e., particles travelling toward the equatorial plane with a pitch angle at the position of the satellite less than  $43^\circ$ ) and therefore its response will not be presented in detail here. In Figure 13, the first four passes of this sequence are presented. The pass recorded on April 2, 1963, (Rev 1372) before the outset of this event presented a typical undisturbed outer zone profile although there was a small, apparent bifurcation in the outer zone maximum for both  $j_{\perp}$  ( $40 \text{ keV} \leq E_e \leq 50 \text{ keV}$ ) and  $j_{\parallel}$  ( $80 \text{ keV} \leq E_e \leq 100 \text{ keV}$ ). The following day, April 3, before any of the magnetic parameters were indicating

activity, an abbreviated pass (Rev 1384) found the intensities of  $j_{\perp}$  ( $40 \text{ keV} \leq E_e \leq 50 \text{ keV}$ ) and  $j_{\perp}$  ( $80 \text{ keV} \leq E_e \leq 100 \text{ keV}$ ) unchanged for invariant latitudes below  $\Lambda = 55^\circ$ , but decreased by factors of 5 and 10 respectively around  $\Lambda \approx 60^\circ$ . On April 4 (Rev 1397), a large increase in both  $j_{\perp}$  ( $40 \text{ keV} \leq E_e \leq 50 \text{ keV}$ ) and  $j_{\perp}$  ( $80 \text{ keV} \leq E_e \leq 100 \text{ keV}$ ) occurred for latitudes above the region of the slot ( $\Lambda > 57^\circ$ ), while these intensities remained unchanged for  $\Lambda < 57^\circ$ . The increase in the intensities of the  $\approx 40 \text{ keV}$  electrons occurred generally over the entire region from  $57^\circ$  to  $\approx 65^\circ$  with an increase of a factor of 30 occurring at  $\Lambda = 60^\circ$  in the twenty-four period from Rev 1384. The increase in the intensities of the  $\approx 90 \text{ keV}$  electrons was concentrated in a narrow region at  $\Lambda \approx 63^\circ$  with an increase of a factor of 7 occurring at  $\Lambda = 60^\circ$ . For  $\Lambda \geq 66^\circ$  both the SpL and SpH detectors were responding essentially to cosmic ray background only. Coincident with the spike of  $90 \text{ keV}$  electrons at  $\Lambda = 63^\circ$ , the flux of electrons with  $E_e \geq 10 \text{ keV}$  travelling toward the equator at a local pitch angle of  $50^\circ \pm 10^\circ$  reached an intensity of  $3.3 \times 10^7 \text{ electrons/cm}^2 \text{ sec. ster.}$  The satellite altitude at this point was  $2610 \text{ km}$ . If the first adiabatic invariant was conserved for these particles, they had mirrored at  $1200 \pm 200 \text{ km}$ . Making the assumptions described in

Chapter III, the spectral slope at  $\Lambda \approx 63^\circ$  for the energy interval from 10 keV to 40 keV was determined to be  $\gamma = 3.4$  and the comparable slope parameter,  $\gamma$ , for interval from 40 keV to 100 keV was approximately the same (see Figure 13). However, at  $\Lambda = 60^\circ$ ,  $\gamma$  for the interval from 40 keV to 100 keV was  $\gamma = 5.9 \pm 0.4$ , whereas its lower energy counterpart was  $\gamma \leq 2.0$ . This large change in the spectral slope over the interval from 10 keV to 100 keV occurred within a  $\Delta \Lambda$  of  $1.5^\circ$  assuming spatial variations or a time interval of  $\approx 30$  seconds assuming temporal variations.

On the following day, April 5, the  $A_p$  and  $\Sigma K_p$  indices reached their maximum values and the pass on that day (Rev 1409) indicated that the intensities of  $\approx 40$  keV and  $\approx 90$  keV electrons had increased generally for all latitudes above  $\Lambda = 54^\circ$  but the  $\approx 40$  keV electrons had decreased somewhat from  $59^\circ$  to  $64^\circ$ , the position of the large maximum in the previous pass (Rev 1397). The latitude profiles revealed no slot and in fact showed a small maximum in the intensity of  $\approx 40$  keV electrons at  $55^\circ$  to  $60^\circ$ , the usual position of the slot during undisturbed conditions. The maximum intensity of  $\approx 40$  keV electrons was found at  $\Lambda = 67.5^\circ$ , a much higher latitude than the preceding day (Rev 1397). In fact, the counting rate of the SpL detector increased by a factor of

$10^3$  at  $\Lambda = 67.5^\circ$  from Rev 1397 to Rev. 1409. The intensity of  $\approx 90$  keV electrons increased at all latitudes from  $54^\circ$  to  $\approx 67^\circ$  reaching approximately the value of  $j_\perp$  ( $80 \text{ keV} \leq E_e \leq 100 \text{ keV}$ ) at the maximum of the spike observed on Rev 1397. The energy spectrum from 40 keV to 100 keV was much harder for  $\Lambda \leq 65^\circ$  when compared to the undisturbed conditions with an exceptionally hard spectrum being present at  $\Lambda = 63.5^\circ \pm .5^\circ$ . For latitudes greater than  $65^\circ$  the value of  $j_\perp$  ( $40 \text{ keV} \leq E_e \leq 50 \text{ keV}$ ) increased rapidly with increasing latitude while the value of  $j_\perp$  ( $80 \text{ keV} \leq E_e \leq 100 \text{ keV}$ ) decreased. This led to a very rapid softening of the electron energy spectrum from 40 keV to 100 keV with the spectral parameter,  $\gamma$ , reaching a maximum value of  $\gamma = 9.6 \pm 0.8$  at  $\Lambda = 68^\circ$ . The large decrease in the value of the spectral parameter for  $\Lambda > 68^\circ$  was real. The rate of the SpH detector stayed sufficiently above background for  $\Lambda > 68^\circ$ , while the value of  $j_\perp$  ( $40 \text{ keV} \leq E_e \leq 50 \text{ keV}$ ) was decreasing with increasing latitude.

It was not possible to determine the value of  $j$  ( $E_e \geq 10 \text{ keV}$ ) over much of the pass due to light contamination of the response of the electron multiplier. This was one of the two passes noted by Fritz and Gurnett [1965] in their study for which it was

believed that the electron multiplier might be responding to light and to particles simultaneously. The response of the electron multiplier for this pass is presented in Figure 13. The maximum response of the electron multiplier (0.3 c/s) which occurred at  $\Lambda = 65.5^\circ$  was approximately equal to the maximum response to light observed during the satellite's lifetime [see Figure 4 of Fritz and Gurnett (1965)].

The value of the spectral parameter,  $\gamma$ , from 10 keV to 40 keV was  $\gamma = 3.1$  at  $\Lambda = 67.5^\circ$ , the position of the peak for  $j_{\perp}$  ( $40 \text{ keV} \leq E_e \leq 50 \text{ keV}$ ). By neglecting the light contamination entirely the maximum value of  $\gamma$  was less than 4.8 for the interval between 10 keV and 40 keV for the entire pass. It will be noted in Rev 1409 that a very large change in the spectrum between 10 keV and 100 keV occurred from  $63^\circ$  to  $67^\circ$ . The spectral slope from 10 keV to 40 keV remained fairly constant with  $\gamma = 3.5 \pm 1$ , but the slope in the interval from 40 keV to 100 keV steepened greatly changing from  $\gamma = 0.7 \pm 0.3$  at  $\Lambda = 63.5^\circ$  to  $\gamma = 9.6 \pm 0.8$  at  $\Lambda = 68^\circ$ .

In Figure 14, four of the next six passes in this sequence are presented. From the pass taken on April 6 (Rev 1421) it will be noted that the value of  $j_{\perp}$  ( $80 \text{ keV} \leq E_e \leq 100 \text{ keV}$ ) had

continued to increase for  $\Lambda > 58^\circ$  while the value of  $j_{\perp}$  (40 keV  $\leq E_e \leq 50$  keV) remained approximately unchanged, although the small maximum observed for these  $\approx 40$  keV electrons at the position of the slot,  $55^\circ$  to  $60^\circ$  had disappeared. This increase of  $j_{\perp}$  (80 keV  $\leq E_e \leq 100$  keV) for  $\Lambda > 58^\circ$  caused the spectrum between 40 keV and 100 keV to harden. On this pass the spectral parameter,  $\gamma$ , was observed to decrease with increasing latitude for  $\Lambda > 55^\circ$ , just the opposite of the usual undisturbed dependence of  $\gamma$  on  $\Lambda$ . An abbreviated pass (Rev 1434, not shown) was recorded on the following day, April 7. This pass reached  $\Lambda = 60^\circ$  and found a very hard spectrum there ( $\gamma = 0.7 \pm 0.3$ ) and a decay of both  $j_{\perp}$  (40 keV  $\leq E_e \leq 50$  keV) and  $j_{\perp}$  (80 keV  $\leq E_e \leq 100$  keV) for  $\Lambda \geq 54^\circ$  from the preceding pass (Rev 1421).

On April 8, the values of the  $A_p$  and  $\Sigma K_p$  indices were indicating near quiet conditions and recovery of the small Dst depression was essentially complete. The pass taken on this day (Rev 1446 in Figure 14) exhibited most of the characteristics of an undisturbed pass discussed in Chapter IV. The value of  $j_{\perp}$  (40 keV  $\leq E_e \leq 50$  keV) at all latitudes was unchanged or slightly increased from the preceding pass, while the value of  $j_{\perp}$  (80 keV  $\leq E_e \leq 100$  keV) indicated a continuing decay for  $\Lambda > 57^\circ$  with the decay occurring more rapidly at  $\Lambda = 60^\circ$  than at  $\Lambda = 65^\circ$ .



On the following day, the next pass in the sequence (Rev 1459) indicated very disturbed conditions. The intensities of  $\approx 40$  keV electrons were increased at all latitudes above  $63^\circ$  and decreased slightly for latitudes from  $57^\circ$  to  $62^\circ$ . The increases of  $j_\perp$  ( $40 \text{ keV} \leq E_e \leq 50 \text{ keV}$ ) for  $\Lambda > 68^\circ$  were by factors of 10 to  $10^3$  over the values of the preceding pass (Rev 1446). In general  $j_\perp$  ( $80 \text{ keV} \leq E_e \leq 100 \text{ keV}$ ) continued to decrease at all latitudes except  $\Lambda \approx 69^\circ$  where an increase of a factor of 10 from background occurred coincident with the peaks of  $j_\perp$  ( $40 \text{ keV} \leq E_e \leq 50 \text{ keV}$ ),  $j_\perp$  ( $E_e \geq 40 \text{ keV}$ ), and  $j$  ( $E_e \geq 40 \text{ keV}$ ) reflected. The ratio of  $j$  ( $E_e \geq 40 \text{ keV}$ ) reflected to  $j_\perp$  ( $E_e \geq 40 \text{ keV}$ ) was  $\approx 0.3$  at  $\Lambda = 69^\circ$  indicating that a very intense precipitation event was occurring. The spectral parameter,  $\gamma$ , increased sharply with latitude for  $\Lambda > 65^\circ$  and reached a maximum value of  $\gamma = 9.2 \pm 0.6$  at  $\Lambda \approx 70^\circ$ . The spectrum from 40 keV to 100 keV was actually slightly harder during the peak intensities of  $\approx 40$  keV and  $\approx 90$  keV electrons which occurred at  $\Lambda \approx 69^\circ$  than it was at adjacent latitudes.

It will be noted that the characteristics of Rev 1459 were very similar to those discussed previously for Rev 243 (Figure 8), Rev 255 (Figure 10), and Rev 2378 (Figure 12). The interpretation

presented here is that the activity observed on Rev 1459 was of the type previously discussed and was not necessarily associated with the magnetic disturbances which are being examined. Since the values of  $j_{\perp}$  ( $80 \text{ keV} \leq E_e \leq 100 \text{ keV}$ ) could be compared directly in this sequence of passes, it was possible to make an estimate of the ratio of the number of electrons from 40 keV to 50 keV present in the precipitation event to the number of electrons with energies from 80 keV to 100 keV present. This estimate indicated that the higher energy electrons constituted no more than 1 part in  $2 \times 10^3$  of the precipitating electrons. (The assumption that the instantaneous electron energy spectrum is not a function of the electron pitch angle is made.)

On the following day, data were recorded on the next pass in the sequence (Rev 1470 - not shown) up to  $\Lambda \approx 64^\circ$ . The values of  $j_{\perp}$  ( $80 \text{ keV} \leq E_e \leq 100 \text{ keV}$ ) for  $\Lambda > 57^\circ$  were slightly smaller than those of Rev 1459, but the large increase of  $j_{\perp}$  ( $40 \text{ keV} \leq E_e \leq 50 \text{ keV}$ ) observed on Rev 1459 was no longer evident in Rev 1470.

The last pass in this sequence, Rev 1483 (Figure 14), exhibited all of the quiet time characteristics discussed in Chapter IV. The values of  $j_{\perp}$  ( $40 \text{ keV} \leq E_e \leq 50 \text{ keV}$ ) and

$j_{\perp}$  ( $80 \text{ keV} \leq E_e \leq 100 \text{ keV}$ ) decreased from  $\Lambda = 45^\circ$  to  $\Lambda \approx 59^\circ$  then increased to a maximum at  $\Lambda \approx 65^\circ$  and fell off rapidly at the high latitude boundary. The position of the slot was well determined for  $j_{\perp}$  ( $80 \text{ keV} \leq E_e \leq 100 \text{ keV}$ ) but fairly broad for  $j_{\perp}$  ( $40 \text{ keV} \leq E_e \leq 50 \text{ keV}$ ). This led to a prominent increase in spectral parameter,  $\gamma$ , around  $58^\circ$  to  $59^\circ$ , but in general the spectrum softened with increasing latitude.

The variations of  $j_{\perp}$  ( $40 \text{ keV} \leq E_e \leq 50 \text{ keV}$ ),  $j_{\perp}$  ( $80 \text{ keV} \leq E_e \leq 100 \text{ keV}$ ), and the spectral parameter,  $\gamma$ , as a function of time during this period at five different latitudes are summarized in Figure 15.

At  $\Lambda = 50^\circ$  and lower latitudes, the values of  $j_{\perp}$  ( $40 \text{ keV} \leq E_e \leq 50 \text{ keV}$ ),  $j_{\perp}$  ( $80 \text{ keV} \leq E_e \leq 100 \text{ keV}$ ) and the spectral parameter remained unchanged throughout the ten day period. For  $\Lambda = 55^\circ$ , the values of  $j_{\perp}$  ( $40 \text{ keV} \leq E_e \leq 50 \text{ keV}$ ) and  $j_{\perp}$  ( $80 \text{ keV} \leq E_e \leq 100 \text{ keV}$ ) each generally increased over the period by approximately a factor of four. The spectral parameter variations indicated that the increase of  $j_{\perp}$  ( $40 \text{ keV} \leq E_e \leq 50 \text{ keV}$ ) occurred at the beginning of the event with the increase of  $j_{\perp}$  ( $80 \text{ keV} \leq E_e \leq 100 \text{ keV}$ ) occurring after the event was well under way. This gave rise to an initial increase in the spectral parameter from  $\gamma \approx 2.4$  to  $\gamma \approx 3.2$  as the  $A_p$  index increased,

followed by a decrease to  $\gamma \approx 2.0$  as  $A_p$  reached its maximum value and began to decrease.

For  $\Lambda > 57^\circ$ , temporal variations of the electron intensities and spectrum became much larger. At  $\Lambda = 60^\circ$ , the values of both  $j_{\perp}$  ( $40 \text{ keV} \leq E_e \leq 50 \text{ keV}$ ) and  $j_{\perp}$  ( $80 \text{ keV} \leq E_e \leq 100 \text{ keV}$ ) decreased abruptly before the magnetic disturbance parameters,  $A_p$ ,  $K_p$ , or Dst, were indicating any increase in activity. The initial decrease of  $j_{\perp}$  ( $80 \text{ keV} \leq E_e \leq 100 \text{ keV}$ ) was larger than the accompanying decrease in  $j_{\perp}$  ( $40 \text{ keV} \leq E_e \leq 50 \text{ keV}$ ) resulting in an increase in the value of the spectral parameter,  $\gamma$ . Following the initial decrease in the intensities, an indication of increased magnetic activity by the magnetic parameters was accompanied by a marked increase in both  $j_{\perp}$  ( $40 \text{ keV} \leq E_e \leq 50 \text{ keV}$ ) and  $j_{\perp}$  ( $80 \text{ keV} \leq E_e \leq 100 \text{ keV}$ ). The increase of the flux of the lower energy electrons was larger than the accompanying increase in the flux of higher energy electrons and this resulted in a further softening of the energy spectrum and a continued marked increase of the spectral parameter,  $\gamma$ .

The value of  $j_{\perp}$  ( $80 \text{ keV} \leq E_e \leq 100 \text{ keV}$ ) continued to increase with time in an exponential manner for approximately 3 days reaching a maximum the day after the magnetic parameters

reached their maximum values." However, the value of  $j_{\perp}$  ( $40 \text{ keV} \leq E_e \leq 50 \text{ keV}$ ), after reaching a maximum value the day before the magnetic parameters reached their maximum values, decreased with time while  $j_{\perp}$  ( $80 \text{ keV} \leq E_e \leq 100 \text{ keV}$ ) was still increasing. This resulted in a large decrease in the spectral parameter,  $\gamma$ , from a value of  $\gamma = 5.9 \pm 0.4$  to a value of  $\gamma = 0.7 \pm 0.3$  in two to three days. After the value of  $j_{\perp}$  ( $80 \text{ keV} \leq E_e \leq 100 \text{ keV}$ ) reached a maximum, the intensity of these higher energy electrons decayed in an exponential manner for about 4 days reaching a value at the end of the disturbance which was approximately a factor of six below their prestorm intensity. The intensity of the  $\approx 40 \text{ keV}$  electrons decreased steadily but not in an exponential manner, reaching a value at the end of the disturbance that was approximately a factor of three below the prestorm intensity.

After the initial decrease observed at  $\Lambda = 60^\circ$ , the value of  $j_{\perp}$  ( $80 \text{ keV} \leq E_e \leq 100 \text{ keV}$ ) was observed to first increase and then decrease in an exponential manner during the event. It was not possible to determine whether the value of  $j_{\perp}$  ( $40 \text{ keV} \leq E_e \leq 50 \text{ keV}$ ) increased in an exponential manner after the initial decrease but it was obvious that it did not exhibit an exponential decay during the recovery period.

The temporal variations of  $j_{\perp}$  ( $40 \text{ keV} \leq E_e \leq 50 \text{ keV}$ ),  $j_{\perp}$  ( $80 \text{ keV} \leq E_e \leq 100 \text{ keV}$ ), and the spectral parameter,  $\gamma$ , for  $\Lambda = 65^\circ$  and  $\Lambda = 68^\circ$  are also presented in Figure 15 for this period. It will be observed that the variations discussed for  $\Lambda = 60^\circ$  were also present in the same form at  $\Lambda = 65^\circ$  and possibly at  $\Lambda = 68^\circ$ . The exponential increase and decrease of  $j_{\perp}$  ( $80 \text{ keV} \leq E_e \leq 100 \text{ keV}$ ) can be observed at  $\Lambda = 65^\circ$  but due to many missing points, it was possible to infer only an apparent exponential decrease in  $j_{\perp}$  ( $80 \text{ keV} \leq E_e \leq 100 \text{ keV}$ ) at  $\Lambda = 68^\circ$ . The initial decrease and then increase of  $j_{\perp}$  ( $40 \text{ keV} \leq E_e \leq 50 \text{ keV}$ ) was present at  $\Lambda = 65^\circ$  and probably at  $\Lambda = 68^\circ$  since a value for  $j_{\perp}$  ( $40 \text{ keV} \leq E_e \leq 50 \text{ keV}$ ) =  $3 \times 10^4$  electrons/cm<sup>2</sup> sec. ster. was found at  $\Lambda \approx 67^\circ$  on the quiet time prestorm pass, Rev 1372 (Figure 13). The variations of  $j_{\perp}$  ( $40 \text{ keV} \leq E_e \leq 50 \text{ keV}$ ) for  $\Lambda \geq 60^\circ$  during the recovery portion of the event exhibited little association with changes in the magnetic activity parameters used in the present discussion.

In summary, during this moderately active period, the region  $\Lambda < 55^\circ$  appeared to be unaffected by magnetic activity occurring whereas the region  $\Lambda > 55^\circ$  exhibited marked temporal variations which were usually associated with the degree of

magnetic activity. For  $\Lambda > 55^\circ$  both  $j_\perp$  ( $40 \text{ keV} \leq E_e \leq 50 \text{ keV}$ ) and  $j_\perp$  ( $80 \text{ keV} \leq E_e \leq 100 \text{ keV}$ ) decreased sharply with the spectral parameter increasing prior to any disturbance being evident in the magnetic records. After the decrease, both  $j_\perp$  ( $40 \text{ keV} \leq E_e \leq 50 \text{ keV}$ ) and  $j_\perp$  ( $80 \text{ keV} \leq E_e \leq 100 \text{ keV}$ ) increased, the latter in an exponential manner, with the spectral parameter continuing to increase. The value of  $j_\perp$  ( $40 \text{ keV} \leq E_e \leq 50 \text{ keV}$ ) reached a maximum before  $j_\perp$  ( $80 \text{ keV} \leq E_e \leq 100 \text{ keV}$ ) and began to decrease while the value of  $j_\perp$  ( $80 \text{ keV} \leq E_e \leq 100 \text{ keV}$ ) was still increasing. This resulted in the value of the spectral parameter decreasing rapidly. After the value of  $j_\perp$  ( $80 \text{ keV} \leq E_e \leq 100 \text{ keV}$ ) reached a maximum, it began to decay in an exponential manner with the spectral parameter again increasing. The exponential time constants for the increases and decreases of  $j_\perp$  ( $80 \text{ keV} \leq E_e \leq 100 \text{ keV}$ ) were somewhat dependent on the latitude. The time constants for this event were

	$\frac{dj_\perp(\text{SpH})}{dt} > 0$	$\frac{dj_\perp(\text{SpH})}{dt} < 0$
	-----	-----
$\Lambda = 60^\circ$	0.75 days	1.35 days
$\Lambda = 65^\circ$	0.65 days	2.2 days
$\Lambda = 68^\circ$	undetermined	2.4 days

These results are in reasonably good agreement with the results of Craven [1966] who found values of the time constant from 2 to 6.5 days for the decay portion of the variation of  $j_{\perp}$  ( $E_e > 40$  keV) for  $3.5 \leq L \leq 6.0$  during four periods of magnetic activity recorded in the Injun 3 data.

### C. Periods of Large Geomagnetic Activity

In the preceding two sections, it has been demonstrated that large amounts of  $\geq 40$  keV electron precipitation, changes in the position of the high latitude  $\geq 40$  keV electron outer zone boundary, and large changes in the electron energy spectrum between 10 keV and 100 keV occur during periods of low and moderate geomagnetic activity.

Craven [1966] examined the variations of the values of  $j_{\perp}$  ( $E_e \geq 40$  keV),  $j_{\perp}$  ( $E_e \geq 230$  keV), and  $J$  ( $E_e \geq 1.6$  MeV) as a function of time during the larger geomagnetic disturbances. His results indicated that the variation of  $j_{\perp}$  ( $40 \text{ keV} \leq E_e \leq 50 \text{ keV}$ ) and  $j_{\perp}$  ( $80 \text{ keV} \leq E_e \leq 100 \text{ keV}$ ) discussed in the previous section for moderate activity will be larger but of the same nature for the larger magnetic disturbances. Therefore, in this section of the present paper, we will be mainly interested in the variations of  $j$  ( $E_e \geq 10$  keV),  $j_{\perp}$  ( $E_e \geq 40$  keV), and  $j$  ( $E_e \geq 40$  keV)



dumped during periods when the various magnetic parameters were indicating the very disturbed conditions. It was found by Fritz and Gurnett [1965] that on approximately 84 passes recorded by Injun 3 during these periods of large magnetic activity, the value of  $j$  ( $E_e \geq 10$  keV) exceeded  $2.5 \times 10^7$  electrons/cm<sup>2</sup> sec. ster. (e.g., Rev 1397 - Figure 13). It was also reported by Fritz and Gurnett that these intense fluxes of 10 keV electrons occurred only between 1700 hours and 0700 hours MLT and were confined in latitude between 58° and 76°. The present section will be concerned mainly with a discussion of the characteristics of these events.

Due to the nature of these events, each occurrence of  $j$  ( $E_e \geq 10$  keV)  $\geq 2.5 \times 10^7$  electrons/cm<sup>2</sup> sec. ster. was a distinct and individual event with little in common with the other events except the restrictions in magnetic local time and invariant latitude. In Figure 16, an example of such an event is presented. This pass was taken near the midnight meridian on June 20, 1963. On this day, the  $\Sigma K_p$  index was 27 (Figure 6) and a large negative bay was being recorded by the College, Alaska magnetometer. It will be noted from Rev 2354 in Figure 16 that the  $\geq 10$  keV electrons appeared near or just inside the high

latitude  $\geq 40$  keV electron outer zone boundary. The lower latitude edge of the region for which the intense flux of  $\geq 10$  keV electrons was observed was marked by a sharp increase in both the value of  $j_{\perp} (E_e \geq 40 \text{ keV})$  and  $j (E_e \geq 40 \text{ keV})$  dumped. From that point the dumping parameter,  $\phi$ , increased with latitude reaching the value of 1 at the high latitude  $\geq 40$  keV electron boundary.

These two properties, (1) the presence of the intense fluxes of  $\geq 10$  keV electrons near and inside rather than outside the  $\geq 40$  keV boundary, and (2) the condition of isotropy or near isotropy for  $\geq 40$  keV electrons over the upper hemisphere at the position of the satellite were the most frequently observed features of these events.

In the example of Figure 16 (Rev 2354) the spectrum between 10 keV and 40 keV was not greatly different from the usual value of  $\gamma$  determined for the interval from 40 keV to 100 keV. The spectral parameter,  $\gamma$ , for the interval from 10 keV to 40 keV ranged from a value of  $\gamma = 2.4$  at  $\Lambda = 62^\circ$  to  $\gamma = 3.8$  at  $\Lambda = 64.6^\circ$ .

Another feature which was characteristic of these events was that values of  $j (E_e \geq 10 \text{ keV}) \geq 2.5 \times 10^7$  electrons/cm<sup>2</sup> sec. were seldom observed on two successive passes and were never observed to occur on three passes in succession through

the same region. To illustrate this feature, the pass preceding Rev 2354 of Figure 16 and the three succeeding passes recorded by Injun 3 in passing through this region of the outer zone near the midnight meridian are presented in Figure 17. In Rev 2353 of Figure 17, it will be noted that there was a large  $\geq 40$  keV electron precipitation event occurring on the outer zone boundary, but the value of  $j$  ( $E_e \geq 10$  keV) never exceeded  $2.0 \times 10^7$  electrons/cm<sup>2</sup> sec. ster. The maximum value of the spectral slope parameter,  $\gamma$ , between 10 keV and 40 keV was  $\gamma = 3.1$  at  $\Lambda \approx 63^\circ$ . The next pass through this region taken approximately two hours later was Rev 2354 (Figure 16) on which the intensity of  $\geq 10$  keV electrons exceeded  $2.5 \times 10^7$  electrons/cm<sup>2</sup> sec. ster. and this pass was considered as an event in the study of Fritz and Gurnett [1965]. During the following pass, Rev 2355 (Figure 17),  $j$  ( $E_e > 10$  keV) again exceeded  $2.5 \times 10^7$  electrons/cm<sup>2</sup> sec. ster. and was also considered in the study by Fritz and Gurnett. It will be noted that the general features described for Rev 2354 were also present in Rev 2355. The position of the intense flux  $\geq 10$  keV electrons was just inside or on the boundary and a sharp increase in both  $j_{\perp}$  ( $E_e \geq 40$  keV) and  $j$  ( $E_e \geq 40$  keV) dumped occurred at the same time that  $j$  ( $E_e \geq 10$  keV) was

observed to increase. Again the dumping parameter increased strongly and reached the value of 1 at and beyond the boundary. In the next two passes, Rev 2356 and Rev 2357 (Figure 17) through this region, the values of  $j$  ( $E_e \geq 10$  keV) remained less than  $1.3 \times 10^7$  electrons/cm<sup>2</sup> sec. ster. throughout both passes, although the value of  $j_{\perp}$  ( $E_e \geq 40$  keV) was equal to or greater than the corresponding values for the two passes, Rev 2354 and Rev 2355. This sequence of passes, Rev 2353-2357, has illustrated that these intense  $\geq 10$  keV electron precipitation events rarely occurred on successive passes. The pair of passes, Rev 2354-2355, was one of fourteen sets of passes found where the value of  $j$  ( $E_e \geq 10$  keV) exceeded  $2.5 \times 10^7$  electrons/cm<sup>2</sup> sec. ster. on successive passes. This condition was never satisfied on three successive passes. The next pass after the sequence presented in Figures 16 and 17 for which  $j$  ( $E_e \geq 10$  keV) exceeded  $2.5 \times 10^7$  electrons/cm<sup>2</sup> sec. ster. occurred approximately one day after Rev 2354-2355. This pass, Rev 2367, is presented in Figure 18 and as will be noted, it had few similarities to the passes, Rev 2354 and Rev 2355.

Now that the characteristics which these events appeared to have in common have been discussed, some of the more noteworthy differences will be discussed.

In Figure 18 and 19 selected examples of these intense  $\geq 10$  keV electron precipitation events are presented. It will be noted that each event was unique and individual. The highest latitude for which any multiplier particle response was observed was  $\Lambda \approx 77^\circ$  (e.g., Rev 2367, Figure 18) and the lowest was  $\Lambda \approx 56^\circ$  (e.g., Rev 3116, Figure 19). The region over which the precipitation was observed could be narrow and confined in latitude (e.g., Rev 2425, Figure 18 and Rev 2603, Figure 19), it could cover a wide range of latitudes (e.g., Rev 2579, Figure 18) or it could be separated into two distinct ranges of latitude (e.g., Rev 2205, Figure 18 and Rev 3451, Figure 19). The electron energy spectrum between 10 keV and 40 keV recorded during these events was quite variable. In Rev 3116 (Figure 19), it can be seen that  $j_{\perp}(E_e \geq 40 \text{ keV}) \approx j_{\alpha=50^\circ}(E_e \geq 10 \text{ keV}) = 1.6 \times 10^7$  electrons/cm<sup>2</sup> sec. ster. at  $\Lambda \approx 57^\circ$ . This would indicate a negative differential energy spectral slope between 10 keV and 40 keV, but due to the large dead time corrections made in the response of Detector 1 for this pass, the above statement should be interpreted to indicate only that the spectrum was very hard ( $\gamma < 1.0$ ) but not necessarily rising toward the higher energies. Another example of a hard spectrum was found on Rev 2579 (Figure 18)

where the spectral parameter,  $\gamma$ , between 10 keV and 40 keV at  $\Lambda = 64.0^\circ$  had a value equal to 1.8. The spectrum was also found to be very soft during some events. In Rev 2367 the spectral parameter,  $\gamma$ , was  $\gamma = 6.2$  at  $76.0^\circ$  and in Rev 2829 (Figure 19) a value of  $\gamma = 6.3$  was found at  $\Lambda = 73.8^\circ$ .

Even with the individual characteristics of each of the events presented in Figures 18 and 19, it will be noted that the intense fluxes of  $\geq 10$  keV electrons were usually associated with the high latitude outer zone  $\geq 40$  keV electron boundary, appearing either on or just inside this boundary. This was not always true. In nine or ten of the events, ( $\approx 12\%$  of the samples) these intense fluxes of  $\geq 10$  keV electrons were observed to occur outside the position of the  $\geq 40$  keV electron high latitude boundary (e.g., Rev 2829 in Figure 19). The two events published by Fritz and Gurnett [1965] (see their Figures 9 and 10) were of this type (Rev 2479 on June 30, 1963, and Rev 2981 on August 9, 1963). These events usually were associated with the declining phases of a magnetic disturbance. This is illustrated in Figure 6 for Rev 2479, Rev 2829, and Rev 2981. Another type of event in which the intense fluxes of  $\geq 10$  keV electrons might be considered to be outside the  $\geq 40$  keV electron high latitude

boundary was illustrated by Rev 2205 (Figure 18). In this pass the satellite appeared to cross the  $\geq 40$  keV electron outer zone boundary at  $\Lambda = 65^\circ$ , then experience a large precipitation event from  $\Lambda \approx 67^\circ$  to  $\Lambda \approx 75^\circ$  in which intense fluxes of  $\geq 10$  keV electrons were observed. However, an alternate interpretation to the latitude profile of Rev 2205 would be that the  $\geq 40$  keV high latitude boundary was crossed only at  $\Lambda \approx 75^\circ$  and the intensity variations observed as a function of latitude were of a temporal nature.

In general, it will be noted that the fluxes of  $> 40$  keV electrons were either approaching isotropy or had attained isotropy over the upper hemisphere at the position of the satellite during these intense  $\geq 10$  keV electron precipitation events. A large portion of the  $\geq 40$  keV electron flux observed in these passes could not have been durably trapped since it would have been lost in the atmosphere before being reflected. Therefore, for these events the concept of a high latitude "trapping" boundary for  $\geq 40$  keV electrons and the connection of the intense fluxes of  $\geq 10$  keV electrons to this boundary lose significance.

In Figure 20, a pass recorded by the Woomera, Australia tracking station is presented. On this pass (Rev 3999) Detector 5

was responding to upward moving particles since its viewing cone "looked" toward the atmosphere in the southern hemisphere. The electron multiplier was also responding to particles which were travelling toward the equatorial plane with a pitch angle at the position of the satellite of  $50^\circ \pm 10^\circ$ . If these intense fluxes of  $> 10$  keV electrons were produced by some mechanism acting below the satellite and then moved in a manner conserving the first adiabatic invariant [Van Allen, 1962], the flux measured by Detector 1 would have been less than the flux measured by Detector 5 because the pitch angle,  $\alpha = 90^\circ$ , could not be obtained by a particle present at a B-value which was larger than the value of B at the position of the satellite. Since the flux measured by Detector 5 was approximately a factor of 10 less than the flux measured by Detector 1 the interpretation is that a large flux of possibly isotropic electrons was incident from above the satellite and the response of Detector 5 was due to electrons which mirrored above the atmosphere or were back-scattered. The altitude of the satellite during this event was 2350 km. The intense flux of  $\geq 10$  keV electrons measured by the electron multiplier mirrored at approximately 1000 km. It is



argued, therefore, that the source of these particles must be well above the region of the satellite (2500 km). This inference will prove to be of importance in subsequent discussion.

## VI. THE "AVERAGE" OUTER ZONE

The discussions and findings of the previous two chapters have been based on the observations of individual passes through the region of the outer zone. In an attempt to summarize these observations for the entire body of Injun 3 data, statistical studies were made on the spectral, spatial, and temporal variations of the outer zone electron fluxes. Two groups of data were selected. The first group was concerned with properties of the outer zone trapping region and the second group was associated only with intense auroral zone particle activity.

### A. Statistical Study of the Outer Zone Trapping Region

Previous statistical studies on the variations of the  $> 40$  keV trapped electron intensities and  $> 40$  keV precipitated electron intensities individually as a function of latitude and local time for the Injun 3 data have been presented by Frank, Van Allen, and Craven [1964] and Armstrong [1965a]. The results of these studies have been noted in Chapters IV and V. Temporal variations of trapped outer zone electrons observed by Injun 3 have been studied by Craven [1966] in connection with large magnetic disturbances.

In the present study, the electron energy spectral variations observed in Chapters IV and V were investigated along with variations in the degree of precipitation of  $> 40$  keV electrons taking place at the position of the satellite.

Due to the uncertainties in the response of the SpH detector after May 1963, the data from Injun 3 for the period from January to May 1963 only, were used in the present statistical study. Data were selected when the satellite was at a position of integral or half integral values of  $L$  in the outer trapping zone ( $2 \leq L \leq 8$ ). Due to a lack of sufficient counting statistics on a frame-by-frame (one-fourth second) basis, the data were summed over eight second intervals containing the appropriate integral or half-integral  $L$ -value. During such an interval each detector on the satellite used in the present study (with the exception of the  $3914 \text{ \AA}$  auroral photometer) was sampled thirty-two times. In order to eliminate errors due to telemetry noise, an error and noise correction computer program was worked out by Armstrong, Halliday, and Fritz [Fritz, 1964]. The computer criteria closely approximated the criteria used for eliminating questionable data points by direct inspection of the complete body of data in their raw form. In the preparation of the eight second sums, this program was applied to all data.

At each position of integral and half-integral values of  $L$ , the spectral parameter,  $\gamma$ , determined from the rates of the differential spectrometer channels, the flux of electrons with energies greater than 40 keV trapped and precipitated at the position of the satellite, and the dumping parameter,  $\phi$ , were calculated from the error corrected data provided the following statistical restrictions were satisfied.

The true response,  $R_i$ , for the two spectrometer channels, SpL and SpH, was determined by taking the observed response,  $r_i$ , and correcting it for background due to penetrating radiation in the following manner:

$$R_i = r_i - \frac{G_i}{G_{\text{SpB}}} r_{\text{SpB}}$$

The statistical restrictions used in the calculation of the spectral parameter,  $\gamma$ , were such that the detector responses,  $R_i$ , for both detectors had to be equal to or greater than 4.0 counts per eight second sum interval. Assuming that  $R_{\text{SpL}}$  and  $R_{\text{SpH}}$  could be approximated as Poissonian variables, the greatest statistical error in  $\gamma$  was  $\Delta\gamma = \pm 0.7$  (corresponding to the minimum acceptable value of  $R_i$ ).

The above restrictions on  $R_{SpL}$  automatically placed an upper limit on the statistical uncertainty in the dumping parameter,  $\varphi$ . This can be seen in the following manner.

$$\frac{R_{SpL}}{g_{SpL}} = j(40 \text{ keV} \leq E_e \leq 50 \text{ keV}) \leq j(E_e \geq 40 \text{ keV}) = \frac{R_{Det.1}}{g_{Det.1}}$$

so

$$\begin{aligned} R_{Det.1} &\geq \frac{R_{SpL}}{g_{SpL}} g_{Det.1} \\ &\geq \frac{(4.0)(0.65 \times 10^{-2})}{(1.6 \times 10^{-4})} = 160 \text{ counts} \end{aligned}$$

Therefore, since  $\varphi = j(\text{Det.5})/j(\text{Det.1})$ , the greatest statistical error in  $\varphi$  (for  $\varphi > 10^{-3}$ ) was approximately ten percent ( $\Delta \varphi / \varphi \approx .1$ ).

In this manner 1840 records, approximately equally divided among the various L-values, were calculated for this study. Each L value had at least 100 calculated points. To each of these points the following quantities were affixed: real time,

$L$ ,  $B$ , local time,  $K_p$ ,  $A_p$ , and the daily  $K_p$  sum. These points were then sorted as a function of the various parameters, first for the spectral parameter,  $\gamma$ , and then for the dumping parameter,  $\phi$ . The variation of  $\gamma$  and  $\phi$  as a function of these parameters is now presented, but a word of caution is introduced here. In the following sections a single parameter study of a multi-parameter problem has been performed on the assumption that there was little coupling between the various parameters. This assumption was not strictly valid, but from the observations of the individual passes presented in Chapters IV and V certain restrictions on the data were introduced which justified the use of this statistical approach. The appropriate restrictions are discussed in each of the following sections. At the end of this chapter a discussion of the observed variations of  $\gamma$  and  $\phi$  as a result of a coupling of the various parameters is given.

#### 1. The Spectral Parameter, $\gamma$ , vs $L$

For the data in each group of integral and half-integral values of  $L$ , the mean and median values of  $\gamma$  were calculated along with the standard deviations, and these are presented in Figure 21 along with a scatter plot of the data.

It is seen that both the mean and median values of  $\gamma$  increased from  $\bar{\gamma} = 1.06$  at  $L = 2.0$  to  $\bar{\gamma} = 2.46$  at  $L = 3.5$  after which these values fell to a minimum around  $L = 4.5$  and then increased slowly with increasing  $L$  to  $\bar{\gamma} = 3.13$  at  $L = 8.0$ . From the scatter plot, it is noted that large variations of  $\gamma$  occurred at a given  $L$ -value. Therefore, the variation of the mean and median values of  $\gamma$  can be interpreted to indicate that on the average the spectrum between 40 keV and 100 keV softened with increasing  $L$  in general but that it was significantly softer at  $L = 3.5$  than at adjacent  $L$  values. These variations are generally the same as those found for selected passes (Chapter IV).

It is also noted in Figure 21 that the standard deviation of the individual observations for each  $L$ -value increased with increasing  $L$  indicating that the spectrum varied less at the lower  $L$ -values than at the higher  $L$ -values (cf., Figures 11 and 15). This result is in agreement with the findings of O'Brien, Laughlin, Van Allen, and Frank [1962] and those of Craven [1966]. The latter author found that the intensities of  $> 40$  keV electrons and  $> 250$  keV electrons at the lower  $L$ -values are rarely affected during geomagnetic storms, whereas the fluxes of these electrons undergo large variations at the large  $L$ -values.

McDiarmid, Burrows, Budzinski, and Wilson [1963] using Geiger tubes sensitive to electrons with energy greater than 40 keV and greater than 250 keV on the Alouette I satellite made an electron energy spectral survey as a function of latitude using a spectral parameter similar to  $\gamma$ . Their study was for electrons which were mirroring at the position of the satellite during periods when  $K_p \leq 4$  between October 1962 and January 1963. They found that on the average their spectral parameter went through a maximum at  $\Lambda = 51^\circ$  ( $L \approx 3$ ) and then through a minimum at  $\Lambda = 59^\circ$  ( $L \approx 4.0$ ). At latitudes above  $59^\circ$ , they found that the spectrum became progressively softer and more variable. These results are consistent with those of the present paper, and also indicate that the position of the "slot" for 40 keV, 100 keV, and 250 keV electrons is different for different energies, being on the average at slightly higher L-values for the lower energy electrons. Mihalov and White [1966] found that the lower energy quiet time outer zone electrons in the range from 170 keV to 4.5 MeV peak at higher L values.

It is noted here that the values for the spectral parameter as a function of L ( $\bar{\gamma} = 2.1 \pm 1.0$ ) are in reasonably



good agreement with the previous spectral measurements of the electron energy spectrum in the range covering the interval from 40 keV to 100 keV at low satellite altitudes reported in the literature [Cladis, Chase, Imhof, and Knecht, 1961; O'Brien, Laughlin, Van Allen, and Frank, 1962; McDiarmid, Burrows, Budzinski, and Wilson, 1963; and Mihalov and White, 1966].

## 2. The Spectral Parameter, $\gamma$ , vs B

Because the orbit of Injun 3 was restricted to low altitudes, the range of the geomagnetic field intensity B was relatively limited ( $0.20 \text{ gauss} \leq B \leq 0.55 \text{ gauss}$ ). This range of B was divided into eight intervals and the mean value of  $\gamma$  was calculated for each interval of B ( $\Delta B = 0.05 \text{ gauss}$ ) for each interval of integral and half integral values of L. Each of these L intervals was examined individually.

For  $L = 2.0$  and  $L = 2.5$ , there was no noticeable dependence on B. With only one exception in the fourteen mean values calculated for these two L interval, the mean values for each B interval were within two standard deviations of the mean values given in Figure 21 for the respective L values. This constancy can be observed in Figures 11 and 15 for  $\Lambda = 50^\circ$  ( $L = 2.4$ ).

The spectral parameter,  $\gamma$ , in the region  $3.0 \leq L \leq 3.5$ , decreased markedly with increasing B (Figure 22). For the region  $L \geq 5.0$ , the mean values of the spectral parameter increased only slightly (indicating a softer spectrum) with increasing B. In the region  $4.0 \leq L \leq 4.5$ , the variations in the mean values of  $\gamma$  were large but appeared to exhibit no dependence on B.

The variations of the individual observations with B for the two regions,  $3.0 \leq L \leq 3.5$  and  $5.0 \leq L \leq 8.0$ , are presented in Figure 22. In order that points in the different L intervals could be plotted together, the mean values of  $\gamma$  as a function of L presented in Figure 21 were set equal to  $\bar{\gamma} = 2.0$  by subtracting the difference,  $\bar{\gamma} - 2.0$ , from each point in a given L interval. This eliminated the scatter in the data which resulted from the dependence of  $\gamma$  on L. The spectral dependence on B noted above for the two L regions is evident in Figure 22. There was a large amount of scatter in both regions. This scatter is evident in Figure 11 and 15 where the variations in the region  $5.0 \leq L \leq 8.0$  appeared to be associated with the degree of magnetic activity occurring but the variations in the region  $3.0 \leq L \leq 3.5$  were confusing.

From the fact that there was no apparent dependence of  $\gamma$  on  $B$  for  $L = 2.0$  and  $2.5$ , we can infer something about the variation of the spectrum in the geomagnetic equatorial plane as a function of the particle's pitch angle for these two  $L$  values. From the first adiabatic invariant, the Alfven magnetic moment, it can be shown that

$$\sin^2 \alpha_o = \frac{B_o}{B_m}$$

where  $B_m$  is the magnitude of the geomagnetic field at the position of the satellite (the particle's mirror point),  $B_o$  is the magnitude of the geomagnetic field for the same  $L$  shell at the equatorial plane, and  $\alpha_o$  is the particle's pitch angle at the equatorial plane. The spectrum was constant to a first approximation for  $18^\circ < \alpha_o < 35^\circ$  for  $L = 2.0$  and  $12^\circ < \alpha_o < 25^\circ$  for  $L = 2.5$ . Cladis, Chase, Imhof, and Knecht [1961], using a four channel rocket-borne magnetic spectrometer which reached an altitude of 1045 km along the magnetic shell  $L = 2.4$ , found that the differential electron spectrum ( $E_e \geq 50$  keV) was not a function of altitude (or therefore  $B$ ) up to the apogee of the rocket. The results of the present paper are consistent with their findings.

### 3. The Spectral Parameter, $\gamma$ , vs Local Time

The variations of the spectral parameter,  $\gamma$ , were investigated as a function of local time. The mean values of the spectral parameter for each three-hour interval of local time were calculated for each L interval. No significant dependence of the spectral parameter,  $\gamma$ , on local time was evident in either the mean values of  $\gamma$  or scatter plots of the data at each L value.

### 4. The Spectral Parameter, $\gamma$ , vs $A_p$ and $K_p$

The variations of the spectral parameter,  $\gamma$ , were investigated as a function of geomagnetic activity using both the  $A_p$  average amplitude index and the  $K_p$  daily sum ( $\Sigma K_p$ ). On the basis of the discussions in Chapter V, magnetic activity appeared to disturb the spectrum, first increasing and then decreasing the value of the spectral parameter as a storm progressed in the region,  $\Lambda \geq 57^\circ$ , but not greatly affecting the spectral parameter in the region below  $\Lambda \approx 57^\circ$ . From these observations no statistical dependence of  $\gamma$  on  $\Sigma K_p$  or  $A_p$  would be expected.

In Figure 23, scatter plots of  $\gamma$  as a function of  $\Sigma K_p$  are presented for the two L regions,  $2.0 \leq L \leq 3.0$  and  $4.5 \leq L \leq 8.0$ , where the L dependence presented in Figure 21 has

again been normalized to  $\gamma = 2.0$  in the manner described in Section A.2 of this chapter. It is noted in Figure 23 that there was no clear dependence of  $\gamma$  on  $\Sigma K_p$  but that the scatter of points for the region  $L \geq 4.5$  was larger than that for the region  $L \leq 3.0$ . These results are consistent with the observations discussed in Chapter V.

It was observed in Chapter V that changes in the intensities of  $> 40$  keV trapped and precipitated electrons and changes in the dumping parameter,  $\phi$ , were not always associated with changes in the magnetic activity indices,  $A_p$  and  $K_p$ . It was, therefore, decided to investigate any possible statistical dependence of  $\gamma$  on the above parameters.

##### 5. The Spectral Parameter, $\gamma$ , vs $j_{\perp}$ ( $E_e \geq 40$ keV)

The variations of the spectral parameter,  $\gamma$ , were investigated as a function of the intensity of electrons with energy greater than 40 keV mirroring at the position of the satellite. The mean value of  $\gamma$  was calculated for each half-order of magnitude increase in  $j_{\perp}$  ( $E_e \geq 40$  keV) from  $10^4$  electrons/cm<sup>2</sup> sec. ster. to  $10^7$  electrons/cm<sup>2</sup> sec. ster. at each  $L$  value. It was noted that for the groups of data centered on  $L = 2.0$ ,  $L = 2.5$ , and  $L = 3.0$ , the mean values

were all within approximately one standard deviation of the mean values given in Figure 21 for the respective L values. No attempt was made to reduce the large B dependence of  $j_{\perp}(E_e > 40 \text{ keV})$  found and reported by Armstrong [1965a] from the data. Armstrong noted that in this region there was only a small variation of  $j_{\perp}(E_e \geq 40 \text{ keV})$  at each B value, but  $j_{\perp}(E_e > 40 \text{ keV})$  varied by approximately three orders of magnitude as a function of B. Therefore, the independence of  $\gamma$  as a function of  $j_{\perp}(E_e \geq 40 \text{ keV})$  for this region,  $2.0 \leq L \leq 3.0$ , confirms the observations of Section A.2 of this chapter that  $\gamma$  was independent of B or altitude for these L values.

The region  $3.5 \leq L \leq 4.0$  is the region where the intensity of electrons with  $E_e \geq 40 \text{ keV}$  has a minimum as a function of L or latitude [McDiarmid, Burrows, Budzinski, and Wilson, 1963; Armstrong, 1965a]. The spectral parameter showed large variations in this region as a function of  $j_{\perp}(E_e \geq 40 \text{ keV})$  but these variations appeared to have no consistent pattern.

In L intervals  $\geq 4.5$  the spectral parameter increased with increasing intensity of  $\geq 40 \text{ keV}$  trapped electrons.

A scatter plot of the spectral parameter,  $\gamma$ , as a function of  $j_{\perp}(E_e \geq 40 \text{ keV})$  is presented in Figure 24 for the

two regions,  $L \leq 3.0$  and  $L \geq 4.5$ , where the L-dependence has again been normalized to  $\gamma = 2.0$ . The variations of the mean values of  $\gamma$  for this normalized data are also presented in Figure 24. The variations noted above for each L region are apparent.

#### 6. The Spectral Parameter, $\gamma$ , vs the Intensity of Precipitating Electrons

In order to investigate the variations of the spectral parameter,  $\gamma$ , as a function of the intensity of  $\geq 40$  keV electrons precipitating into the atmosphere, all data in the southern hemisphere and all data taken when  $B < .300$  gauss were eliminated from consideration. These restrictions assured that Detector 5 was responding only to particles which were being precipitated into the atmosphere.

No attempt was made to investigate the dependence of the spectral parameter,  $\gamma$ , on the intensity of precipitating electrons at each L-value, due to the large variations of  $j$  ( $E_e \geq 40$  keV) dumped at a given latitude. In Figure 25 a scatter plot of the spectral parameter,  $\gamma$ , as a function of  $j$  ( $E_e \geq 40$  keV) dumped in the region from  $L = 5.0$  to  $L = 8.0$  is presented. It will be noted that there was a tendency for

the spectral parameter to increase (indicating a softer spectrum) with increasing intensity of  $j$  ( $E_e \geq 40$  keV) dumped.

Another measure of the  $\geq 40$  keV precipitating electrons was the dumping parameter,  $\phi$ . This parameter was a measure of the degree of precipitation occurring below the satellite rather than just the intensity of precipitation as was presented in Figure 25. A scatter plot of the same points presented in Figure 25 is presented as a function of the dumping parameter,  $\phi$ , in Figure 26. A similar tendency for the spectral parameter,  $\gamma$ , to be large when the dumping parameter was close to 1 and somewhat smaller when  $\phi$  was smaller is again evident in Figure 26. These two dependences together with the discussion of Section A in Chapter V about the passes, Rev 243 (Figure 8) and Rev 255 (Figure 10), are considered to demonstrate that the mechanism which produced large increases in the intensity of particles being precipitated into the atmosphere was energy dependent and acted to precipitate a softer spectrum of electrons than that which was normally present in the trapped radiation. This result is in agreement with the observations of McIlwain [1960] and Maehlum and O'Brien [1963], but is in disagreement with the conclusions of O'Brien [1964]. McIlwain



found very soft electron energy spectrums being precipitated into the region of active aurorae. Maehlum and O'Brien found that the spectrum for precipitating electrons was significantly softer than the spectrum of trapped particles observed on magnetically quiet days. In the context of the present paper, they found that the spectral parameter,  $\gamma$ , changed from  $\approx 2$  on quiet days to  $\approx 5$  on disturbed days and that there was no enhancement of the intensity of the 90 keV electrons during these disturbed periods. However, O'Brien [1964] after examining a few "splashes", concluded tentatively that the electron energy spectrum in the range  $40 \leq E_e \leq 110$  keV was not responsive to precipitation.

An inference from the present evidence is that the electron energy spectrum would soften as the intensity of visible auroral light emission beneath the satellite increased. With the auroral photometer ( $3914 \text{ \AA}$ ) flown on Injun 3, this point could be investigated. Due to the problem of spurious light contamination of the auroral photometer, the intensity of auroral light emission was measured only when this contamination was absent. For each of these measurements, the spectral parameter,  $\gamma$ , was calculated at the same time and the results of this

investigation are presented in Figure 27. It is observed that the expected variation was present, the spectral parameter,  $\gamma$ , being on the average two units larger for auroral emissions greater than one kilorayleigh than for auroral emissions of less than 0.1 kilorayleigh. (For a discussion of the calibrations of the auroral photometer, see O'Brien and Taylor (1964)).

#### 7. The Dumping Parameter, $\phi$ , vs L

In the exemplary data of Chapters IV and V, the dumping parameter,  $\phi$ , appeared to be independent of latitude up to the high latitude  $\geq 40$  keV electron boundary. At the boundary the parameter usually increased sharply toward the value of one. In Figure 28 the dependence of the dumping parameter,  $\phi$ , on latitude is presented using the data points in this study. In the upper portion of Figure 28 a scatter plot of the points at each L-value is presented for all points recorded in the northern hemisphere. Below that scatter plot another scatter plot is presented in which just the points of the study were used for which the value of the local geomagnetic field intensity, B, was equal to or greater than 0.300 gauss. This condition assured that the value of the dumping parameter,  $\phi$ , was not contaminated by trapped particles (See Appendix II). The values of the statistical parameters associated with the two scatter plots are also presented in Figure 28.




It will be noted that the scatter of the points for the region,  $2.0 \leq L \leq 4.5$ , in the lower scatter plot is much less than for the same region in the upper scatter plot. In the lower scatter plot which restricted B to be greater than or equal to 0.300 gauss, the points clustered around  $10^{-2}$  for the lower L values ( $L \leq 5.5$ ). These results confirm the observations made in Chapter IV that when the response of Detector 5 was due solely to precipitating electrons, the value of the dumping parameter,  $\phi$ , was independent of latitude up to the high latitude boundary and was approximately equal to  $10^{-2}$ . This value is significant in that it represented the ratio of the  $\geq 40$  keV electron flux in the loss cone to the  $\geq 40$  keV electron flux locally trapped at the position of the satellite. Since a background correction was made on the rates of both Detector 1 and Detector 5 values of the dumping parameter,  $\phi$ , down to zero were possible. However, since the background correction was made by subtracting a nominal 0.6 c/s from the detector rates, it could be argued that the lower limit on  $\phi$  was determined by the uncertainty in this background correction. In Figure 37, it will be noted that the outer zone rate of Detector 5 was nominally two orders of magnitude above the

corresponding background rate to penetrating radiation. Therefore a lower limit on  $\varphi$  of  $10^{-4}$  was possible even without a background correction. It is significant therefore that no values of  $\varphi > 4.5 \times 10^{-2}$  and no values of  $\varphi < 2.5 \times 10^{-3}$  were observed for this region.

In Chapter IV, it was noted that at the high latitude boundary which usually occurred beyond  $L = 5.5$  ( $\Lambda > 65^\circ$ ), the value of the dumping parameter increased rapidly toward one and the condition of near isotropy usually existed on and beyond the high latitude boundary. This effect is also evident in the lower scatter plot of Figure 28. No values of the dumping parameter  $\varphi \geq 0.32$  were observed for  $L < 4.5$  and as the value of  $L$  increased the frequency of occurrence of the values of  $\varphi$  representing near isotropic fluxes became larger. In fact the scatter of points in both scatter plots of Figure 28 for the higher latitudes,  $L \geq 5.0$ , indicate that the degree of the precipitation was of a bimodal nature. That is, either the value of the dumping parameter was of the order of a few times  $10^{-2}$  or it was nearly one. This observation is consistent with the observation of the rapid change of  $\varphi$  from  $10^{-2}$  to  $\approx 1$  near the high latitude boundary noted in Chapter IV.

### 8. The Dumping Parameter, $\varphi$ , vs B

Using all the data (top scatter plot in Figure 28) in the study, the variations of  $\varphi$  as a function of B were investigated. For the low L region,  $\varphi$  remained constant as B decreased, until B decreased past the point where Detector 5 could respond to trapped particles. This variation is apparent in the undisturbed passes presented in Chapter IV (Figures 3-5) and is summarized for these passes in the following table for  $\Lambda = 60^\circ$ :

Rev	B (gauss)	$\varphi$	Detector 5 response
503	.512	$0.8 \times 10^{-2}$	 precipitating particles only
634	.468	$0.7 \times 10^{-2}$	
302	.385	$1.5 \times 10^{-2}$	
1981	.375	$0.9 \times 10^{-2}$	
240	.357	$1.4 \times 10^{-2}$	
transition altitude			
1626	.239	$2.8 \times 10^{-2}$	 contaminated by trapped particles
1700	.222	$3.0 \times 10^{-2}$	
1923	.198	$3.1 \times 10^{-2}$	

It will be noted that substantial fluxes of  $\geq 40$  keV electrons were always observed in the loss cone at the low latitudes. For example at  $\Lambda = 65^\circ$  in Rev 503 of Figure 4 the loss cone encompassed all local pitch angles with  $\alpha \leq 73^\circ$  and yet the ratio  $j_{\alpha < 43^\circ} (E_e \geq 40 \text{ keV}) / j_{\alpha = 90^\circ \pm 13^\circ} (E_e \geq 40 \text{ keV})$  remained  $\approx 10^{-2}$ .

However, for the higher latitudes ( $L \geq 5.0$ ),  $\phi$  was consistently larger at the higher values of  $B$ . The reason for this variation can be seen from an inspection of the two scatter plots in Figure 28. It will be noted that most of the points for  $L \geq 5.0$  with  $\phi > 0.1$  occurred in both plots but a large number of the points with  $\phi < 0.1$  had values of  $B < .300$  gauss and did not appear in the lower scatter plot. This variation implied that the near isotropic distributions occurred at the larger  $B$  values. This variation was investigated further.

In Figure 29 the frequency of occurrence for near isotropic distributions ( $\phi \geq 0.32$ ) for the region  $5.0 \leq L \leq 8.0$  is presented as a function of the geomagnetic field intensity,  $B$ , where the values of the dumping parameter,  $\phi$ , presented in the upper scatter plot of Figure 28 for the  $L$  intervals from  $L = 5.0$  to  $L = 8.0$  have been used as a sample space. This sample

space is also presented in Figure 29. It will be noted that the frequency of occurrence of the near isotropic distributions was a strong function of B and that these near isotropic distributions occurred much more frequently at low altitudes (high B values).

These near isotropic distributions could be produced primarily at the top of the atmosphere by the action of each of the following mechanisms:

- 1) A mechanism acting in the region of the satellite ( $\sim 1000$  km) which directionally accelerates electrons toward the atmosphere.
- 2) A mechanism acting near the equatorial plane which produces a pitch angle distribution which is strongly peaked at  $\alpha < 3^\circ$  (that is, few electrons are produced with  $4^\circ < \alpha_o^o < 8^\circ$ .)
- 3) A mechanism acting in the region of the satellite which produces an isotropic distribution of electrons at low altitudes.
- 4) Scattering of locally trapped electrons by atmospheric constituents. This mechanism would become more effective as the atmospheric density increased with decreasing height.

Each of these mechanisms will produce near isotropic distributions which occur much more frequently at low altitudes. However, mechanism #2 would produce values of  $\phi \gg 1.0$  when it was

operative and the satellite was at an altitude where Detector 1 was responding to particles whose equatorial pitch angle,  $\alpha_0$ , were within the range  $4^\circ < \alpha_0 < 8^\circ$  since Detector 5 would still be responding to particles with  $\alpha_0 < 3^\circ$ . Values of  $\varphi$  much greater than 1.0 were never observed and mechanism #2 can be eliminated as a possibility. Mechanism #3 can be eliminated for the same reason since when it operated in the southern hemisphere values of  $\varphi \gg 1$  would occur when Detector 1 was responding to particles with  $4^\circ < \alpha_0 < 8^\circ$  in the northern hemisphere. Mechanism #3 would also predict that when the satellite was in the southern hemisphere and this mechanism operative there, the upflux of particles measured by Detector 5 would exceed the locally trapped particle flux measured by Detector 1. This was never observed.

Mechanism #4 plausibly could produce the observed altitude dependence of  $\varphi$  but appears unable to produce the observed latitude dependence of  $\varphi$ . For example, in Rev 243 of Figure 8, the precipitated flux was observed to increase by two orders of magnitude from  $\Lambda = 65^\circ$  to  $\Lambda = 66.5^\circ$  while the locally trapped flux increased by less than a factor of two. This variation would require the scattering efficiency to change abruptly from  $\sim 10^{-2}$  to  $\sim 1$  in  $\Delta\Lambda = 1.5^\circ$ . Since atmospheric density gradients as a function of latitude are



not first order effects [Walt and MacDonald, 1964], it would be very difficult to explain the latitude variation of  $\phi$  with a scattering mechanism. Also, it will be noted in Rev 2378 (Figure 12) that the satellite was at a lower altitude and recorded a larger trapped flux at  $\Lambda = 62^\circ$  than at  $\Lambda = 70^\circ$  but the precipitated flux was  $\sim 10^2$  greater at  $\Lambda = 70^\circ$  than at  $\Lambda = 62^\circ$ , just the opposite variation expected of a scattering mechanism.

Therefore, it is concluded that this mechanism which produces a tendency toward isotropy, and hence increases in precipitation, acts primarily at low altitudes just above the top of the atmosphere (200 to 1000 km) and preferentially produces electrons moving toward the atmosphere.

#### B. Statistical Study of Intense Auroral Zone Particle Activity

In the present study, data were used from passes through the outer zone in which the response of the electron multiplier equaled or exceeded 0.12 c/s at some point during the pass and in which this response was not due to contamination by light or noise. For a complete discussion of the selection criteria for these passes, see Fritz and Gurnett [1965]. Eighty-four passes were selected in this manner.

Stilwell [1963] in calibrating the electron multiplier prior to launch determined that the associated electrometer was

linear over the range from  $10^2$  c/s down to less than  $1.5 \times 10^{-2}$  c/s. The lower limit of the electrometer response determined the threshold of the electron multiplier. Fritz and Gurnett [1965] performed an extensive inflight calibration of the electron multiplier and confirmed that the electrometer was linear down to at least  $1.5 \times 10^{-2}$  c/s. With no extrapolation of the electrometer linearity, the value (0.015 c/s) corresponded to a flux threshold of approximately  $3.0 \times 10^6$  electrons/cm<sup>2</sup> sec. ster. If the linearity was assumed to hold down to (0.010 c/s) the flux threshold was approximately  $2 \times 10^6$  electrons/cm<sup>2</sup> sec. ster. [see Figure 2 of Fritz and Gurnett (1965)]. The lower threshold was used in Chapters IV and V in an attempt to place an upper limit on the flux of trapped  $\geq 10$  keV electrons. In the present statistical study, only the threshold equal to  $3.0 \times 10^6$  electrons/cm<sup>2</sup> sec. ster. was used.

With the 84 passes selected as described above, all instances when  $j$  ( $E_e \geq 10$  keV) exceeded  $3.0 \times 10^6$  electrons/cm<sup>2</sup> sec. ster. in these passes were determined. These periods constituted the data sample for the present statistical study. To each of these periods the coordinates  $L$ ,  $B$ , magnetic local time, and the invariant latitude of the satellite were affixed to each data point. The  $K_p$ ,  $\Sigma K_p$ , and  $A_p$  indices for the particular periods were also affixed to each data point. With the recorded data the spectral parameter,  $\gamma$ , for the interval

between 10 keV and 40 keV was calculated for each period using the responses of the electron multiplier and Detector 1 as described in Section A of Chapter III. The spectral parameter,  $E_0$ , in an exponential spectral form ( $dN = N_0 \exp(E/E_0) dE$ ) was also determined from the responses of these two detectors. It was not possible to calculate the spectral parameter,  $\gamma$ , from 40 keV to 100 keV because most of these electron multiplier responses occurred during the summer of 1963 and the SpH detector was not considered trustworthy after the middle of May, 1963 (See discussion in Section F of Chapter II). From the responses of Detector 1 and Detector 5, the dumping parameter,  $\phi$ , was also calculated for these periods.

The spatial and temporal variations of these intense fluxes of  $\geq 10$  keV electrons were discussed in detail by Fritz and Gurnett [1965] and in Section C of Chapter V in the present paper. In general these intense fluxes of low energy electrons,  $j(E_e \geq 10 \text{ keV}) \geq 2.5 \times 10^7$  electron/cm<sup>2</sup> sec. ster., occurred only during local night between 1700 and 0700 hours (magnetic local time) and only between 58° and 76° invariant latitude. In the present statistical study, the spectral variations found for the range from 10 keV to 40 keV during these intense events will be discussed.

### 1. The Spectral Parameter, $\gamma$ , vs Invariant Latitude, $\Lambda$

The variations of the spectral parameter,  $\gamma$ , for the energy interval from 10 keV to 40 keV were investigated as a function of invariant latitude by calculating the average value of  $\gamma$  for the data in each one degree interval of latitude. These variations are presented in Figure 30 along with a scatter plot of the data. It will be noted that the value of  $\gamma$  generally increased with increasing latitude. However the scatter plot is more informative. Below  $\Lambda \approx 65^\circ$ , the spectral parameter,  $\gamma$ , was always less than  $\gamma = 4.5$ , whereas for  $\Lambda \geq 73^\circ$ ,  $\gamma$  was always greater than  $\gamma = 4.0$ . In the region  $65^\circ \leq \Lambda \leq 73^\circ$ ,  $\gamma$  varied over a range from  $\gamma = 1.5$  to  $\gamma = 7.4$ .

### 2. The Spectral Parameter, $\gamma$ , vs Magnetic Local Time

The variations of the spectral parameter,  $\gamma$ , for the energy interval from 10 keV to 40 keV were investigated as a function of magnetic local time by calculating the average value of  $\gamma$  for the data in each one hour interval of MLT. These variations are presented in Figure 31 along with a scatter plot of the data. The impression from both the mean values and the scatter plot is that the energy spectrum between 10 keV and 40 keV was much softer

during the early evening hours (1700 to 2100 hours MLT) than at any other time during local night. The smaller values of  $\gamma$  which occurred around the dusk meridian (1800 hours MLT) were investigated individually. It was found that almost all of these values were recorded on Rev 3451 (Figure 19). Therefore the impression of the spectrum becoming harder again around 1700 hours MLT may have been the result of a temporal variation observed on Rev 3451 which occurred during the largest magnetic disturbance observed by Injun 3 (see Figure 6). Otherwise the absence of very soft spectra on the morning side of the midnight meridian and the absence of the hard spectra from 1800 hours to 2200 hours on the evening side of the midnight meridian appear genuine and significant.

Johansen [1965] using simultaneous auroral luminosity and auroral absorption measurements taken during the three winters 1961/62, 1962/63, 1963/64 was able to study the variations in the energy spectrum of auroral electrons as a function of local time. He concluded that between 2000 hours and 0100 hours local time there was a significant hardening of the energy spectrum with maximum hardness between 2200 and 2300 hours, a result consistent with Figure 31 herein. Johansen also concluded that the energy spectrum appeared to be fairly independent of the intensity of the auroral luminosity (see next paragraph).

### 3. The Spectral Parameter, $\gamma$ , vs $j$ ( $E_e \geq 10$ keV)

The variations of the spectral parameter,  $\gamma$ , for the energy interval from 10 keV to 40 keV were investigated as a function of the intensity of  $\geq 10$  keV electrons measured at the position of the satellite by calculating the average value of  $\gamma$  for the data over each incremental increase of a factor of 2.5 in the value of  $j$  ( $E_e \geq 10$  keV). These variations are presented in Figure 32 along with a scatter plot of the data. From Figure 32, it will be noted that almost any value of the spectral parameter possible occurred at any given value of  $j$  ( $E_e \geq 10$  keV). The average value of  $\gamma$  for each incremental increase in  $j$  ( $E_e \geq 10$  keV) exhibited very little dependence on the value of  $j$  ( $E_e \geq 10$  keV). These results are in good agreement with the observation of Johansen [1965] noted above. From the scatter plot it will be noted that the largest values of  $j$  ( $E_e \geq 10$  keV) observed were  $\approx 10^9$  electrons/cm<sup>2</sup> sec. ster. and these represent the most intense fluxes of electrons observed by Injun 3. The smallest values exhibited in the scatter plot,  $\approx 4 \times 10^6$  electrons/cm<sup>2</sup> sec. ster., were set by the threshold of the multiplier ( $3 \times 10^6$  electrons/cm<sup>2</sup> sec. ster.).

#### 4. The Spectral Parameter, $\gamma$ , vs the Dumping Parameter, $\phi$

There was little meaning in investigating the variations of the spectral parameter,  $\gamma$ , as a function of the dumping parameter,  $\phi$ , because in almost all of the cases  $\phi$  was greater than 0.1 and the effective range in the dumping parameter was only the order of magnitude from 0.1 to 1.0.

#### 5. The Spectral Parameter, $\gamma$ vs $K_p$

As a final point, the variations of the spectral parameter,  $\gamma$ , were investigated as a function of the 3 hour  $K_p$  index. The average value of the spectral parameter,  $\gamma$ , was calculated for the data recorded at each value of the  $K_p$  index from 0 to 7. These average values are presented in Figure 33 along with a scatter plot of the data. Almost no events occurred when  $K_p < 2$ . From the scatter plot it will be noted that when  $K_p$  was in the range from 2 to 4 a wide range of the spectral parameter occurred, but as  $K_p$  increased the softer spectra were never observed. This type of variation led to an average overall hardening of the energy spectrum from 10 keV to 40 keV with increasing  $K_p$ .

Therefore the mechanism responsible for the production of these intense fluxes of  $\geq 10$  keV precipitating electrons was

strongly dependent on  $K_p$  or magnetic activity. The mechanism worked for energies  $\geq 10$  keV when  $K_p \geq 2$  but very seldom below that. As the degree of magnetic activity increased this mechanism was able to increase the intensity of  $j$  ( $E_e \approx 40$  keV) relatively more than  $j$  ( $E_e \geq 10$  keV). In Rev 1397 (Figure 13) at  $\Lambda \approx 63^\circ$  this mechanism appeared to increase the intensity of  $j$  ( $E_e \approx 90$  keV) as well as  $j$  ( $E_e \approx 40$  keV). The  $K_p$  index at that time was 4<sub>0</sub>.

It is noted again that most of the smaller values of  $\gamma$  plotted in Figure 31 near 1700 hours MLT were computed from data taken on Rev 3451 (Figure 19). The  $K_p$  index during Rev 3451 was 5+ and it is noted that the apparent hardening of the spectrum at 1700 hours MLT in Figure 31 may have been the result of the very large September storm and not necessarily an effect associated with that region of MLT.



## VII. SUMMARY OF PRINCIPAL FINDINGS

In the present study of the spectral, spatial, and temporal variations observed for outer zone electrons with energies from 10 keV to 100 keV, a number of the observations were inter-related with one another. In this chapter the principal findings of the present study are summarized.

### A. Precipitation of Electrons Into the Atmosphere

In the present paper, it has been shown that electrons with  $E_e \geq 40$  keV were constantly observed in the loss cone (i.e., particles which would mirror below 100 km before being reflected) at all latitudes of the outer zone for  $L \geq 2.0$  (Chapter VI.A.8). The flux of precipitating electrons was always approximately  $10^{-2}$  that of the locally mirroring flux. This meant that the degree of precipitation occurring for the region of the outer zone with  $L \geq 2.0$  was independent of latitude up to the high latitude boundary at which point it usually increased rapidly (Chapter IV and VI.A.7). For latitudes below the high latitude boundary the ratio of the precipitated flux to the locally trapped flux was independent of altitude (B) up to the point where Detector 5 could respond to trapped particles (Chapter VI.A.8).

These lower latitude variations of the locally trapped and precipitated flux imply that both types of particles originated in the same manner and their characteristics noted here are strongly suggestive of a pitch angle scattering or diffusion mechanism which operates constantly and at all latitude from  $\Lambda = 45^\circ$  up to the high latitude boundary of the outer trapping region, producing both the locally trapped and precipitating flux observed by Injun 3. This will be examined in more detail later.

At the high latitude boundary there was usually a "spike" of precipitating electrons present and in many cases the flux of  $\geq 40$  keV electrons was isotropic over the upper hemisphere at the position of the satellite as the satellite passed through the boundary. The dumping parameter,  $\phi$ , was usually observed to break sharply from  $10^{-2}$  toward one at that point and beyond that latitude large amounts of  $\geq 40$  keV electron precipitation were observed during magnetically quiet as well as active periods (Chapter V). The characteristics associated with these large precipitation events are discussed later in this chapter.

#### B. High Latitude Outer Zone Boundary

It was noted in Figure 12 that large variations ( $\Delta \Lambda = 7^\circ$ ) occurred in the apparent position of the  $\geq 40$  keV electron high

latitude boundary during a magnetically quiet period (Chapter V.A). It was also noted that in each of the four passes presented, the latitude at which the dumping parameter,  $\phi$ , started to increase sharply was approximately  $65^\circ$  for each pass. In Figure 12 it will be noted that there was no variation in the value of  $j_{\perp}$  ( $E_e \geq 40$  keV) and  $j$  ( $E_e \geq 40$  keV) dumped for  $\Lambda < 65^\circ$  from pass to pass in each of the four passes but very large variations in these quantities occurred for  $\Lambda > 65^\circ$ . For example at  $\Lambda = 70^\circ$   $j_{\perp}$  ( $E_e \geq 40$  keV) varied from  $3.0 \times 10^5$  electrons/cm<sup>2</sup>. sec. ster. on Rev 2378 to  $< 10^2$  electrons/cm<sup>2</sup>. sec. ster. on Rev 2380. This represented a change of over three and a half orders of magnitude in  $j_{\perp}$  ( $E_e \geq 40$  keV) in less than four hours and therefore it would be difficult to call the electron fluxes observed at  $\Lambda > 65^\circ$  durably trapped.

The concept of a high latitude outer zone "trapping" boundary for  $\geq 40$  keV electrons has usually been associated with a point where the counting rate of a given detector dropped rapidly toward background as a function of latitude. This concept probably should be revised to include two regions, the trapping region and the auroral zone, which overlap somewhat in latitude. The auroral zone can be disturbed by a variety of mechanisms (the variations which some of them produce are discussed in the next section).

The lower latitude trapping region is disturbed only during magnetically active periods but remains undisturbed otherwise and exists in the manner outlined in the preceding section of this chapter.

The position at which the dumping parameter,  $\phi$ , is observed to break sharply from  $\approx 10^{-2}$  toward 1 should be a more meaningful concept of the high latitude limit to durably trapped particles than the usual intensity cutoff.

### C. Observed Particle Variations

In the present study a large number of particle observations have been presented. In the present section an attempt is made to group the observations into a set of distinct particle variations which can later be associated with the presently proposed mechanisms reported in the literature.

In the low altitude trapping region (as opposed to the auroral zone) there appeared to be four distinct variations of the characteristics of electrons with energies from 40 keV to 100 keV. Three of these variations were associated with magnetic activity and are discussed later. The fourth group of observations deals with the quiet time trapping region. In this region

there was always a significant flux of  $\geq 40$  keV electrons observed in the loss cone (i.e., particles which would mirror below 100 km before being reflected). A source for these particles was necessary since they would be lost in the atmosphere before completing a latitudinal oscillation. The lifetimes of these particles was therefore less than  $10^{-1}$  seconds ( $\approx$  one quarter of their bounce period) but they were observed constantly. From the discussion of Section A of this chapter, the characteristics noted there were strongly suggestive of a pitch angle scattering or diffusion mechanism which operated constantly and at all latitudes for  $L \geq 2.0$  with equal effectiveness. The variations of the intensity of locally trapped and precipitating electrons as a function of latitude then could be attributed to a source mechanism operating nearer the equatorial plane which supplied the electrons that were eventually observed by Injun 3 at the lower altitudes through a pitch angle scattering process. This interpretation of the observed particle variation, although suggestive, is of course not unique.

During the occurrence of magnetic activity there appeared to be three distinct variations of the flux of electrons with energies between 40 keV and 100 keV in the outer zone for  $\Lambda > 57^\circ$ .

These were

1. Rapid Loss
2. Replenishment
3. Persistent Decay

At the onset of a magnetic storm the values of  $j_{\perp}$  ( $40 \text{ keV} \leq E_e \leq 50 \text{ keV}$ ) and  $j_{\perp}$  ( $80 \text{ keV} \leq E \leq 100 \text{ keV}$ ) were observed here and the value of  $j_{\perp}$  ( $E_e \geq 40 \text{ keV}$ ) was observed by Craven [1966] to decrease by factors of 10 to  $10^3$ . It was not possible to determine from the Injun 3 data whether these particles were completely lost to the outer zone or whether their pitch angles were perturbed in such a fashion that they mirrored above the satellite.

However, observation of a similar rapid loss near the equatorial plane at  $L \approx 5$  by Explorer 14 [Frank, 1965] indicates that the particles were completely lost to the outer zone. After the rapid loss occurred, a replenishment of  $\approx 40 \text{ keV}$  and  $\approx 90 \text{ keV}$  particles was observed to occur in which the value of  $j_{\perp}$  ( $40 \text{ keV} \leq E_e \leq 50 \text{ keV}$ ) was increased by a factor of 30 in less than a day. The increase of  $j_{\perp}$  ( $80 \text{ keV} \leq E_e \leq 100 \text{ keV}$ ) was observed to occur over a period of days reaching a maximum after the  $\approx 40 \text{ keV}$  fluxes had already begun to decay. After the fluxes of  $\approx 40 \text{ keV}$  and  $\approx 90 \text{ keV}$  electrons reached their respective peak intensities, they began a

persistent decay which lasted over a period of days. The values of  $j_1$  ( $80 \text{ keV} \leq E_e \leq 100 \text{ keV}$ ) decayed in an exponential manner with a time constant of the order of  $\approx 2$  days. The observed decay of  $j_1$  ( $40 \text{ keV} \leq E_e \leq 50 \text{ keV}$ ) was not of an exponential nature (as found by Craven [1966] for  $j_1$  ( $E_e \geq 40 \text{ keV}$ )) due to other variations superimposed on the decay (Chapter V.B).

In the next chapter, various mechanisms reported in the literature are discussed to determine the possible mechanisms which may cause the above observed particle variations.

In the auroral zone region,  $\Lambda > 65^\circ$ , there were at least two distinct groups of variations which were observed in the present study of Injun 3 data. These groups of observed variations were very distinct from each other and in the summary presented here each group is associated with a mechanism (source or acceleration) for the purpose of summarizing the collective variations. In this manner the properties and characteristics of the mechanism (or mechanisms) which must exist and which cause the observed particle characteristics are delineated.

The first group of observations to be discussed here was associated with the variations observed in Rev 243 (Figure 8), Rev 255 (Figure 10), Rev 2378 (Figure 12) and probably Rev 1459 (Figure

14). The "mechanism" associated with this group was observed to produce fluxes of  $\geq 40$  keV electrons which were isotropic or nearly isotropic over the upper hemisphere at the position of the satellite and it appeared to be independent of the amount of magnetic activity occurring, being observed to operate during periods of little magnetic activity (e.g., Rev 255 of Figure 10). It was observed to occur at all local times and produced the sharp change in the dumping parameter,  $\phi$ , from a value of  $10^{-2}$  to  $\approx 1$  associated with the high latitude boundary. It operated almost continually in the region  $\Lambda > 65^\circ$  with only a few passes found where the sharp increase in  $\phi$  was not observed at the boundary (e.g., Figure 5). As this mechanism increased in intensity, it usually produced isotropic distributions at latitudes higher than  $\Lambda \approx 65^\circ$  (e.g.,  $65^\circ < \Lambda < 70^\circ$  in Rev 243 of Figure 8 and  $65^\circ < \Lambda < 74^\circ$  in Rev 2378 of Figure 12) but it could expand to lower latitudes also (e.g.,  $60^\circ < \Lambda < 75^\circ$  in Rev 255 of Figure 10). It was not observed to occur below  $\Lambda = 60^\circ$  (see Figure 28). From the results of Chapter VI.A.6 this mechanism was found to be energy dependent and would act to precipitate a softer spectrum of electrons than that which was normally present in the trapped radiation. In the only pass where this mechanism was observed to affect the value of  $j_1$  ( $80 \text{ keV} \leq$



$E_e \leq 100$  keV) (Rev 1459 of Figure 14), the spectral slope parameter from 40 keV to 100 keV was  $\gamma \approx 8.0$ , one of the softest spectra observed in the Injun 3 data, while the spectral slope between 10 keV and 40 keV was  $\gamma \approx 2.5$ , indicating a fairly hard spectrum for that energy interval. The most surprising feature of the mechanism was that it tended to produce the isotropic fluxes predominantly right on top of the atmosphere (Figure 29). From the discussion of Chapter VI.A.8, this dependence was interpreted to demonstrate that this mechanism must operate in the region of the satellite near the end of the geomagnetic field line and preferentially produce electrons moving toward the atmosphere.

The second group of observations was associated with the variations observed in connection with the intense fluxes of  $\geq 10$  keV electrons precipitating into the atmosphere. The "mechanism" associated with this group was observed to operate only during disturbed conditions ( $K_p \geq 2$ ). This mechanism occurred only in the classical auroral zone between  $\Lambda \approx 56^\circ$  and  $\Lambda \approx 77^\circ$  and only during local night between 1700 hours and 0700 hours MLT. It was responsible for the intense fluxes,  $j(E_e \geq 10 \text{ keV}) \geq 2.5 \times 10^7$  electrons/cm<sup>2</sup> sec. ster. observed by Injun 3 and reported by Fritz and Gurnett [1965] that were associated with the high latitude  $\geq 40$  keV electron intensity cutoff.

From the discussion of Chapter V.C, it was shown that this mechanism acted in a region high above the satellite. It produced a much softer spectrum in the interval from 10 keV to 40 keV in the early evening hours (1800 hours to 2000 hours) of local night than it did during the early morning hours ( $2200 \text{ hours} < \text{MLT} < 0700 \text{ hours}$ ) (Figure 31). As a function of latitude the spectrum was always much harder ( $\gamma < 4.5$ ) for  $\Lambda < 65^\circ$  and was always very soft ( $\gamma > 4.0$ ) for  $\Lambda > 73^\circ$  (Figure 30). The energy this mechanism was able to give to a particle was dependent on the amount of magnetic activity occurring (Figure 33). That is, it was seldom observed for  $K_p < 2$ . For  $K_p > 2$  it produced intense fluxes of  $\geq 10 \text{ keV}$  electrons and as  $K_p$  increased it could enhance the flux of  $\approx 40 \text{ keV}$  ( $K_p > 4$ ) and  $\approx 90 \text{ keV}$  electrons.

Various particle acceleration and source mechanisms reported in the literature are discussed in the next chapter to determine the actual mechanisms associated with the particle variations presented above.

## VIII. DISCUSSION

A number of different acceleration and/or source mechanisms for outer zone electrons have been proposed [Dessler and Karplus, 1961; Dragt, 1961; Wentzel, 1961; Cornwall, 1964; Stix, 1964; Chang and Pearlstein, 1965; Dungey, 1965; Fälthammar, 1965; Taylor and Hones, 1965; Trakhtengerts, 1965; Block, 1966; Eviatar, 1966; Kennel and Petschek, 1966a; Persson, 1966; Roberts, 1966; Evans, 1967]. Many of these mechanisms are only in the conceptual stage and do not predict detailed particle characteristics and behavior. However a few have been developed to the point of making such detailed predictions. In the present chapter, some of these mechanisms will be examined in detail in order to determine whether the particle characteristics observed in the present study may be understood.

### A. The Pitch Angle Diffusion Mechanism of Kennel and Petschek [1966a]

One of the pitch angle diffusion mechanisms proposed, the mechanism of Kennel and Petschek [1966a] has been developed to a large extent [Thorne and Kennel, 1966; Kennel and Thorne, 1966; Kennel and Petschek, 1966b; Kennel, 1967]. This mechanism uses the concept of a whistler cyclotron resonance interaction which is

generated and maintained near the equatorial plane by an anisotropic particle pitch angle distribution to scatter particles toward smaller equatorial pitch angles. This mechanism acts to limit the number of trapped particles observed at the equatorial plane and is non linear in nature. That is, if the trapped flux present near the equatorial plane is less than the limit imposed by this mechanism there will be no pitch angle diffusion taking place. However, as the trapped particle flux exceeds this limit, the diffusion mechanism takes over and reduces the intensity of the trapped flux to the limiting level. Kennel and Petschek [1966a, b] calculated the limiting values that this mechanism would impose on fluxes near the equatorial plane. It was found that the Explorer 14 values of  $j(E_e \geq 40 \text{ keV})$  reported by Frank [1965] were approximately equal to these limiting fluxes for  $L \geq 4$ . With this ground work, Kennel and Petschek [1966a, b] were able to predict the following particle characteristics observable in the low altitude outer zone:

1. There should be a steady state "weak" diffusion of particles into the pitch angle region of the loss cone, resulting in a "dizzle" of precipitating particles.

This effect was anticipated because the equatorial fluxes were observed to be approximately equal to the limiting values imposed by

this mechanism for  $L \geq 4.0$ , thus suggesting the possibility of a constantly active source mechanism near the equatorial plane and a corresponding "dizzle" of precipitating particles or steady state diffusion loss .

2. If the equatorial trapped electron fluxes are built up to their limiting values by an acceleration mechanism, the observed energy spectrum will be hard since the limiting flux is essentially independent of energy. However there should be a transition energy beyond which the flux is no longer near its limit and a softer spectrum should exist at higher energies.

Kennel and Petschek suggested after an examination of the data that at  $L = 6$  electrons with  $E_e \geq 40$  keV are frequently near the limiting value imposed by this mechanism while electrons with  $E_e \geq 240$  keV are only occasionally at their limiting value. Therefore for this latitude ( $L=6$ ), the transition energy should be greater than 40 keV but less than 240 keV.

3. If spectra are measured using two channels - one above and one below the transition energy, the trapped particles should have a harder spectrum than the precipitating particles. In fact there should not be any precipitating particles at the higher energies.

4. This mechanism does not require any gross change in the geomagnetic or geoelectric fields to produce an increase in precipitation.
5. When acceleration is continuous, more and more of the electron energy distribution reaches the limiting flux and the transition energy increases with time. Thus, observed trapped particle energy spectra should become progressively harder with time. Also when acceleration is enhanced high energy electrons should have their peak after the low energy electron fluxes.

These five consequences of the basic whistler mode instability theory of Kennel and Petschek can now be examined in the context of the present study. An extension of the theory to include parasitic precipitation of higher energy electrons at latitudes below the latitude of generation of the whistler is able to predict exponential type decays with time constants of the order of days [Kennel and Petschek, 1966b; Kennel, 1967].

In the present paper it was found that the value of the dumping parameter,  $\phi$ , was essentially independent of latitude up to the high latitude boundary during undisturbed periods, that there was always a significant flux of  $\geq 40$  keV electrons in the

loss cone, and that this flux was equal to approximately  $10^{-2}$  that of the locally trapped fluxes at all latitudes for  $\Lambda \geq 45^\circ$ . Prediction 1 above states that there should be a steady state "dizzle" of precipitating electrons and appears to agree with these observed electron characteristics very well. However from the discussion by Kennel and Petschek [1966a, b] Prediction 1 should not be operative below  $L \approx 4.0$  and even for  $L > 4.0$  the observed equatorial electron intensities were more often subcritical than unstable. There was a large drop in the intensities of both the locally trapped and precipitated  $\geq 40$  keV electron fluxes below  $L \approx 4.0$  ( $\Lambda < 60^\circ$ ) associated with the slot but the ratio of these two fluxes remained unaffected. The fact that  $\phi$  was independent of latitude from  $\Lambda = 45^\circ$  up to the high latitude boundary implies that any pitch angle scattering mechanism should also be independent of latitude for  $\Lambda > 45^\circ$  and the observed low altitude intensity variations of the locally trapped and the precipitated  $\geq 40$  keV electrons probably were reflecting the variation in the source mechanism(s) of these particles near the equatorial plane. In its present form the pitch angle scattering mechanism resulting from the whistler mode instability does not appear to agree with the observed undisturbed particle variations at the lower latitudes ( $\Lambda < 60^\circ$ ).

Since this mechanism does not appear to be operative much below  $L \approx 4.0$  ( $\Lambda \approx 60^\circ$ ), it is a possible candidate to explain the large variation observed during a magnetic storm which appeared to occur only for  $\Lambda > 57^\circ$  (Figure 15). In Chapter VII, it was shown that three types of particle behavior were observed during a magnetic storm. These were (1) rapid loss, (2) replenishment, and (3) persistent decay. The pitch angle diffusion mechanism is unable to explain the rapid loss phase of the magnetic storm since it can act only to increase the flux observed at low altitudes. However if a steady state source mechanism near the equatorial plane is assumed [Kennel and Petschek, 1966a and b] and which appeared to be implied by the results of the present study, the entire storm time variations observed at low altitudes can be predicted qualitatively by assuming some rather ad hoc but not unreasonable variations of the equatorial source. First this equatorial source is momentarily shut off at the beginning of a magnetic storm (e.g., at the sudden commencement) and then is turned on again (e.g., during the initial phase) acting continuously through the storm.

By turning off the source at the beginning of the storm the steady state pitch angle scattering mechanism suggested in



Chapter VII would decrease the intensities of the equatorially trapped fluxes until either the reservoir of particles was depleted or the mechanism was unable to operate. The same decrease would be observed at low altitudes giving rise to the rapid loss phase of the observed particle variations. As the source mechanism is turned on again Prediction 5 of the mechanism of Kennel and Petschek would become important. From Figure 15, it is noted that the intensity of the lower energy electrons reaches its maximum value before that of the higher energy electrons at  $\Lambda = 60^\circ$  in agreement with Prediction 5. It is also noted in Figure 15 that after the values of the intensities of both the  $\approx 40$  keV and  $\approx 90$  keV electrons began to rise, the energy spectrum became progressively harder with time and this is again in good agreement with Prediction 5. The subsequent persistent decay could be explained by requiring the source mechanism to lose strength as the magnetic activity subsides and be unable to maintain the intensity of  $\approx 90$  keV electrons near their limiting values. The transition energy would move to a point between  $\approx 40$  keV and  $\approx 90$  keV. Parasitic precipitation of  $\approx 90$  keV electrons [Kennel, 1967] would begin and give the observed exponential decays. With the  $\approx 90$  keV electrons above the transition energy, Prediction 2 could be tested. The values of  $j(E_e > 10 \text{ keV})$  and  $j(E_e \approx 40 \text{ keV})$  would still be maintained near their limiting values, while the value of

$j$  ( $E_e \approx 90$  keV) would continue to decrease. Therefore the fact that the spectral slope between 10 keV and 40 keV was observed to be much harder than the slope from 40 keV to 100 keV after the maximum intensities were reached is also in good agreement with Prediction 2 (see Rev 1459 of Figure 14).

The pitch angle diffusion mechanism of Kennel and Petschek has been shown here in a qualitative manner to be able to produce the particle variations observed at low altitudes with reasonable assumptions about a source mechanism acting near the equatorial plane. The consistency of these observations and predictions however does not, of course, prove the existence of this mechanism, but does support it.

Since this mechanism can act to increase the amount of precipitation occurring at low altitudes without requiring any change in the geomagnetic field (Prediction 4), it is also a possible candidate for the phenomenon described in Chapter VII which operates in the auroral zone during quiet times. This pitch angle diffusion mechanism being non linear in nature acts to drive the value of an enhanced flux of trapped particles near the equatorial plane down to the value of the limiting flux for that L shell. If the equatorial trapped fluxes were enhanced well above the limiting values the diffusion mechanism becomes much

stronger and a large amount of precipitation will occur at low altitudes. These large increases in the values of the precipitating flux were observed frequently with Injun 3. If we assume that the transition energy for these quiet time precipitation events was between 40 keV and 90 keV, then Prediction 3 should be observed. In Chapter VI it was shown that the energy spectrum from 40 keV to 100 keV became much softer as the degree of precipitation ( $\phi$ ) increased. This is in agreement with Prediction 3. In the series of passes presented in Figures 7 to 11, it was found that the intensity of the  $\approx 90$  keV electrons was not observably effected during these large  $\geq 40$  keV precipitation events (e.g., Rev 243 of Figure 8 and Rev 255 of Figure 10). This again is in good agreement with Prediction 3.

However it was shown in Chapter VI that the mechanism which generated these large precipitation events acted to produce the isotropic distributions predominantly right on top of the atmosphere near the end of the geomagnetic field line. It appears to be conceptually very difficult to diffuse particles in pitch angle with a mechanism acting near the equatorial plane in such a way that large fluxes of particles can be produced with equatorial pitch angles,  $\alpha_0 < 3^\circ$ , but the same large fluxes are not found to

occur in the equatorial pitch angle interval,  $3^\circ \leq \alpha_0 \leq 7^\circ$ . Therefore, in its present form this pitch angle scattering mechanism does not appear to be the mechanism causing these quiet time auroral zone precipitation events.

In summary, the pitch angle diffusion mechanism resulting from the whistler mode instability does not appear to be adequate to predict the variations observed in the quiet time outer trapping region ("dizzle" precipitation) or the large  $\geq 40$  keV electron precipitation events which are observed in the auroral zone, neither the quiet time precipitation events nor the intense  $\geq 10$  keV electron precipitation events. However during the development of a magnetic disturbance, this mechanism is able to predict the observed low altitude particle variations very well (with a few reasonable, although ad hoc, assumptions about the equatorial source mechanism(s)) and appears to play an important role in such disturbances. This role would be consistent with the observation that the equatorial electron intensities were more often subcritical than supercritical for  $L > 4.0$ .

#### B. The Magnetospheric Model of Taylor and Hones [1965]

Taylor and Hones [1965] have constructed a model of the earth's magnetosphere which used an empirically deduced geomagnetic

and geoelectric field configuration. The model of the magnetic field included the effects of the solar wind pressure on the sunward side of the magnetosphere and of the neutral or current sheet in the magnetospheric tail. The electric field was deduced in the ionosphere from the  $S_D$  current system which accompanied magnetic bays and therefore represented magnetically disturbed conditions. The magnetic field lines were assumed to be equipotentials and the electric field was projected throughout the magnetosphere. The motion of the solar wind electrons (kinetic energy at the magnetospheric boundary  $< 1$  keV) was studied in quantitative detail. The motion of these electrons was followed by allowing them to drift into the magnetosphere from the boundary surface while conserving their first and second adiabatic invariants. With the model set up in this manner Taylor and Hones [1965] were able to predict the following particle variations observable in the low altitude outer zone:

1. These electrons will not remain in trapped orbits (without invoking additional mechanisms), but will either precipitate into the atmosphere and be absorbed, or will drift back out of the magnetosphere again.

2. The maximum energy which these solar wind electrons can achieve at low altitudes is  $\approx 40$  keV.
3. These electrons will precipitate only on the local night side of the magnetosphere. They should be found between  $70^\circ$  and  $78^\circ$  invariant latitude between 1800 hours and 2400 hours MLT and should be found about  $5^\circ$  southward from the above values after local midnight.
4. These electrons should precipitate in a region north of the  $\geq 40$  keV outer zone electron trapping boundary.
5. The electron energy spectrum between 1 keV and 100 keV should be much softer north of the boundary than south of it.
6. Particles precipitating at a given latitude will have energies of a few keV during the early evening hours and get progressively more energetic reaching 35 to 40 keV a few hours after local midnight.

These six consequences of letting solar wind particles drift into this model of Taylor and Hones [1965] can now be examined in the context of the present study.

Since the model used an electric field which was associated with magnetic bay activity in the auroral zone, it should be associated with the mechanism discussed in Chapter VII which produced the intense fluxes of  $\geq 10$  keV electrons observed by Injun 3.

Prediction 1 above states that these intense fluxes of  $\geq 10$  keV electrons should not remain in trapped orbits. Since the Injun 3 electron multiplier sampled particles with pitch angles,  $\alpha = 50^\circ \pm 10^\circ$ , it usually sampled both particles which would mirror above the atmosphere and particles which would mirror in the atmosphere and be lost. Therefore it was sensitive to both locally trapped and precipitated particles. In Section C of Chapter V it was noted that these intense events,  $j(E > 10 \text{ keV}) \geq 2.5 \times 10^7$  electrons/cm<sup>2</sup> sec. ster. were never observed on three consecutive passes (over a period of > four hours). In Figures 16 and 17 it will be noted that the latitude at which the intense fluxes of  $\geq 10$  keV electrons occurred was not constant from pass to pass. In Chapter V.C. it was argued that these intense fluxes of  $\geq 10$  keV electrons originated high above the region of the satellite on lines of force intersecting the surface of the earth in the classical auroral zone. These observations indicated that these intense fluxes of  $\geq 10$  keV electrons were introduced into the region of the auroral zone and precipitated without remaining in stably trapped orbits. This is in good agreement with Prediction 1 of the model of Taylor and Hones [1965].

Most of the intense fluxes of  $\geq 10$  keV electrons were observed during the summer of 1963 during a period when the SpH channel was considered untrustworthy. For this reason, it was not possible to determine whether the flux of  $\approx 90$  keV electrons was usually influenced during the periods of these intense  $\geq 10$  keV electron precipitation events but in the event presented in Figure 13 (Rev 1397), it did appear that the value of  $j_{\perp}$  ( $80 \text{ keV} \leq E_e \leq 100 \text{ keV}$ ) was enhanced at the same latitude at which the intense flux of  $\geq 10$  keV electrons was observed. To investigate this point more fully, fifteen of the events were investigated for which the SpH detector was considered to be trustworthy. It was found that there was a detectable increase of  $j_{\perp}$  ( $80 \text{ keV} \leq E_e \leq 100 \text{ keV}$ ) associated in time with the intense flux of  $\geq 10$  keV electrons in about half of these events (seven) with three of the increases being as observable as Rev 1397 in Figure 13. Therefore increases in the flux of  $\approx 90$  keV electrons were observable for some of these events. This does not agree with Prediction 2 of the model of Taylor and Hones.

Prediction 3 is the most stringent of the predictions to satisfy. Taylor and Hones [1965] compared this prediction with the region of occurrence of the observed intense  $\geq 10$  keV electron



precipitation events reported by Fritz and Gurnett [1965] and concluded that the observed and predicted regions of precipitation were in reasonable agreement with each other.

It would appear from Prediction 4 that these intense fluxes of  $\geq 10$  keV electrons should be found in a region north of the intensity cutoff for  $\geq 40$  keV electrons as for example, Rev 2829 in Figure 19. However most of the  $\geq 10$  keV electrons fluxes were observed to occur on or inside the latitude of the intensity cutoff for  $\geq 40$  keV electrons. The observations appear to disagree with Prediction 4. However from the discussion of Section B in Chapter VII a more meaningful definition of the high latitude boundary for durably trapped  $\geq 40$  keV outer zone electrons would be the latitude at which the dumping parameter,  $\phi$ , broke away from  $\phi \approx 10^{-2}$  toward  $\phi \approx 1$ . With this definition of the high latitude  $\geq 40$  keV "trapping" boundary, the intense fluxes of  $\geq 10$  keV electrons were observed almost without exception in the region where  $\phi$  was approaching one and therefore in good agreement with Prediction 4.

Prediction 5 of the model of Taylor and Hones [1965] is associated with the discussion given above for Prediction 4 but the consequences of Prediction 5 are readily apparent in Figure 30. It will be noted that for  $\Lambda < 65^\circ$ , the spectral slope between 10 keV

and 40 keV was always less than  $\gamma \approx 4.5$  but for  $\Lambda > 73^\circ$  the spectral parameter was always greater than  $\gamma = 4.0$ . For the region  $65^\circ \leq \Lambda \leq 73^\circ$  any value of the spectral parameter from  $\gamma = 1.5$  to  $\gamma = 7.0$  was possible. The wide statistical variations of the spectral parameter in this region can be interpreted to mean variations in the position of the outer zone boundary.

Since Prediction 6 is a prediction about the presence of electrons of various energies as a function of local time, it is informative to investigate the variation of the  $\geq 10$  keV and  $\geq 40$  keV electrons associated with these intense precipitation events. Scatter plots of the fluxes of these electrons were constructed as a function of local time. It was found that there was little change in the median intensity of the  $\geq 10$  keV electrons as a function of local time, but there were relatively fewer occasions when appreciable fluxes of  $\geq 10$  keV electrons were present for local times earlier than 2000 hours [see Figure 6 of Fritz and Gurnett, 1965]. It was found that the median intensity of  $\geq 40$  keV electrons had a minimum between 1800 hours and 2000 hours, then increased by approximately two orders of magnitude between 2000 hours and 2200 hours, and remained approximately constant for local times after 2200 hours. These variations can be observed in Figure 31 since it was noted above that there was little change in the median value of  $j(E_e \geq 10 \text{ keV})$  as a function of local time. From Figure 31, it was noted that there was a marked absence of the smaller values of the spectral parameter in the early

evening hours from 1800 hours to 2200 hours MLT. This can be interpreted to indicate that the value of  $j(E_e \geq 40 \text{ keV})$  was not enhanced for those local times. Also in Figure 31, it was noted that there was an almost complete lack of the very soft spectra on the morning side of the midnight meridian ( $0200 \text{ hours} \leq \text{MLT} \leq 0800 \text{ hours}$ ). This can be interpreted to indicate that the value of  $j(E_e \geq 40 \text{ keV})$  was always enhanced during this local time interval. These variations are in good agreement with Prediction 6 of the model of Taylor and Hones.

The auroral zone mechanism discussed here and in Chapter VII was found also to have a dependence on the degree of magnetic activity occurring at the time the intense flux of  $\geq 10 \text{ keV}$  electrons was observed. This dependence indicated that the mechanism was able to create more and more energetic electrons as the degree of activity increased. The model of Taylor and Hones [1965] included no specifications for variations with magnetic activity. However, a few qualitative arguments can be made here. Since the electric field configuration of the model was deduced from a twelve-month average current system in the polar ionosphere derived from magnetic bays, the actual current system and hence the electric field should be a function of the degree of magnetic activity occurring. This was confirmed by Fairfield [1963, 1964] who made a statistical study of the orientation and intensity of very high latitude current systems in quiet and disturbed times. He

concluded that the time variations both in intensity and direction were large but that the direction was rotated by some  $30^\circ$  with respect to the earth sun line from quiet to disturbed times. Therefore it is not unreasonable to expect that large potentials and different electric field configurations exist during the periods of large magnetic activity, and thereby permit the solar wind electrons to gain larger amounts of energy in reaching the auroral zone regions. This would be a possible explanation of the difference between the observation of  $\approx 90$  keV electrons associated with these intense  $\geq 10$  keV precipitation events and Prediction 2 of the model of Taylor and Hones [1965]. The large amount of scatter in Figure 31 between 2100 hours and 0200 hours MLT may be associated with the variations of the energy which a solar wind electron can derive during various phases of magnetic activity.

In summary, the model of Taylor and Hones [1965] appears to be very successful in explaining the observed variations of the outer zone electrons from 10 keV to 40 keV associated with the intense fluxes of  $\geq 10$  keV precipitating electrons reported by Fritz and Gurnett [1965]. This model provides both a source and an acceleration mechanism for these particles. It is suggested that an extension of the model to include various degrees of magnetic activity will be important.

### C. The Two Stream Plasma Instability Mechanism of Stix [1964]

An acceleration mechanism, which is still in the conceptual stage as far as application to magnetospheric phenomena is concerned, was proposed by Stix [1964] to explain the results of certain laboratory plasma experiments. Smullin and Getty [1962] reported that when a beam of monoenergetic electrons (with energy equal to a few keV) was introduced into a plasma immersed in a magnetic field within a very short time ( $\approx 10^{-6}$  seconds) electrons with energies greater than 100 keV were produced. Stix [1964] proposed that the interaction of monoenergetic beam of electrons with the plasma led to the production of various modes of plasma waves. He showed that certain of these waves could grow in amplitude, drawing their energy from the monoenergetic beam. A resonance between the gyrofrequency of these keV electrons and the wave frequency could then lead to a rapid acceleration of some favored keV energy electrons to energies of  $> 100$  keV.

Evans [1967] pointed out that this situation possibly occurs during intense auroral zone precipitation. In a rocket flight by Evans into the break up phase of an auroral display, the primary auroral electron beam was observed to have a strong nearly monoenergetic component with  $E_e \approx 5$  to 6 keV. Higher energy electrons

( $\approx 16$  keV,  $> 60$  keV,  $> 120$  keV) were observed to be present in substantial numbers and to demonstrate a 10 cps periodicity. Doing a cross-correlation analysis of the fluctuations of the 16 keV, 60 keV and 120 keV detector counting rates, Evans concluded that these fluctuations were simultaneous in real time. He then argued that the process responsible for the generation of the periodic fluctuations must lie close to the earth and also that the 16 keV and 120 keV electrons must be affected nearly simultaneously at the source. Evans [1967] proposed the following mechanism to explain both the presence of energetic electrons in the auroral electron beam and the occurrence of a 10 cps periodicity.

1. A monoenergetic beam ( $E \approx 6$  keV) of electrons (possibly produced in the outer magnetosphere by an electric field acceleration of the type proposed by Taylor and Hones [1965]) enters the enhanced electron density of the upper F layer.
2. The interaction of these electrons with the local plasma excites a wide range of plasma oscillations.
3. Some of these oscillations propagate and grow in an exponential fashion.

4. A gyrofrequency of certain favored electrons in the monoenergetic beam resonates with these waves and these electrons are accelerated.
5. The transfer of energy from wave to particles can progress to the point where it exceeds the growth of the wave, thus damping the wave.

These five steps were suggested by Evans to occur during a time interval of 0.1 seconds. He also pointed out that this wave-particle interaction favors energization perpendicular to the local magnetic field line thus tending to trap the accelerated electrons rather than precipitate them.

This mechanism is discussed here because it was a possible source of the higher energy ( $\approx 90$  keV) observed during many of the intense  $\geq 10$  keV precipitation events (e.g., Rev 1397 of Figure 13). It will be noted here that in Rev 1397 of Figure 13 all of the necessary features of this mechanism were present. An intense beam of possibly nearly monoenergetic electrons was entering the ionosphere and enhancement of the locally trapped electrons with  $E_e \approx 90$  keV was observed. Included in the detector complement of the Injun 3 payload was a VLF receiver which was sensitive to the

magnetic component of an electromagnetic wave with frequencies from 500 cps to 7.0 kc/s [Gurnett and O'Brien, 1964]. Since this mechanism involves a wave-particle interaction, there is a distinct possibility that the Injun 3 VLF receivers could detect the presence of such a wave. The frequency-time spectrograms recorded during Rev 1397 of Figure 13 were examined. It was found that coincident with the beginning of the intense flux of  $\geq 10$  keV electrons an intense banded noise appeared below 1.5 kc/s. This noise lasted approximately 30 seconds which was the duration of the intense flux of  $\geq 10$  keV electrons. This short burst of intense low frequency noise was not common to the Injun 3 VLF data especially during periods of local night [D. A. Gurnett and W. W. L. Taylor, private communication]. This observation indicated that some unusual waves were observed coincident with the  $\geq 10$  keV fluxes on this pass. However, the waves postulated by Stix [1964] were electrostatic in nature and would necessarily have had frequencies of the order of megacycles. It was not possible to observe such waves with the Injun 3 VLF experiment.

In summary, the generation of energetic electrons through the mechanism of a two-stream plasma instability proposed by Stix [1964] and observed in the laboratory by Smullin and Getty [1962] and in the low altitude auroral zone by Evans [1967] is believed to



be responsible for the generation of the  $\approx 90$  keV electrons observed in connection with the intense fluxes of  $\geq 10$  keV electrons observed by Injun 3 (e.g., Rev 1397 of Figure 13).

It is noted here that if this mechanism is responsible for the generation of the  $\approx 90$  keV electrons observed in connection with the intense fluxes of  $\geq 10$  keV electrons, the only disagreement between the predictions of the model of Taylor and Hones [1965] and the experimental observations presented here is removed. (See Prediction 2 of the model of Taylor and Hones in the preceeding section.)

## Appendix I

## MAGNETIC ORIENTATION OF INJUN 3

In many of the discussions of the present paper the orientation of the various Injun 3 detectors with respect to the local geomagnetic B vector played an important role in reaching the conclusions. For this reason a study of the effectiveness of the Injun 3 passive magnetic orientation system in maintaining alignment was undertaken and reported by Fritz [1965]. The results of this study will be presented here.

Magnetic orientation of Injun 3 was accomplished by using a large permanent bar magnet and orienting the satellite much like a three-dimensional compass needle. Although this mechanism for satellite orientation was used on the two previous satellites in the Injun series, no experimental verification of its effectiveness was obtained until the launch of Injun 3. The principal element of the orientation system was an Alnico V bar magnet one-inch square and twenty-two inches long with a magnetic moment (M) of  $\approx 1.4 \times 10^5$  ergs/gauss oriented along the  $\theta = 0^\circ - \theta = 180^\circ$  axis [O'Brien, Laughlin, and Gurnett, 1964].

Injun 3 had a moment of inertia (I) of  $\approx 10^7$  gm cm<sup>2</sup> transverse to its magnetic axis and when the satellite was in a geomagnetic

field (B) of 0.3 gauss, it had a natural period of oscillation (T),

$$T = 2 \pi \sqrt{\frac{I}{M B}} \simeq 2 \text{ minutes},$$

which is sufficiently small to maintain alignment continuously even while the direction of the local geomagnetic vector  $\vec{B}$  changes [see Figure 2, O'Brien, Laughlin, and Gurnett, 1964].

The initial angular kinetic energy which the satellite had soon after launch was dissipated by hysteresis losses in twenty-two permalloy rods one-eighth inch in diameter and about 11 inches long mounted perpendicular to the magnetic axis. Fourteen of the rods were mutually perpendicular to the  $\theta = 0^\circ$  and  $\theta = 90^\circ$  axes and the other eight were parallel to  $\theta = 90^\circ$  axis. These rods were also important in maintaining dynamic alignment later. The alignment was measured by two Schonstedt flux gate magnetometers mounted with their axes parallel to the  $\theta = 90^\circ$  and  $\theta = 130^\circ$  axes, respectively. The preflight calibrations of these magnetometers were performed in the Model Ships Magnetic Laboratory of the Naval Ordnance Laboratory and the inflight checks on these calibrations and their constancy found that they were accurate and that they remained constant during the 10 month lifetime of Injun 3 [Fritz, 1965].

Effectiveness of Orientation Mechanism  
in Attaining Alignment with the Geo-  
magnetic Vector  $\vec{B}$

Soon after launch the satellite's rotational motion showed a sluggish behavior with an oscillation period in excess of an hour. At the beginning of the fifth day in orbit, the satellite's rotational motion changed suddenly to an oscillation about the geomagnetic vector  $\vec{B}$  with a period of  $\approx 1$  to 2 minutes. These circumstances were interpreted to mean that the satellite had failed to separate initially from the last stage of the launch vehicle but became disengaged from the rocket during the fifth day in orbit.

After separation occurred, the angular motion of the satellite appeared to be magnetically controlled (i.e., simple harmonic in nature) oscillating about the geomagnetic vector  $\vec{B}$  with an angular deviation from alignment in excess of  $115^\circ$ . Figure 3<sup>4</sup> shows the maximum deviation from alignment recorded during each revolution. It is evident from this figure that the hysteresis damping mechanism was able to dissipate the initial angular kinetic energy of the satellite such that the maximum angular deviation was damped from a deviation in excess of  $115^\circ$  to less than  $10^\circ$  in approximately two weeks. Figure 3<sup>4</sup> demonstrates that the passive magnetic

orientation system of Injun 3 is an effective mechanism for attaining magnetic alignment in a low altitude satellite. The effectiveness of this system in maintaining alignment of Injun 3 was then investigated.

Effectiveness of Orientation Mechanism  
in Maintaining Alignment with the  
Geomagnetic Vector  $\vec{B}$

The Injun 3 magnetometer data were divided into five sample intervals in the McIlwain L parameter. These intervals were:

- |                             |   |
|-----------------------------|---|
| (1) $1.25 \leq L \leq 1.30$ | $(26.6^\circ \leq \Lambda \leq 28.7^\circ)$ |
| (2) $1.80 \leq L \leq 2.00$ | $(41.8^\circ \leq \Lambda \leq 45.0^\circ)$ |
| (3) $3.0 \leq L \leq 3.5$   | $(54.7^\circ \leq \Lambda \leq 57.7^\circ)$ |
| (4) $5.0 \leq L \leq 6.0$   | $(63.4^\circ \leq \Lambda \leq 65.9^\circ)$ |
| (5) $10.0 \leq L \leq 12.0$ | $(71.6^\circ \leq \Lambda \leq 73.2^\circ)$ |

Within each of these intervals, the angular deviation from orientation was calculated every eight seconds for both magnetometers for all data (System A) available after January 1, 1963, within a particular interval. These calculated deviations were then sorted in three different ways:

### 1. As a Function of Time

The deviations were grouped into half-month intervals and the maximum deviation, the mean deviation, and the mean of the absolute value of the deviations were computed for each half-month interval. These quantities were plotted for each of the above L intervals and a representative plot for  $5.0 \leq L \leq 6.0$  is presented in Figure 35.

On examination of these plots, it was found that the maximum deviation for all L intervals varied in a random way between  $5^\circ$  and  $15^\circ$  for the full 10 month period except for the period during the first part of April 1963, when angular deviations from alignment as high as  $25^\circ$  were observed. No satisfactory explanation for these large deviations has been found. The mean of the absolute value of deviations always remained less than  $5^\circ$  except for this period during April 1963 when unusually large deviations occurred.

### 2. As a Histogram of Deviations

Within each of the L intervals, the data were further divided into two groups: The first group was data taken while the satellite was traveling away from the magnetic equator,  $d\Lambda/dt > 0$  ( $\Lambda$  being the invariant latitude defined by the equation  $L \cos^2 \Lambda = 1$ ); and the second group was taken while the satellite was traveling toward

the magnetic equator,  $d\Lambda/dt < 0$ . This division was made because the direction of the geomagnetic vector  $\vec{B}$  changes rapidly near the magnetic equator [see Figure 2, O'Brien, Laughlin, and Gurnett, 1964]. This changing direction of  $\vec{B}$  could introduce disturbances into the system and cause larger deviations.

The number of times a given angular deviation was observed was presented in a histogram type of plot for both magnetometers. The Root-Mean-Square (RMS) deviations were also calculated for each of the groups and these are presented in Figure 36. On examination of each of the histograms, it was found that the form of the histogram and the RMS values for  $d\Lambda/dt > 0$  were not significantly different from the values for  $d\Lambda/dt < 0$  for each magnetometer, but the RMS deviation was approximately one degree larger for the low L values when compared to the higher L values (Figure 36). These results indicated that the satellite was not as well aligned when the direction of the geomagnetic vector  $\vec{B}$  was changing rapidly, but that the rapidly changing direction of  $\vec{B}$  introduced no long term ( $> \text{minutes}$ ) disturbances into the system.

### 3. As a Function of the Scalar Magnitude of $\vec{B}$

The angular deviations from alignment were grouped into the following intervals of  $|\vec{B}|$ :

- (1)  $B < .200$  (B in gauss)
- (2)  $.200 \leq B < .300$
- (3)  $.300 \leq B < .400$
- (4)  $.400 \leq B < .500$
- (5)  $.500 \leq B$

for each of the L groups. Within each of the intervals of  $|\vec{B}|$ , the mean deviation and the standard deviations of the individual readings were calculated. The results of this study showed that the strength of the geomagnetic field had little effect on the capability of the orientation mechanism to orient the satellite.

### Conclusion

The passive magnetic orientation system described in this appendix was successful in attaining and maintaining alignment with respect to the geomagnetic vector  $\vec{B}$  in the Injun 3 satellite.

Specifically, the orientation mechanism was able to dissipate the initial angular kinetic energy of the satellite such that the maximum angular deviation from alignment was damped from a deviation in excess of  $115^\circ$  to less than  $10^\circ$  in approximately two weeks to attain initial alignment. Over the 10 month active



lifetime of the satellite, the orientation mechanism was able to maintain alignment so that the RMS deviation was less than  $5^\circ$  at all latitudes (L). The capability of the orientation mechanism to maintain alignment was slightly dependent on the rate of change of the direction of the geomagnetic vector  $\vec{B}$  (the RMS deviation was approximately one degree larger at low latitudes where the direction of  $\vec{B}$  is changing rapidly when compared to the higher latitudes) but showed little dependence on the strength of the geomagnetic field or on the sense of travel with respect to the magnetic equator (toward or away).

## Appendix II

## THE RESPONSE OF DETECTOR 5

In the present paper many of the findings were based on the response of Detector 5. Since Detector 5 was a thin-windowed, open-end Geiger tube, its response could have been due to or contaminated by the following:

- (a) Electrons with  $E_e \geq 40$  keV travelling with pitch angles at the position of the satellite such that they would have been precipitated (i.e., mirror below 100 km altitude).
- (b) Electrons with  $E_e \geq 40$  keV mirroring near the satellite which were counted directly or scattered into the aperture and counted as precipitated electrons.
- (c) Higher energy penetrating electrons and/or bremsstrahlung produced by electrons bombarding the satellite.
- (d) Soft solar x-rays when the detector viewed the sun.

In this appendix we will try to demonstrate that the response of Detector 5 was primarily due to (a) with (b), (c), and (d) contributing negligible amounts.

The contamination of the response of Detector 5 due to soft x-ray was discussed in Chapter IV. Periods when Detector 5 viewed the sun were easily identified by the response of the companion solar aspect sensor and therefore (d) can be eliminated.

The contamination of the response of Detector 5 due to bremsstrahlung or to high energy penetrating electrons was investigated with the SpB detector. Both Detector 5 and SpB have approximately the same omnidirectional geometric factors and similar omnidirectional shielding [O'Brien, Laughlin, and Gurnett, 1964]. SpB was sensitive only to the higher energy penetrating protons ( $E_p > 70$  MeV) or to bremsstrahlung produced by electrons with  $E_e \gtrsim 2$  MeV. Two latitude profiles of the responses of Detector 5 and SpB are presented in Figure 37 using two of the undisturbed passes presented in Figures 3 and 4. The large variations in the SpB counting rates were mostly statistical (1 count/second corresponded to 8 counts). It will be noted that the SpB rate as a function of latitude was rarely more than a few times the cosmic ray background rate whereas the Detector 5 response was never less than a factor 20 greater than its response to cosmic ray background. Since a nominal 0.6 cts/second was always subtracted from the Detector 5 response when the dumping parameter,  $\phi$ , was calculated, the contribution of (c) can be neglected as possible source of contamination.

The response of Detector 5 due to trapped electrons being counted directly or scattered into the aperture was regarded as the most serious possible source of contamination. Since latitude profiles of the counting rates of Detector 5 and Detector 1 were very similar (i.e.,  $\phi$  was independent of latitude), the problem appeared even more serious.

The approach to this problem was to use the experimentally determined angular response function for Detector 5 and determine whether the detector could respond to trapped electrons when the satellite was properly aligned. The rate of any Geiger tube can be expressed by the integral,

$$\text{Rate} = \int g(E, \theta) F(\alpha, E) dE d\Omega$$

where

$g(E, \theta)$  is the Geiger tube response characteristic as a function of incident particle energy and aperture opening angle,  $\theta$ .

$F(\alpha, E)$  is the particle distribution function depending on particle energy and pitch angle,  $\alpha$ .

The above functions are usually assumed to be separable in each variable, so

$$g(E, \theta) = \epsilon(E) \epsilon(\theta) A$$

where  $A$  is the effective area of the tube

$$F(\alpha, E) = f(\alpha) f(E) .$$

Therefore

$$\text{Rate} = A \int_0^{\infty} \epsilon(E) f(E) dE \int \epsilon(\theta) f(\alpha) d\Omega .$$

Solid  
Angle

In the present case we are really interested in the ratio of the response of Detector 5 to the response of Detector 1.

$$\begin{aligned} \text{Ratio} &= \frac{\text{Rate (Det. 5)}}{\text{Rate (Det. 1)}} \\ &= \frac{A_5 \int \epsilon_5 (E) f (E) dE \int \epsilon_5 (\theta) f (\alpha) d\Omega}{A_1 \int \epsilon_1 (E) f (E) dE \int \epsilon_1 (\theta) f (\alpha) d\Omega} . \end{aligned}$$

Assuming similar window thicknesses and effective areas for the two 213 Geiger tubes, we have

$$\text{Ratio} = \frac{\int \epsilon_5 (\theta) f (\alpha) d\Omega}{\int \epsilon_1 (\theta) f (\alpha) d\Omega} .$$

A form for the particle pitch angle distribution,  $f (\alpha)$  must be assumed. The usual assumption is

$$f (\alpha) = \sin^n \alpha$$

where  $n$  is a variable controlling the width of the angular distribution. From the work of Armstrong [1965b],  $n$  was determined to be in the range  $1 \leq n \leq 2$  for the low altitude outer zone using the same detector at various  $B$  values on a given  $L$  shell.

The function  $\epsilon_5 (\theta)$  was experimentally determined using the identical flight back-up detector [J. D. Craven and H. K. Hills, private communication]. By assuming a pitch angle distribution

Now, if there are no particles being precipitated, there must be some angle,  $\alpha_D$ , for which there is a cutoff in the pitch angle distribution. (That is, all particles with  $\alpha < \alpha_D$  will mirror below 100 km and be lost to the atmosphere.) Therefore for evaluating the response integral for Detector 5, we assume

$$\begin{aligned} f(\alpha) &= \sin^n \alpha & \alpha &\geq \alpha_D \\ &= 0 & \alpha &< \alpha_D \end{aligned}$$

and evaluate numerically the integral

$$2\pi \int_{\alpha_D}^{\pi} \epsilon_5(\alpha) \sin^{n+1} \alpha \, d\alpha$$

as a function of  $\alpha_D$  for various values of  $n$ . The ratio of the rates of the two detectors is calculated then as a function of  $n$  and  $\alpha_D$ . Using the correction for the geometric factors, the ratio of  $j(>40 \text{ keV})$  dumped to  $j(>40 \text{ keV})$  trapped is also calculated as a function of  $n$  and  $\alpha_D$ . This functional dependence is presented in Figure 38.

It was found that Detector 5 had a vanishing response to any particle with a pitch angle  $\alpha > 48^\circ$  (independent of  $n$ ). Therefore if the ratio of the fluxes  $j(\text{Det. 5})/j(\text{Det. 1})$  was greater than  $10^{-3}$  and all particle pitch angles less than  $48^\circ$

of the above form, the function  $\epsilon_5(\theta)$  becomes  $\epsilon_5(\alpha)$  since the viewing cone of Detector 5 was centered at  $\alpha = 0^\circ$  (i.e., parallel to the field line). The function  $\epsilon_1(\theta)$  however becomes a complicated function of  $\alpha$  and  $\varphi$ . Therefore

$$\text{Ratio} = \frac{\int \epsilon_5(\alpha) \sin^{n+1} \alpha \, d\alpha \, d\varphi}{\int \epsilon_1(\alpha, \varphi) \sin^{n+1} \alpha \, d\alpha \, d\varphi}.$$

The top integral is the one of interest to us and can be evaluated numerically since the variables are separable. The bottom integral is used only as a normalizing function but is very difficult to evaluate due to the dependence of  $\epsilon_1$  on both  $\alpha$  and  $\varphi$ . T. P. Armstrong [private communication] has written a computer program which evaluates the bottom integral assuming,

$$\begin{aligned} \epsilon(\theta) &= \cos \theta & \theta < \theta_{1/2} \\ &= 0 & \theta \geq \theta_{1/2} \end{aligned}$$

where  $\theta_{1/2}$  is the opening half angle of the detector aperture. This approximation should be sufficient here. Using  $\theta_{1/2} = 13^\circ$  for Detector 1, the computer integrations gives,

$$\begin{aligned} \int \epsilon(\alpha, \varphi) \sin^{n+1} \alpha \, d\alpha \, d\varphi &= 0.1006 & \text{for } n = 0 \\ &0.0998 & \text{for } n = 1 \\ &0.0991 & \text{for } n = 2 \end{aligned}$$

# REFERENCES

- Akasofu, S.-I., "Electrodynamics of the magnetosphere: geomagnetic storms," Space Science Reviews 6, 21-143 (1966).
- Armstrong, T., "Morphology of the outer zone electron distribution at low altitudes from January through July and September, 1963 from Injun 3," J. Geophys. Res. 70, 2077-2110 (1965a).
- Armstrong, T., "Angular distribution of outer zone electrons at 250- to 2500-km altitude," Trans. AGU 46, 528-529 (1965b).
- Block, Lars P., "Coupling between the outer magnetosphere and the high latitude ionosphere," Royal Institute of Technology Research Report, Nr 65-13 (1966).
- Chang, D. B. and L. D. Pearlstein, "On the effect of resonant magnetic-moment violation on trapped particles," J. Geophys. Res. 70, 3075-3083 (1965).
- Cladis, J. D., L. F. Chase, W. L. Imhof, and D. J. Knecht, "Energy spectrum and angular distributions of electrons trapped in the geomagnetic field," J. Geophys. Res. 66, 2297-2312 (1961).
- Cornwall, John M., "Scattering of energetic trapped electrons by very-low frequency waves," J. Geophys. Res. 69, 1251-1258 (1964).
- Craven, J. D., "Temporal variations of electron intensities at low altitudes in the outer radiation zone as observed with satellite Injun 3," J. Geophys. Res. 71, 5643-5663 (1966).
- Dessler, A. J. and R. Karplus, "Some effects of diamagnetic ring currents on Van Allen radiation," J. Geophys. Res. 66, 2289-2295 (1961).
- Dragt, A. J., "Effects of hydromagnetic waves on the lifetime of Van Allen radiation protons," J. Geophys. Res. 66, 1641-1649 (1961).



mirrored below the atmosphere (100 km), then it must be concluded that Detector 5 was responding to precipitated particles.

Over North America where most of the satellite data were taken  $B_{100 \text{ km}} = 0.47$  to  $0.58$  gauss for outer zone latitudes. This corresponded to the restriction that Detector 5 was responding to precipitated particles at the position of the satellite when

$$B_{\text{local}} \geq B_{(100 \text{ km})} \sin^2 48^\circ$$

or

$$\begin{aligned} B_{\text{local}} &\geq 0.26 \text{ gauss for } \Lambda \approx 45^\circ \\ &0.28 \text{ gauss for } \Lambda \approx 55^\circ \\ &0.32 \text{ gauss for } \Lambda \approx 70^\circ \end{aligned}$$

conditions which were easy to satisfy.

- Fritz, T. A. and D. A. Gurnett, "Diurnal and latitudinal effects observed for 10-keV electrons at low satellite altitudes," J. Geophys. Res. 70, 2485-2502 (1965).
- Gurnett, D. A. and B. J. O'Brien, "High-latitude geophysical studies with satellite Injun 3. 5. Very low frequency electromagnetic radiation," J. Geophys. Res. 69, 65-90 (1964).
- Johansen, O. E., "Variations in energy spectrum of auroral electrons detected by simultaneous observation with photometer and riometer," Planet. Space Sci. 13, 225-235 (1965).
- Kennel, Charles F., "Parasitic electron precipitation," Trans. AGU 48, 180 (1967).
- Kennel, C. F. and H. E. Petschek, "Limit on stably trapped particle fluxes," J. Geophys. Res. 71, 1-29 (1966a).
- Kennel, C. F. and H. E. Petachek, "Van Allen belt plasma physics," Avco Everett Res. Rept. 259, December 1966b.
- Kennel, C. F. and R. M. Thorne, "Unstable growth of unducted whistlers propagating at an angle to the geomagnetic field," J. Geophys. Res. 72, 871-878 (1967).
- Laughlin, C. D., "A satellite borne magnetic electron spectrometer, U. of Iowa Research Report 60-14 (1960).
- Maehlum, B. and B. J. O'Brien, "Study of energetic electrons and their relationship to auroral absorption of radio waves," J. Geophys. Res. 68, 997-1010 (1963).
- McDiarmid, I. B. and J. R. Burrows, "Diurnal intensity variations in the outer radiation zone at 1000 km," Can. J. Phys. 42, 1135-1148 (1964).
- McDiarmid, I. B., J. R. Burrows, E. E. Budzinski, and Margaret D. Wilson, "Some average properties of the outer radiation zone at 1000 km," Can. J. Phys. 41, 2064-2079 (1963).

- Dungey, J. W., "Effects of electromagnetic perturbations on particles trapped in the radiation belts," Space Science Reviews 4, 199-222 (1965).
- Evans, David S., "A 10 cps periodicity in the precipitation of auroral zone electrons," NASA GSFC Res. Rept. X-611-67-216, May 1967.
- Eviatar, Aharon, "The role of electrostatic plasma oscillations in electron scattering in the earth's outer magnetosphere," J. Geophys. Res. 71, 2715-2728 (1966).
- Fairfield, D. H., "Ionospheric current patterns in high latitudes," J. Geophys. Res. 68, 3589-3602 (1963).
- Fairfield, D. H., "A study of the high latitude ionospheric current patterns--with emphasis on the 12th hour UT," Penn. State Ionospheric Res. Rept. 217 (1964).
- Fälthammer, Carl-Gunne, "Effects of time dependent electric fields on geomagnetically trapped radiation," J. Geophys. Res. 70, 2503-2516 (1965).
- Farley, T. A., "The growth of our knowledge of the earth's outer radiation zone," Reviews of Geophysics 1, 3-34 (1963).
- Frank, L. A., "A survey of electrons beyond 5  $R_E$  with Explorer 14," J. Geophys. Res. 70, 1593-1626 (1965).
- Frank, L. A., J. A. Van Allen, and J. D. Craven, "Large diurnal variations of geomagnetically trapped and of precipitated electrons observed at low altitudes," J. Geophys. Res. 69, 3155-3167 (1964).
- Fritz, T. A., "A latitude survey of the electron energy spectrum in the outer zone (unpublished Master's thesis, Department of Physics and Astronomy, University of Iowa, 1964).
- Fritz, T. A., "The passive magnetic orientation of satellite Injun 3," U. of Iowa Research Report 65-21 (1965).

- O'Brien, B. J. and H. Taylor, "High-latitude geophysical studies with satellite Injun 3. 4. Auroras and their excitation," J. Geophys. Res. 69, 45-63 (1964).
- O'Brien, B. J., J. A. Van Allen, C. D. Laughlin, and L. A. Frank, "Absolute electron intensities in the heart of the earth's outer radiation zone," J. Geophys. Res. 67, 397-403 (1962).
- Parthasarathy, R., F. T. Berkey, and D. Venkatesan, "Auroral zone electron flux and its relation to broadbeam radiowave absorption," Planet. Space Sci. 14, 65-83 (1966).
- Persson, H., "Electric field parallel to magnetic field in a low density plasma," Phys. Fluids 9, 1090-1098 (1966).
- Rao, C. S. R., "Study of the temporal variations of 40 keV electrons in the magnetosphere during and after the magnetic storm on April 18, 1965," U. of Iowa Research Report 67-16, 1-60 (1967).
- Roberts, C. S., "Electron loss from the Van Allen zones due to pitch angle scattering by electromagnetic disturbances, Radiation Trapped in the Earth's Magnetic Field," Proceedings of Advanced Study Institute, 403-421 (1966).
- Smullin, L. D. and W. D. Getty, "Generation of a hot, dense plasma by a collective beam-plasma interaction," Phys. Rev. Letters 9, 3-6 (1962).
- Stilwell, D. E., "Observations of intense, low energy electron fluxes in the outer zone during January and March, 1963," U. of Iowa Research Report 63-28, 1-111 (1963).
- Stix, Thomas H., "Energetic electrons from a beam-plasma overstability," Phys. Fluids 7, 1960-1979 (1964).
- Taylor, Harold E. and Edward W. Hones, Jr., "Adiabatic motion of auroral particles in a model of the electric and magnetic fields surrounding the earth," J. Geophys. Res. 70, 3605-3628 (1965).
- Thorne, R. M. and C. F. Kennel, "Quasi-trapped VLF propagation in the outer magnetosphere," J. Geophys. Res. 72, 857-870 (1967).

- McIlwain, C. E., "Coordinates for mapping the distribution of magnetically trapped particles," J. Geophys. Res. 66, 3681-3691 (1961).
- McIlwain, C. E., "Direct measurements of particles producing visible aurorae," J. Geophys. Res. 65, 2727-2747 (1960).
- McIlwain, C. E., "Processes acting upon outer zone electrons. I. Adiabatic perturbations, presented at Inter-Union Symposium on Solar-Terrestrial Physics, Belgrade, Yugoslavia, September 1, 1966.
- Mihalov, J. D. and R. S. White, "Energetic electron spectra in the radiation belts," J. Geophys. Res. 71, 2217-2226 (1966).
- Mozer, F. S. and P. Bruston, "Electric field measurements in the auroral ionosphere," J. Geophys. Res. 72, 1109-1114 (1967).
- O'Brien, B. J., "High latitude geophysical studies with satellite Injun 3. 3. Precipitation of electrons into the atmosphere," J. Geophys. Res. 69, 13-43 (1964).
- O'Brien, B. J., "Lifetimes of outer-zone electrons and their precipitation into the atmosphere," J. Geophys. Res. 67, 3687-3706 (1962).
- O'Brien, B. J. and C. D. Laughlin, "Electron precipitation and the outer radiation zone, Space Research III, Proceedings of the Third International Space Science Symposium," edited by W. Priest, North Holland Publishing Co., 399-417 (1963).
- O'Brien, B. J., C. D. Laughlin, and D. A. Gurnett, "High-latitude geophysical studies with satellite Injun 3. 1. Description of the satellite," J. Geophys. Res. 69, 1-12 (1964).
- O'Brien, B. J., C. D. Laughlin, J. A. Van Allen, and L. A. Frank, "Measurements of the intensity and spectrum of electrons at 1000 km altitude and high latitudes," J. Geophys. Res. 67, 1209-1225 (1962).

## FIGURE CAPTIONS

- Figure 1. Spectral response passbands of several Injun 3 detectors.
- Figure 2. Background responses of the Injun 3 differential spectrometer channels to galactic cosmic rays over the polar caps of the earth.
- Figure 3. A sample pass through the outer zone exhibiting undisturbed electron characteristics.
- Figure 4. Four examples of undisturbed passes taken in different sectors of local time.
- Figure 5. Four examples of undisturbed passes. Rev 1700, Rev 1923, and Rev 1981 exhibited the absence of a "spike" of precipitating electrons at the boundary and Rev 1708 illustrated contamination of the Detector 5 response by solar x-rays near the local noon meridian.
- Figure 6. Magnetic conditions during the active lifetime of Injun 3.
- Figure 7. Two passes (Rev 239 and Rev 241) of a series taken on January 1-2, 1963 during a magnetically quiet period in which large amounts of  $\geq 40$  keV electrons were observed precipitating into the atmosphere.
- Figure 8. Continuation of the series of Figure 7 (Rev 243 and Rev 244).
- Figure 9. Continuation of the series of Figure 7 (Rev 252 and Rev 253).

- Trakhtengerts, V. Yu., "Kinetic instability of the outer radiation zone of the earth," *Geomagnetism and Aeronomy* (English Transl.) V, 865-867 (1965).
- Van Allen, J. A., "Dynamics, composition, and origin of the geomagnetically-trapped corpuscular radiation," *Trans. Intern. Astron. Union* 11B, 99-136 (1962).
- Van Allen, J. A., G. H. Ludwig, E. C. Ray, and C. E. McIlwain, "Observations of high-intensity radiation by satellites 1958 $\alpha$  and  $\gamma$ , *IGY Satellite Report Series No. 3: Some preliminary reports of experiments in satellites 1958 $\alpha$  and  $\gamma$* ," National Academy of Sciences, Washington, D. C., 73-92 (1958).
- Van Allen, J. A., L. A. Frank, B. Maehlum, and L. W. Acton, "Solar x-ray observations by Injun 1," *J. Geophys. Res.* 70, 1639-1645 (1965).
- Van Allen, J. A. and L. A. Frank, "Radiation around the earth to a radial distance of 107,400 km," *Nature* 183, 430-434 (1959).
- Van Allen, J. A., C. E. McIlwain, and G. H. Ludwig, "Radiation observations with satellite 1958 $\epsilon$ ," *J. Geophys. Res.* 64, 271-286 (1959).
- Walt, Martin and William M. MacDonald, "The influence of the earth's atmosphere on geomagnetically trapped particles," *Reviews of Geophysics* 2, 543-577 (1964).
- Wende, Charles D., "Solar x-ray observations by the satellites Injun 1 and Injun 3," U. of Iowa Master's Thesis, unpublished, 1-132 (1966).
- Wentzel, D. G., "Hydromagnetic waves and the trapped radiation-- Part 1. Breakdown of the adiabatic invariance; Part 2. Displacement of the mirror points," *J. Geophys. Res.* 66, 359-369 (1961).

Figure 20. An example of a pass (Rev 3999) taken in the southern hemisphere in which the intense flux of  $\geq 10$  keV electrons mirrored at 1000 km and was observed at the satellite moving toward the equatorial plane.

Figure 21. A scatter plot of the spectral parameter,  $\gamma$ , for the interval from 40 keV to 100 keV calculated at positions of integral and half-integral L values. The statistical parameters for the data are also shown.

Figure 22. Scatter plots of the spectral parameter,  $\gamma$ , for the interval from 40 keV to 100 keV as a function of the scalar value of the geomagnetic field intensity, B, for the regions  $3.0 \leq L \leq 3.5$  and  $5.0 \leq L \leq 8.0$  with the dependence of  $\gamma$  on L normalized (see text) to  $\gamma = 2.0$  in each plot. The statistical parameters associated with each plot are also shown.

Figure 23. Scatter plots of the spectral parameter,  $\gamma$ , for the interval from 40 keV to 100 keV as a function of the daily  $K_p$  sums geomagnetic activity index for the regions  $2.0 \leq L \leq 3.0$  and  $4.5 \leq L \leq 8.0$  with the dependence of  $\gamma$  on L normalized (see text) to  $\gamma = 2.0$  in each plot. The statistical parameters associated with each plot are also shown.

Figure 24. Scatter plots of the spectral parameter,  $\gamma$ , for the interval from 40 keV to 100 keV as a function of the intensity of trapped electrons with  $E_e \geq 40$  keV for the region  $2.0 \leq L \leq 3.0$  and  $L \geq 4.5$  with the dependence of  $\gamma$  on L normalized (see text) to  $\gamma = 2.0$  in each plot. The statistical parameters associated with each plot are also shown.



Figure 10. Continuation of the series of Figure 7 (Rev 255).

Rev 243 is a pass through the outer zone in the southern hemisphere recorded between Rev 243 and Rev 244 of Figure 8.

Figure 11. A summary of the variations observed in the series of passes Rev 239--Rev 255 at  $\Lambda = 50^\circ$ ,  $\Lambda = 55^\circ$ ,  $\Lambda = 60^\circ$ ,  $\Lambda = 65^\circ$ , and  $\Lambda = 68^\circ$  for January 1-2, 1963.

Figure 12. Four consecutive passes through the high latitude boundary recorded near the midnight meridian.

Figure 13. Four passes taken a day apart through similar L, B, MLT coordinates which were recorded during the magnetic disturbance of April 2-11, 1963.

Figure 14. Continuation of Figure 13.

Figure 15. A summary of the variations observed in the series of passes presented in Figures 13 and 14 at  $\Lambda = 50^\circ$ ,  $\Lambda = 55^\circ$ ,  $\Lambda = 60^\circ$ ,  $\Lambda = 65^\circ$ , and  $\Lambda = 68^\circ$  for April 2-11, 1963.

Figure 16. An example of a pass (Rev 2354) on which an intense flux of  $\geq 10$  keV electrons was observed precipitating into the atmosphere.

Figure 17. Consecutive passes around Rev 2354 of Figure 16 illustrating the temporal characteristics associated with the intense fluxes of  $\geq 10$  keV precipitating electrons.

Figure 18. Four examples of passes on which an intense flux of  $\geq 10$  keV electrons was observed precipitating into the atmosphere.

Figure 19. Continuation of Figure 18.

Figure 32. A scatter plot of the spectral parameter,  $\gamma$ , for the interval from 10 keV to 40 keV as a function of  $j$  ( $E_e \geq 10$  keV) with the statistical parameters associated with the plot.

Figure 33. A scatter plot of the spectral parameter,  $\gamma$ , for the interval from 10 keV to 40 keV as a function of the three hour planetary  $K_p$  index with the statistical parameters associated with the plot.

Figure 34. The maximum initial angular deviation from alignment as a function of time for satellite Injun 3.

Figure 35. An example of the results of the study of the angular deviation from magnetic alignment as a function of time for  $5.0 \leq L \leq 6.0$  during the active lifetime of satellite Injun 3.

Figure 36. The rms deviation from alignment during the satellite active lifetime as a function of latitude.

Figure 37. Sample counting rate profiles as a function of latitude for Detector 5 and SpB during undisturbed conditions.

Figure 38. Variation of the ratio of  $j$  ( $E_e \geq 40$  keV) dumped to  $j$  ( $E_e \geq 40$  keV) trapped as a function of the loss cone cutoff angle,  $\alpha_D$ , for various assumed particle pitch angle distributions.

Figure 25. A scatter plot of the spectral parameter,  $\gamma$ , for the interval from 40 keV to 100 keV as a function of the intensity of precipitated electrons with  $E_e \geq 40$  keV for the region  $5.0 \leq L \leq 8.0$ . The statistical parameters for the data are also shown.

Figure 26. A scatter plot of the spectral parameter,  $\gamma$ , for the interval from 40 keV to 100 keV as a function of the degree of precipitation occurring in the region  $5.0 \leq L \leq 8.0$ . The statistical parameters for the data are also shown.

Figure 27. A scatter plot of the spectral parameter,  $\gamma$ , for the interval from 40 keV to 100 keV as a function of the intensity of the 3914 Å auroral light emission.

Figure 28. Scatter plots of the dumping parameter,  $\phi$ , as a function of  $L$  for all data and for data only with  $B \geq 0.300$  gauss. The statistical parameters for the data are also shown.

Figure 29. Frequency of occurrence for near isotropic distributions ( $\phi \geq 0.32$ ) as a function of the geomagnetic field intensity,  $B$ .

Figure 30. A scatter plot of the spectral parameter,  $\gamma$ , for the interval from 10 keV to 40 keV as a function of invariant latitude,  $\Lambda$ , with the statistical parameters associated with the plot.

Figure 31. A scatter plot of the spectral parameter,  $\gamma$ , for the interval from 10 keV to 40 keV as a function of magnetic local time, MLT, with the statistical parameters associated with the plot.

G67-517

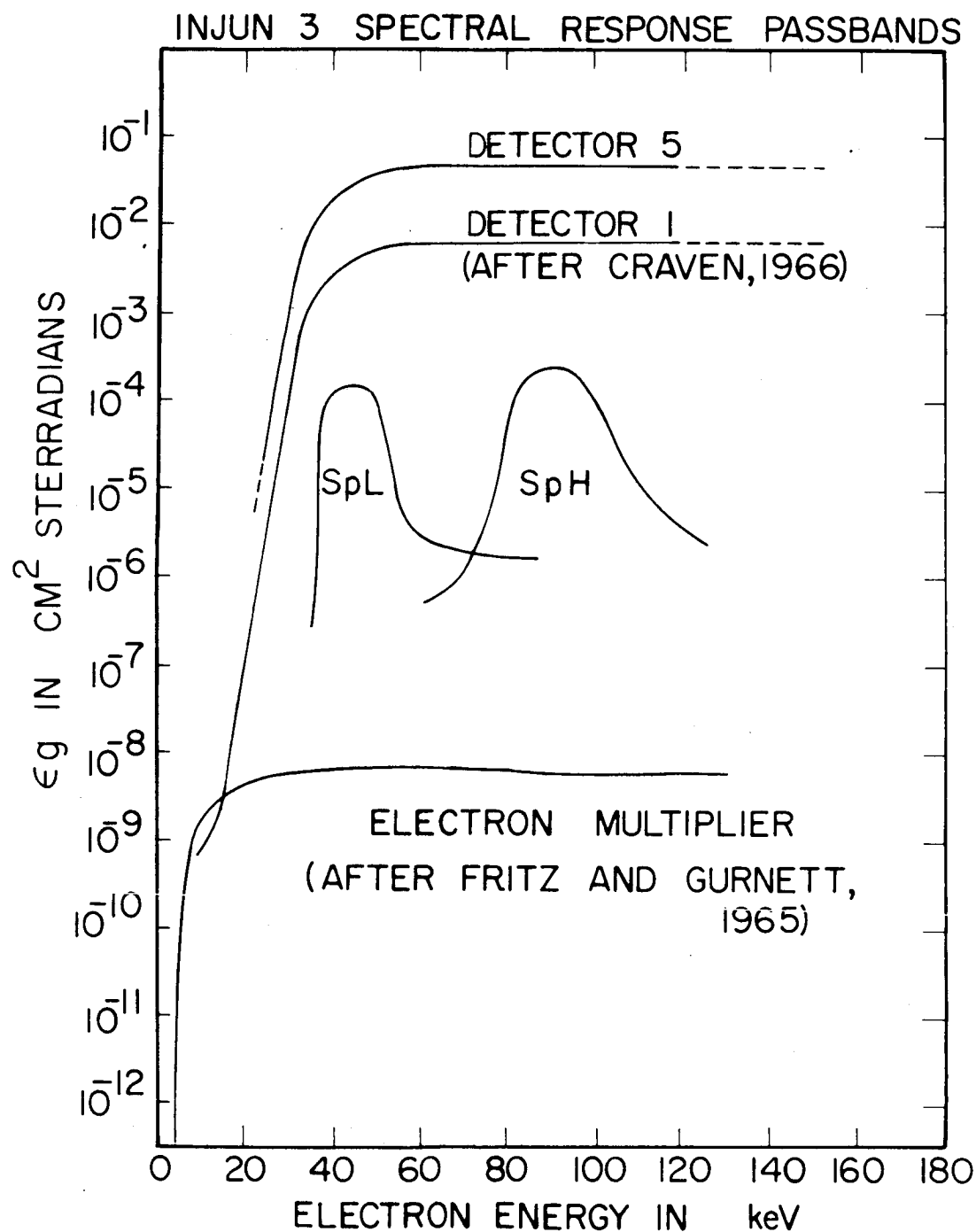


FIGURE 1

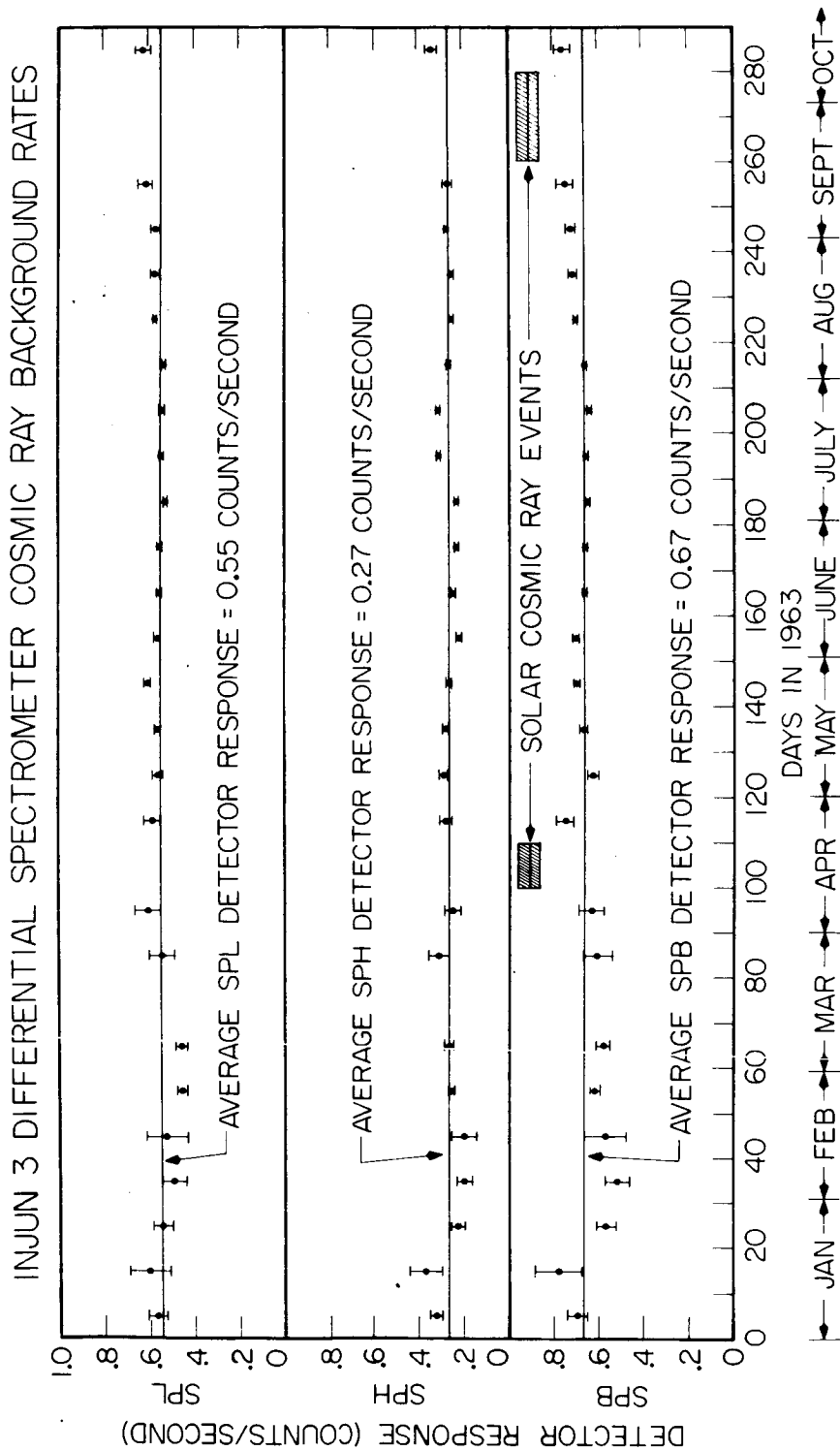


FIGURE 2

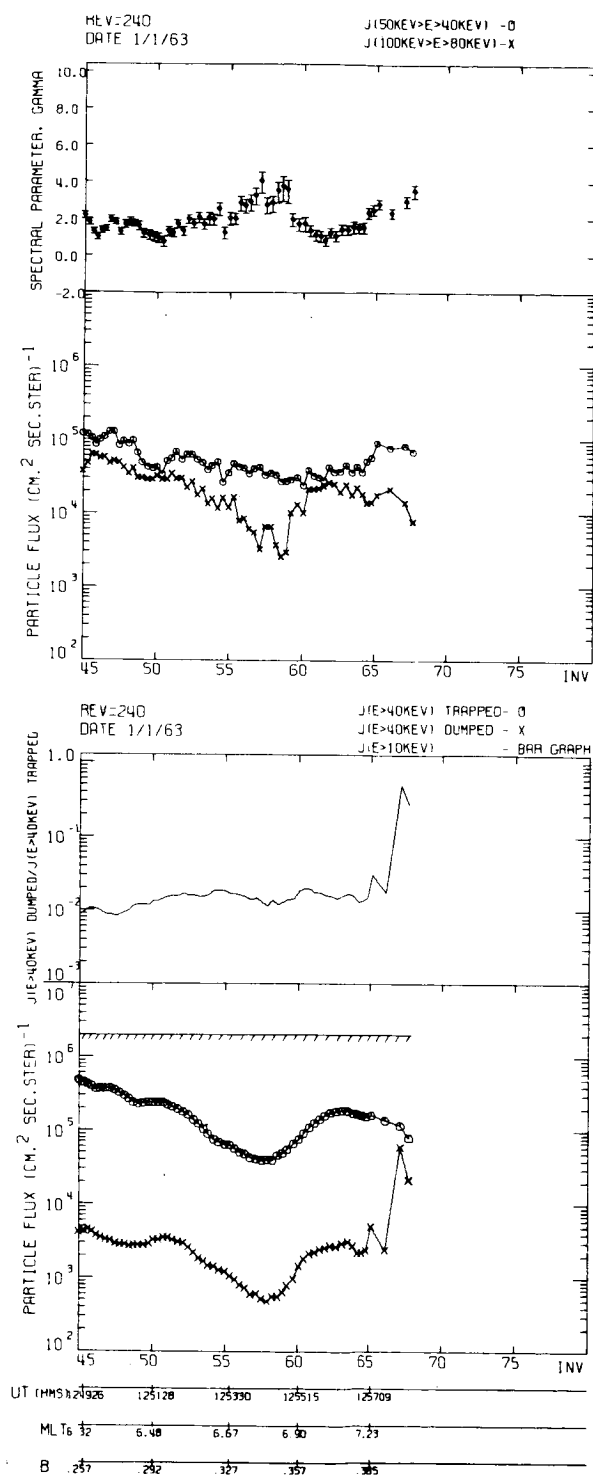


FIGURE 3

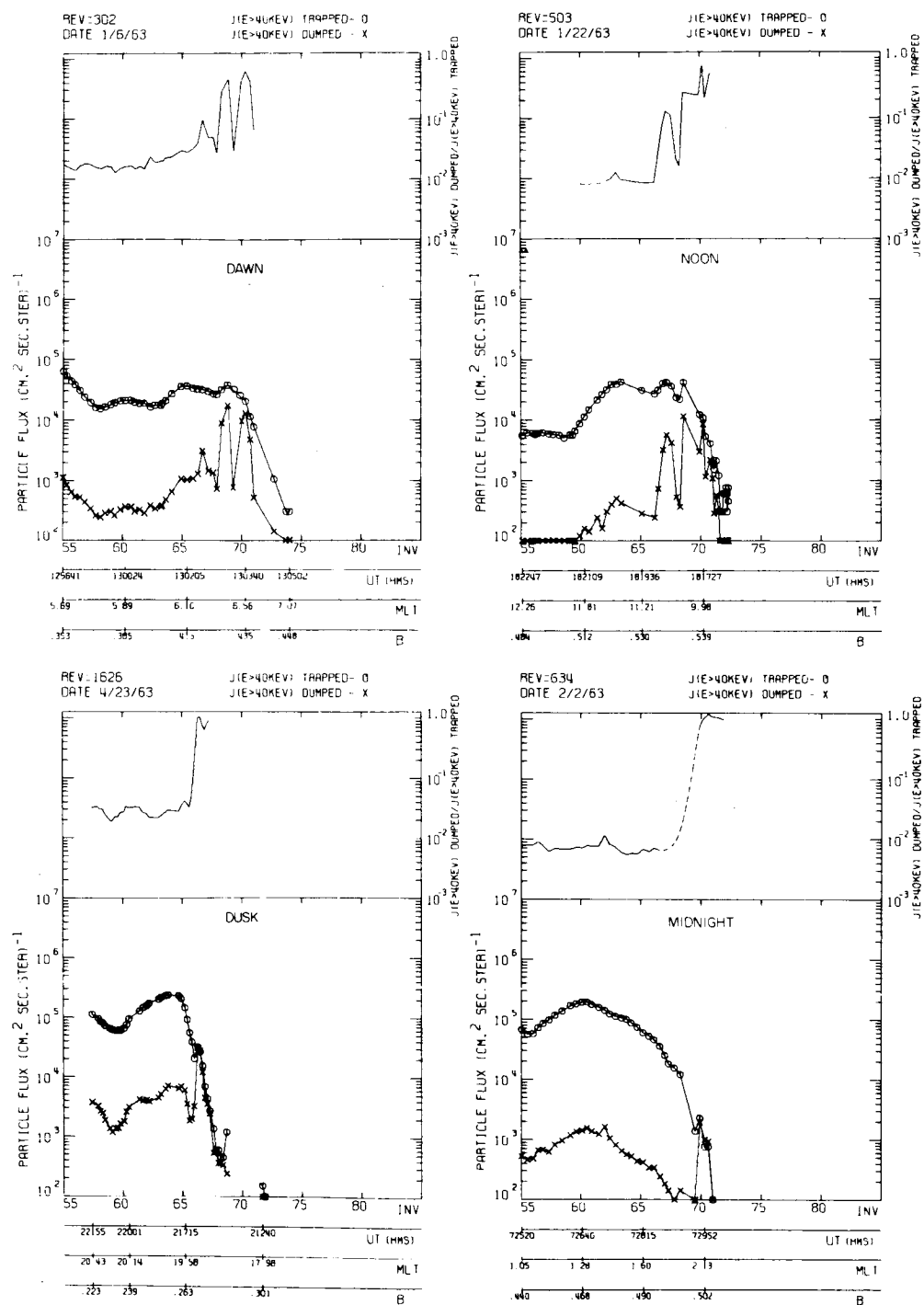


FIGURE 4

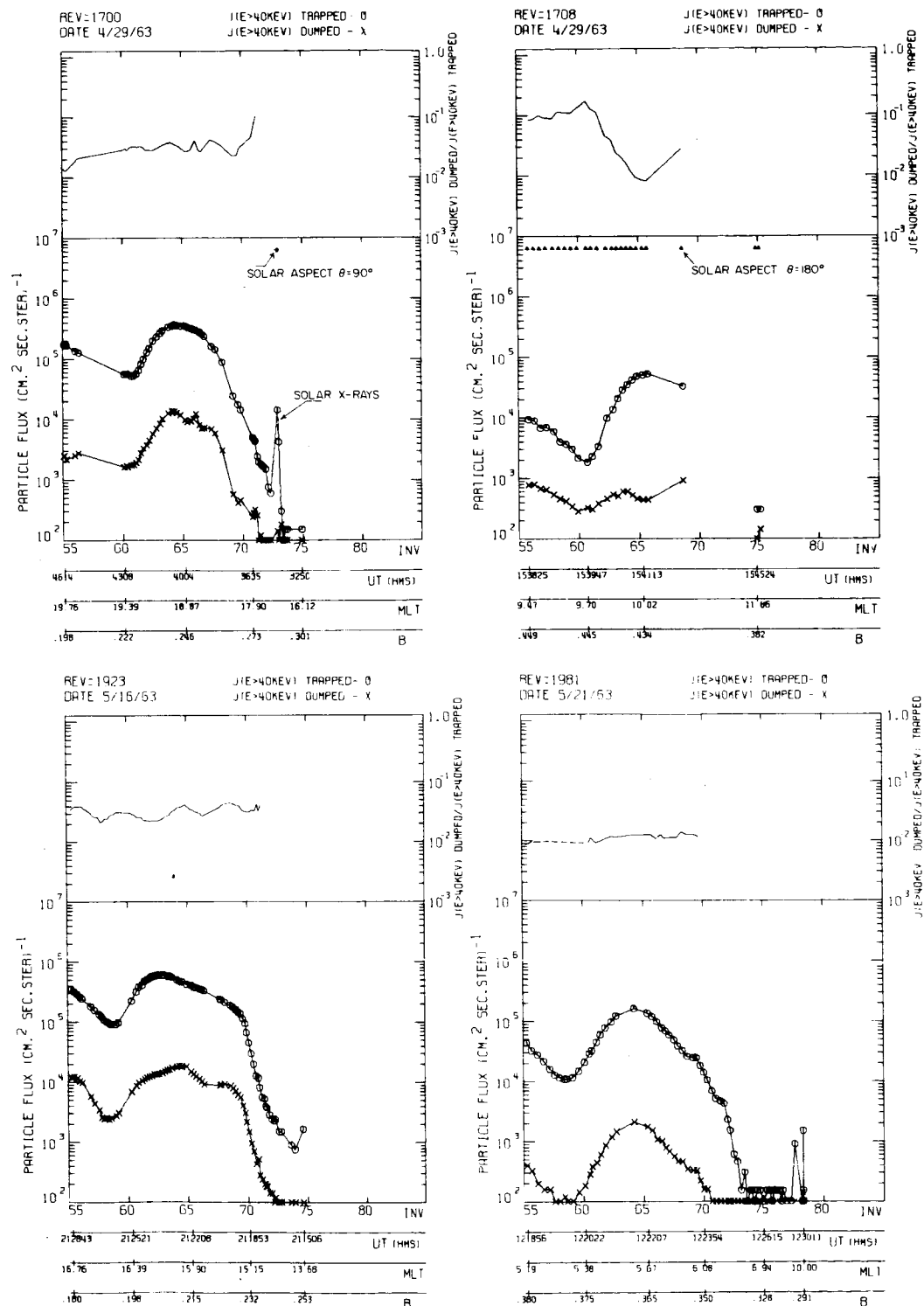


FIGURE 5



667-621

## MAGNETIC CONDITIONS DURING INJUN 3 ACTIVE LIFETIME

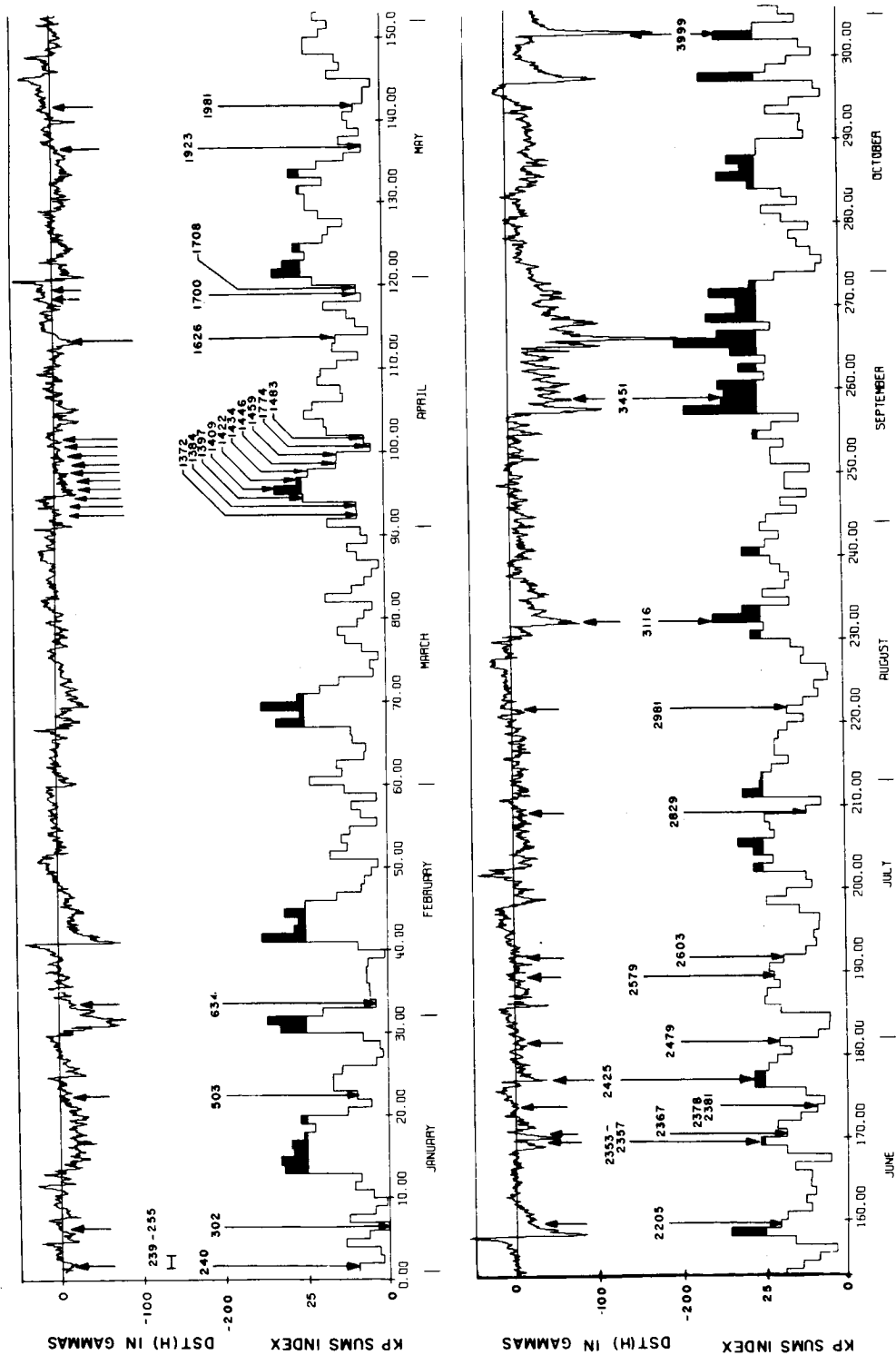


FIGURE 6

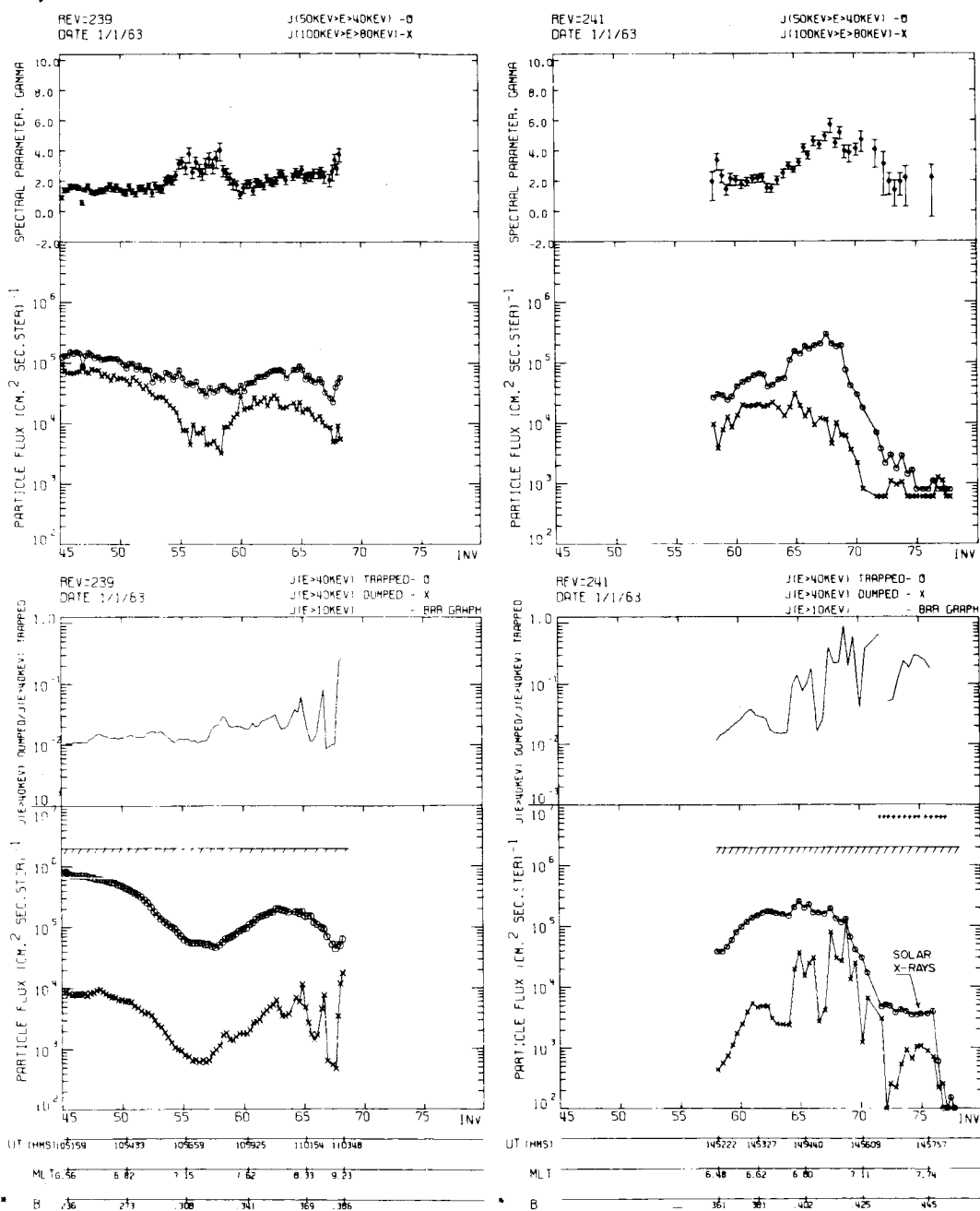


FIGURE 7

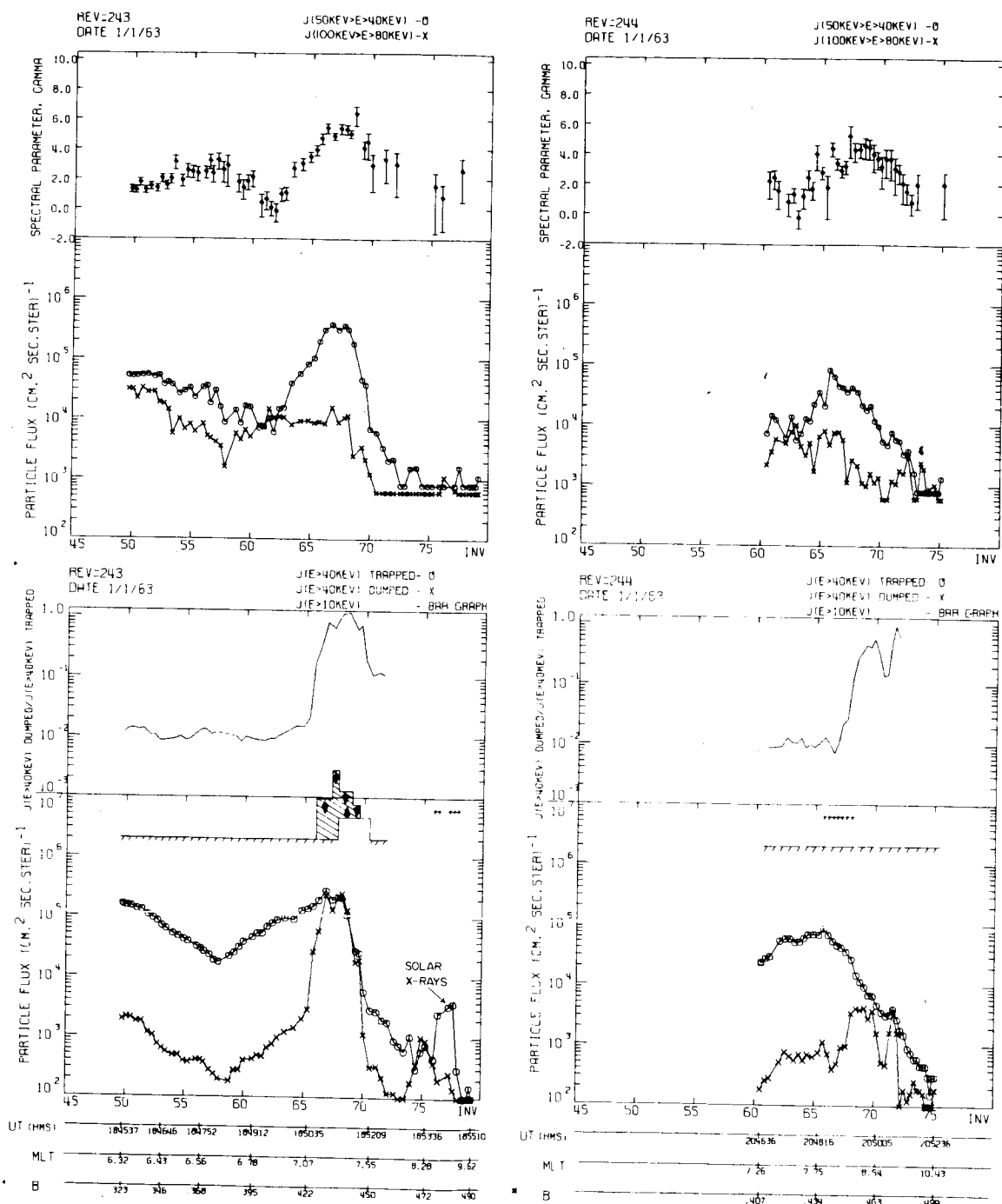
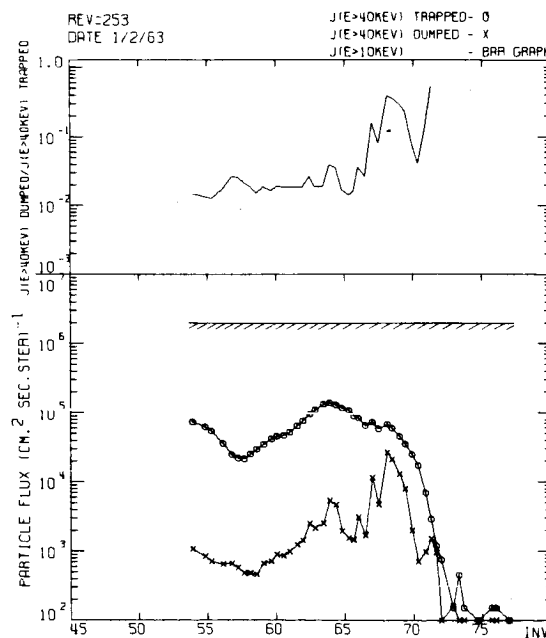
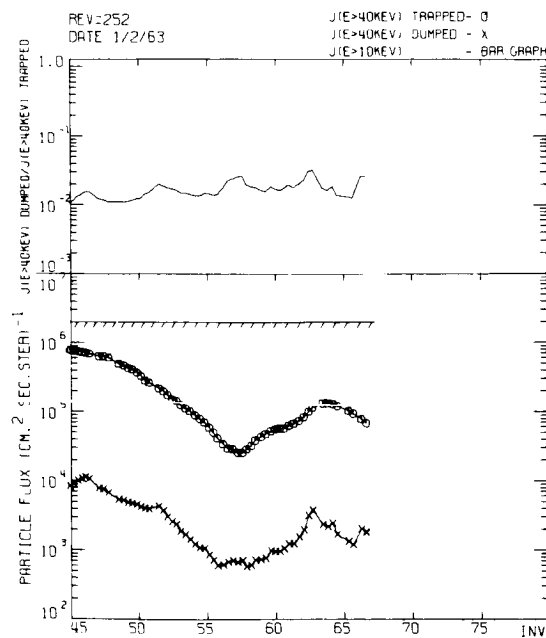
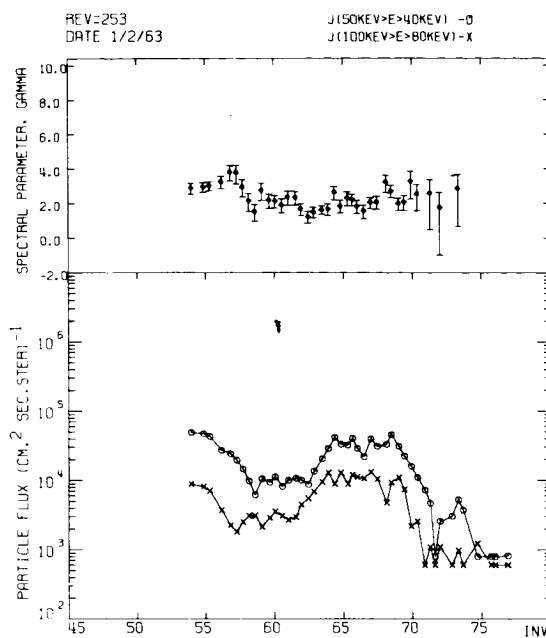
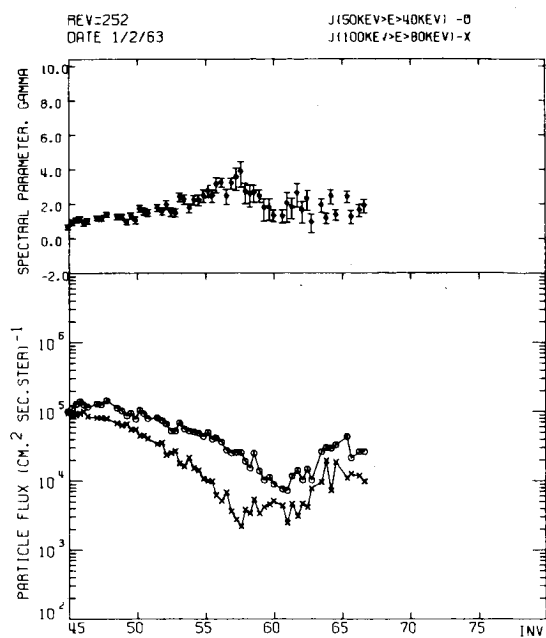


FIGURE 8



UT (HMS)	120329	120539	120741	120943	121143
MLT	6.32	6.40	6.60	6.89	7.29
B	.53	.269	.324	.356	.383

UT (HMS)	140500	140607	140711	140842	141020	141215
MLT	6.27	6.36	6.46	6.71	7.10	7.84
B	.335	.356	.376	.401	.424	.443

FIGURE 9

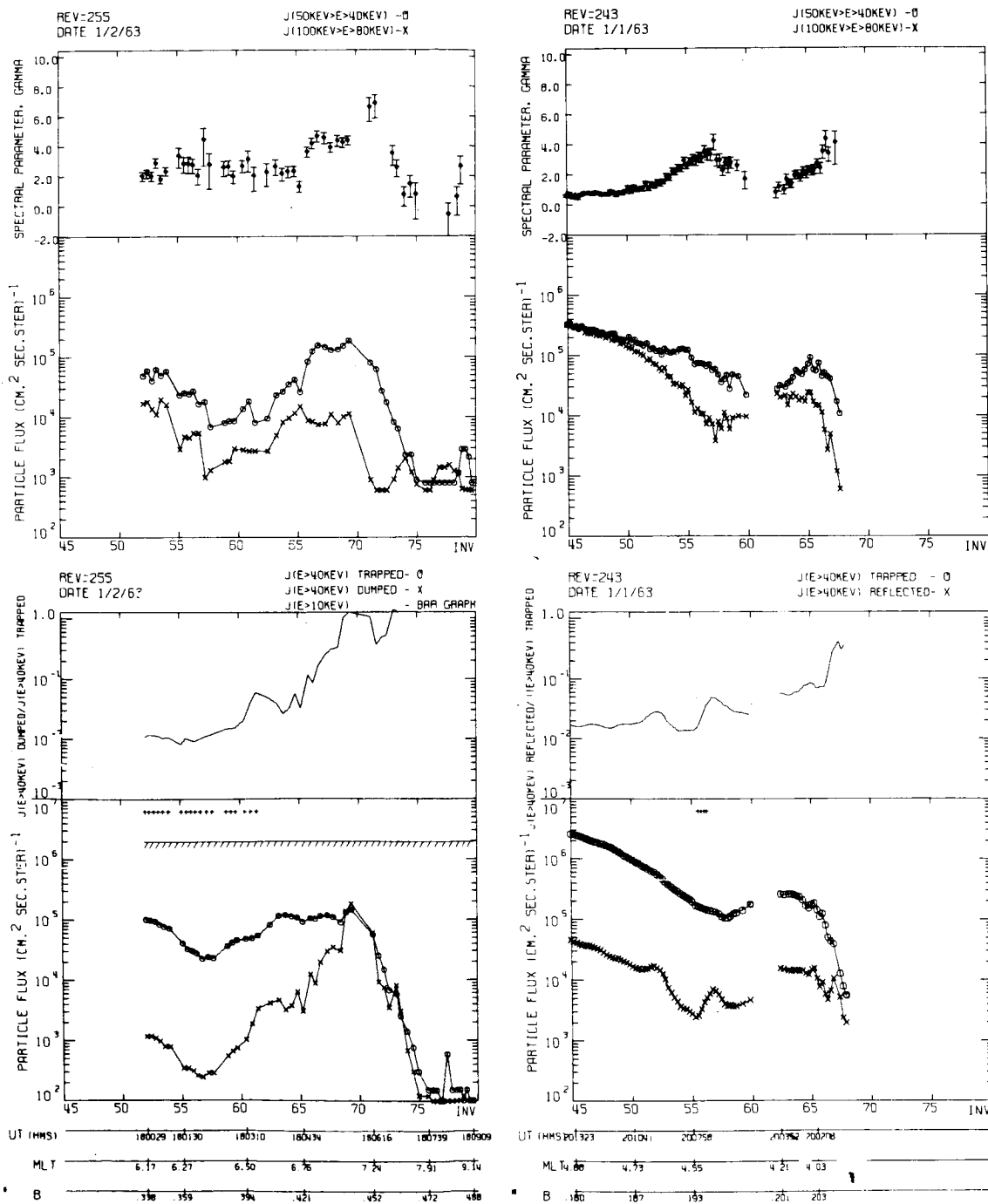


FIGURE 10

MAGNETIC FIELD

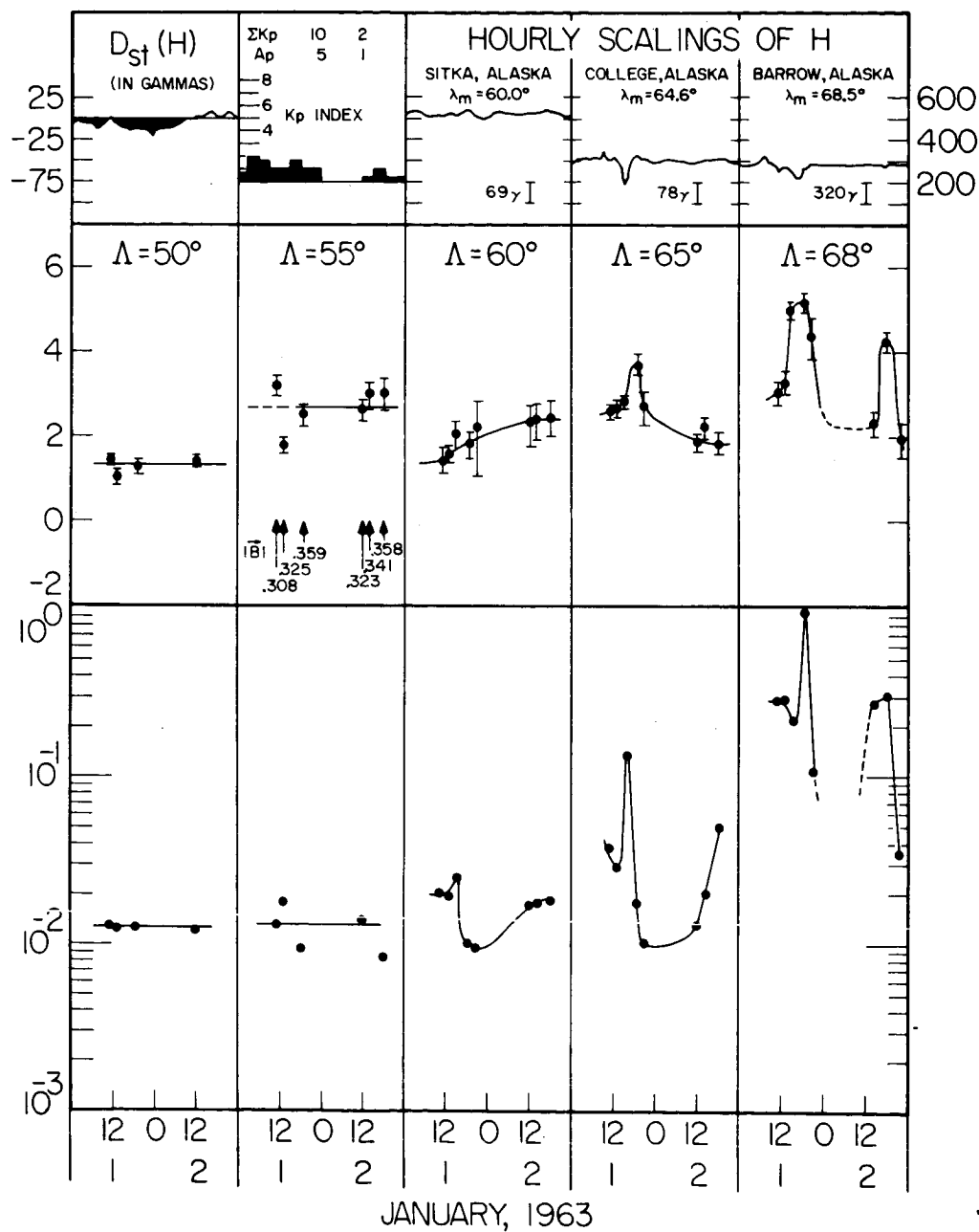
SPECTRAL PARAMETER,  $\gamma$ DUMPING PARAMETER,  $\phi$ 

FIGURE 11

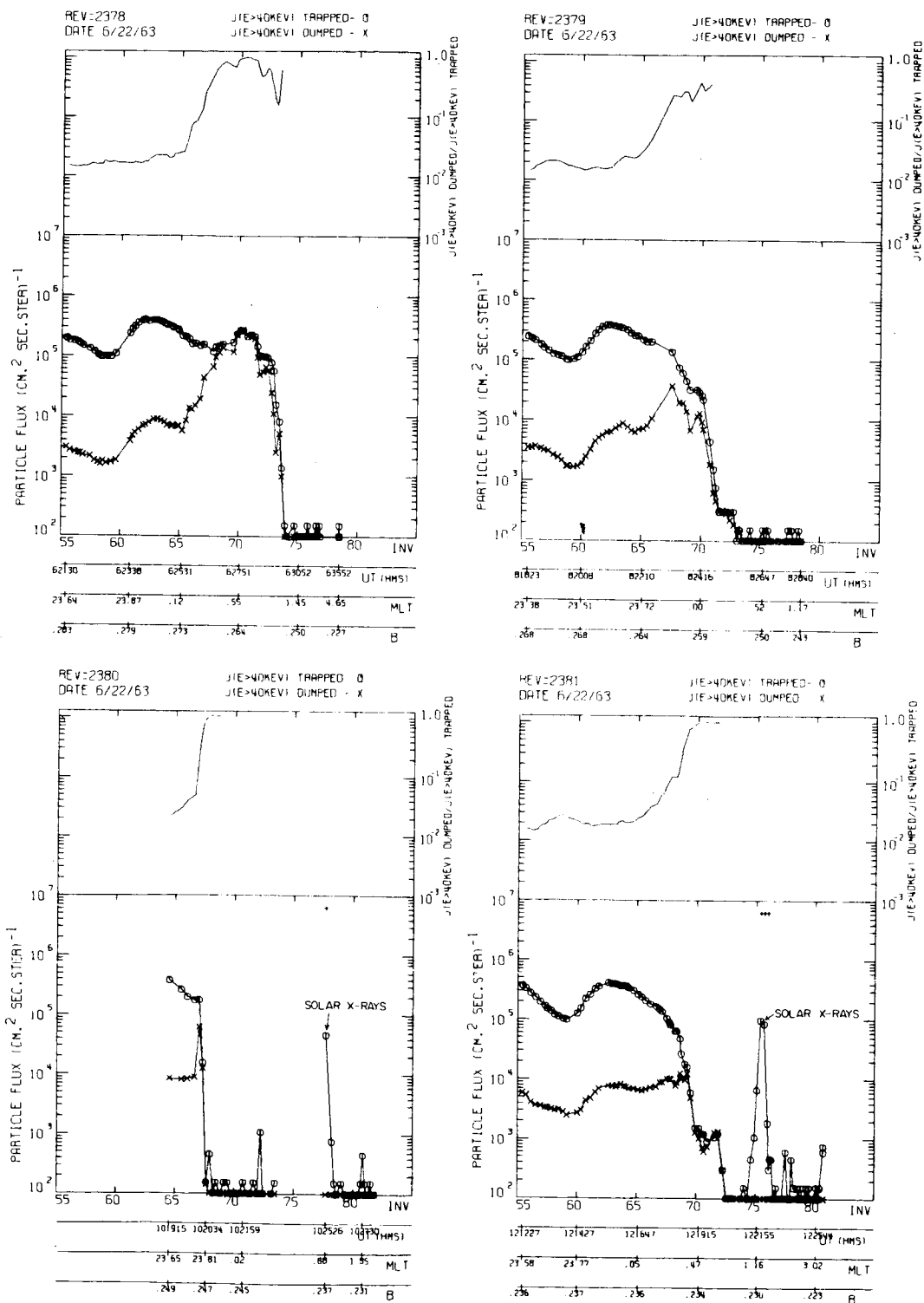


FIGURE 12

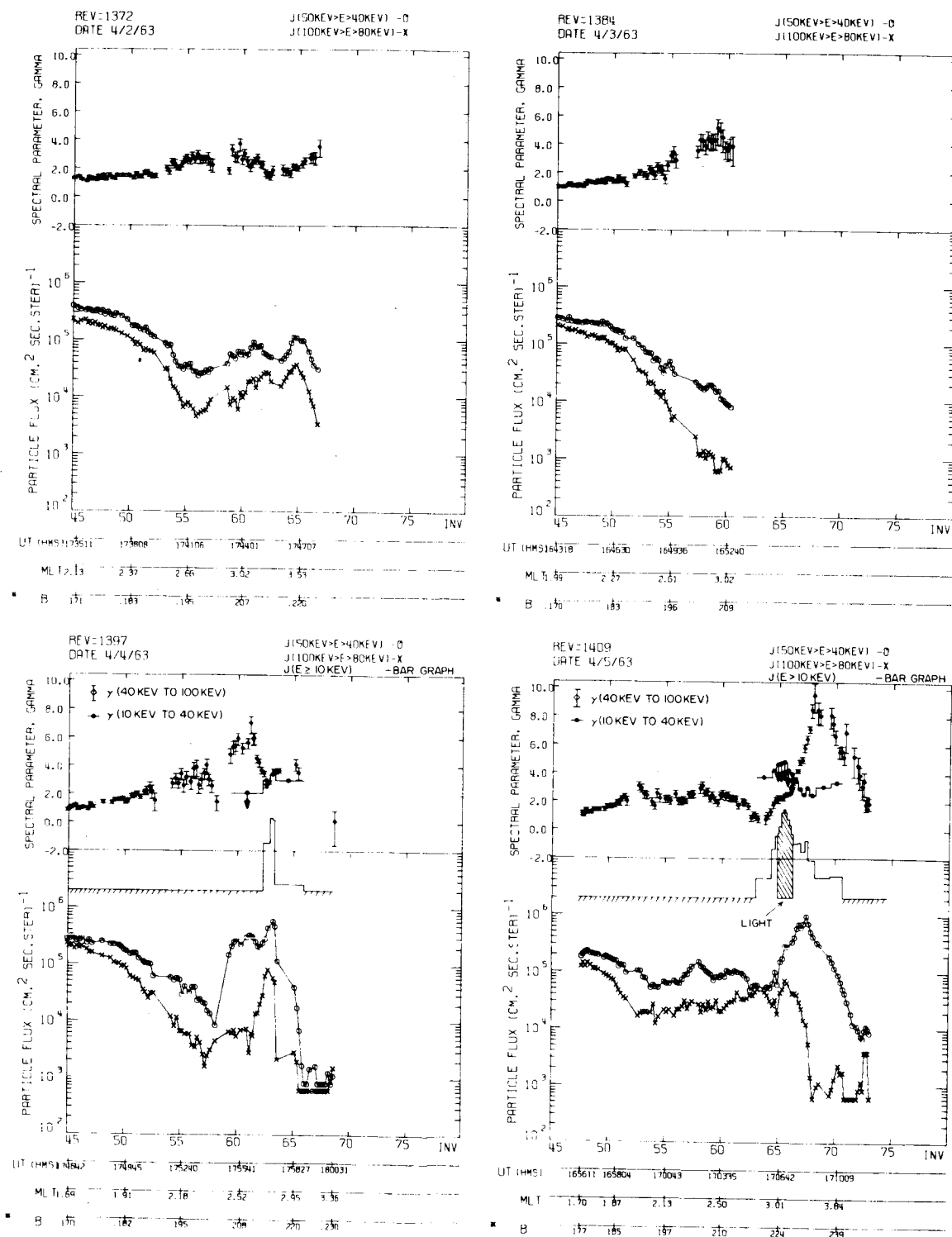


FIGURE 13



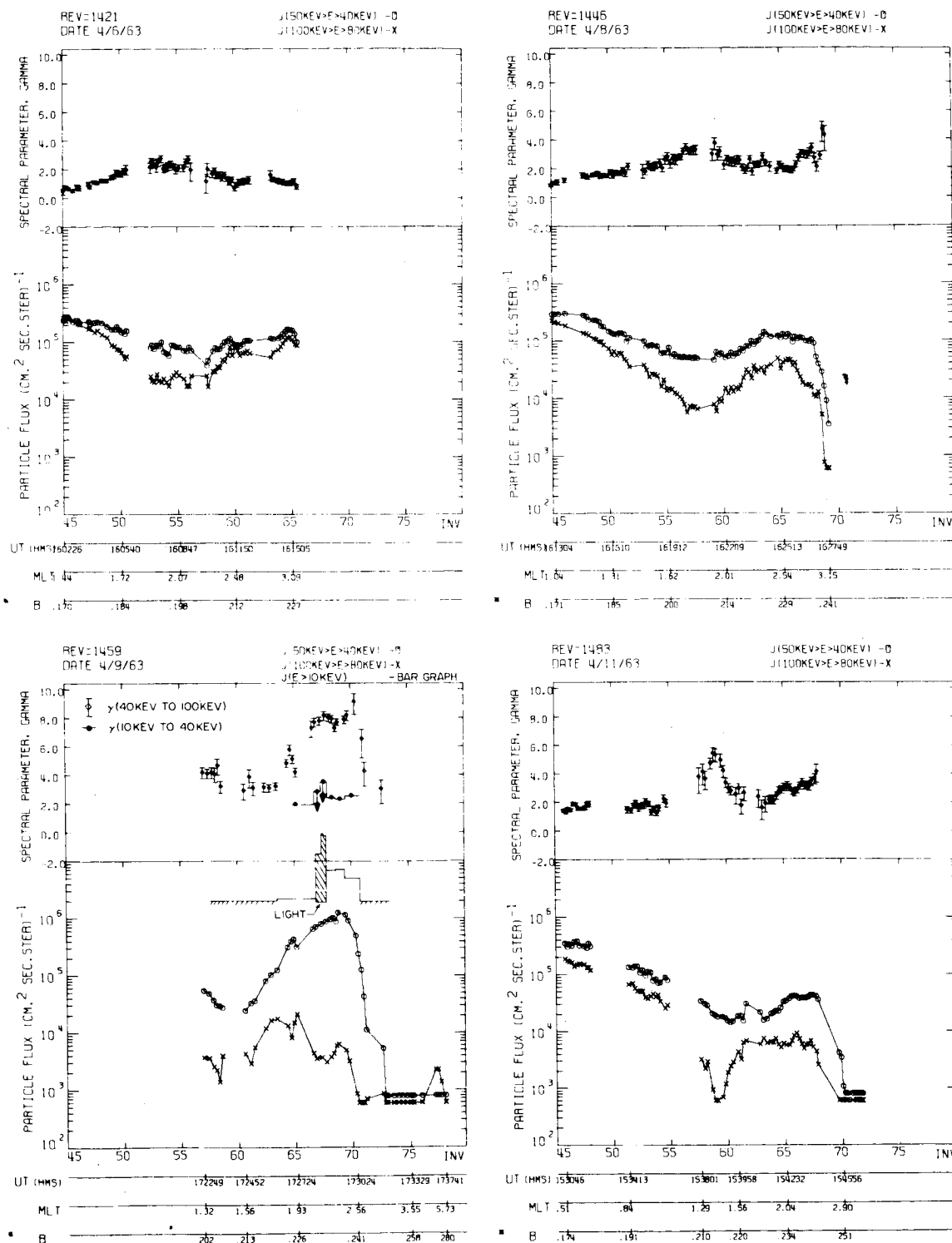


FIGURE 14

G 67-538

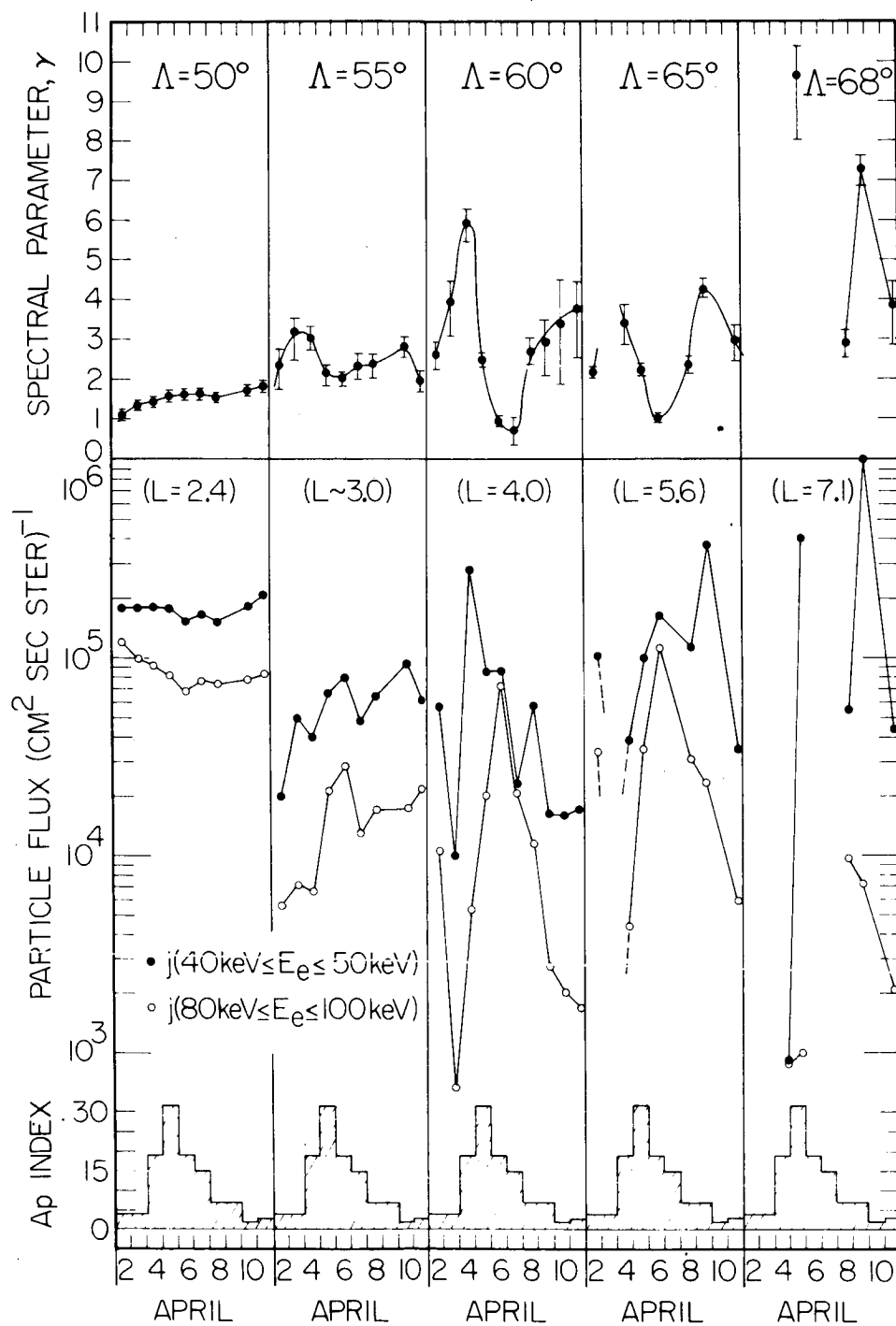


FIGURE 15

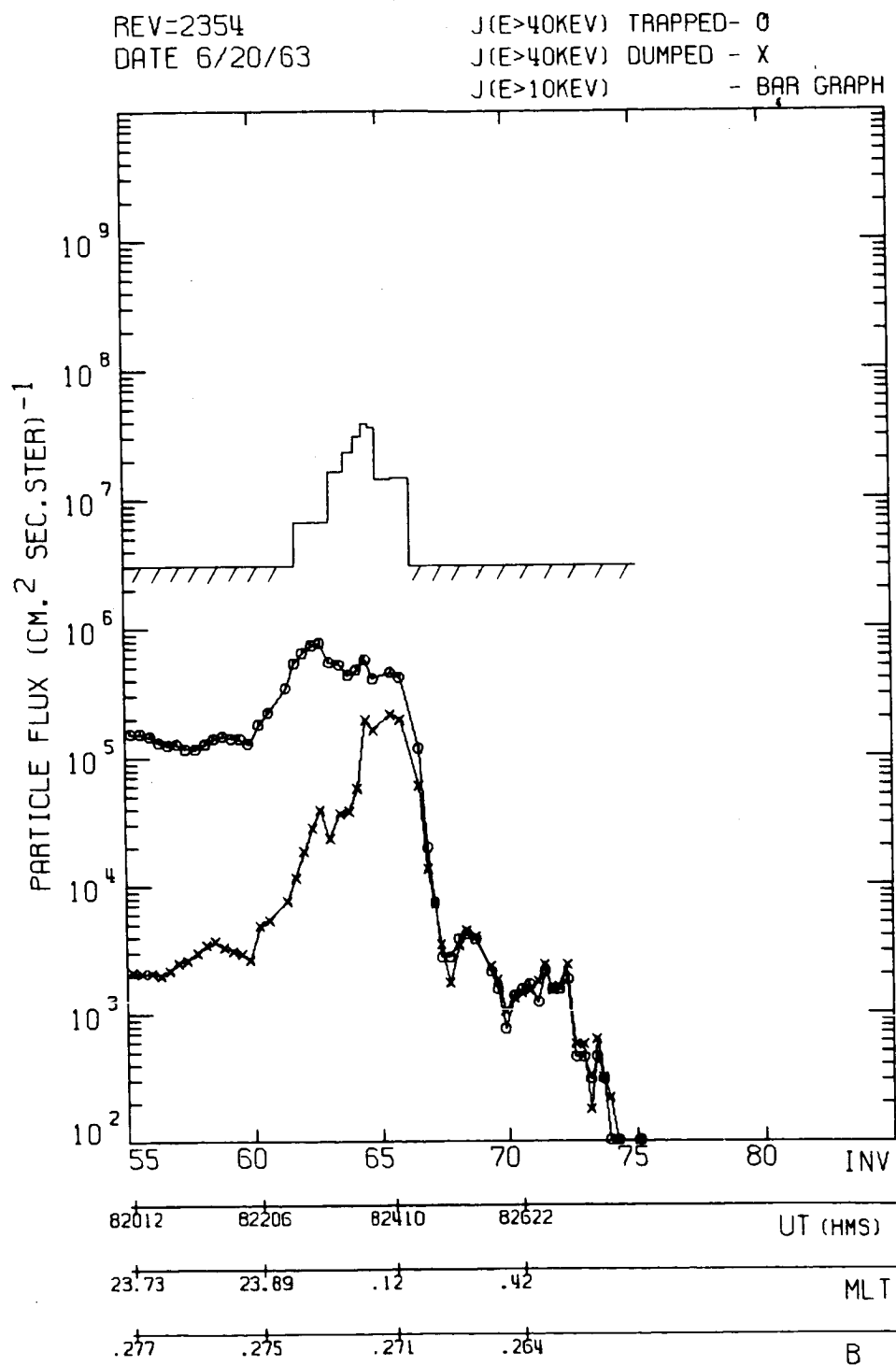


FIGURE 16

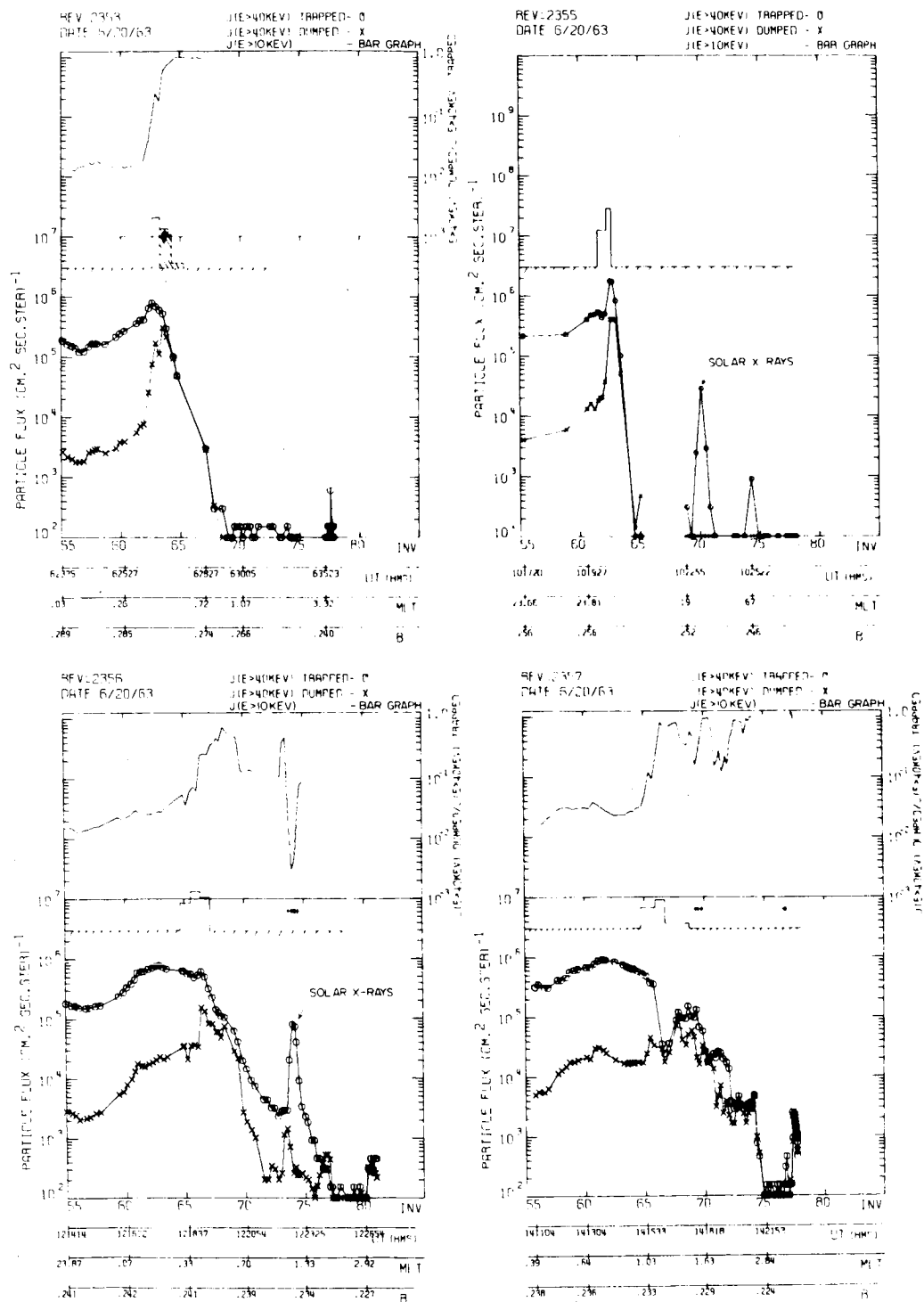


FIGURE 17

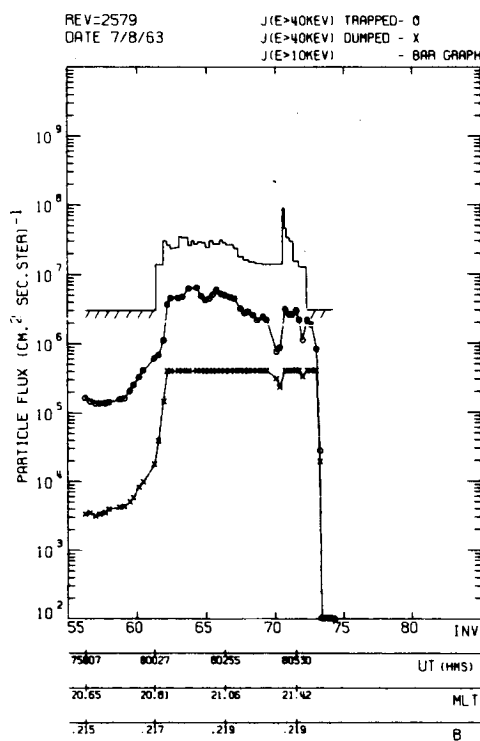
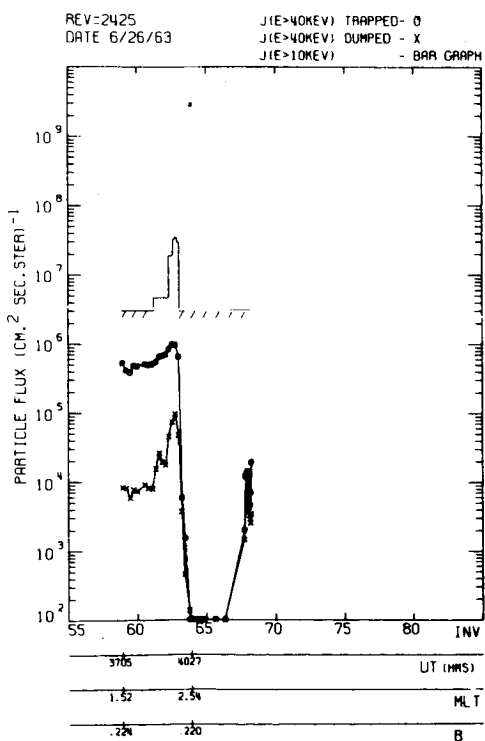
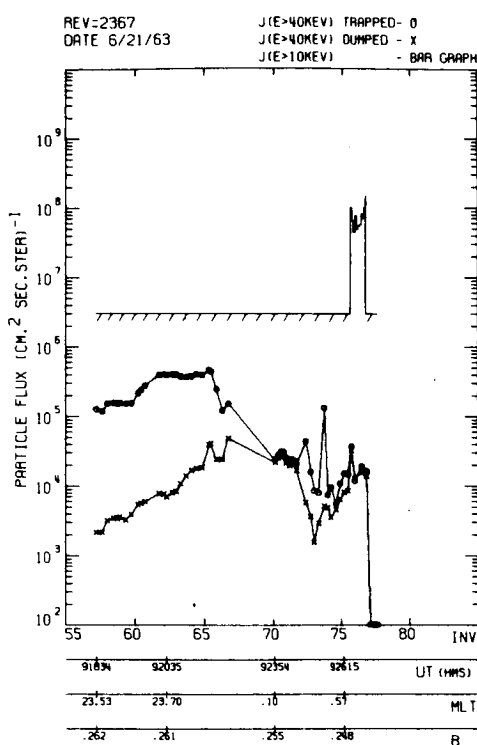
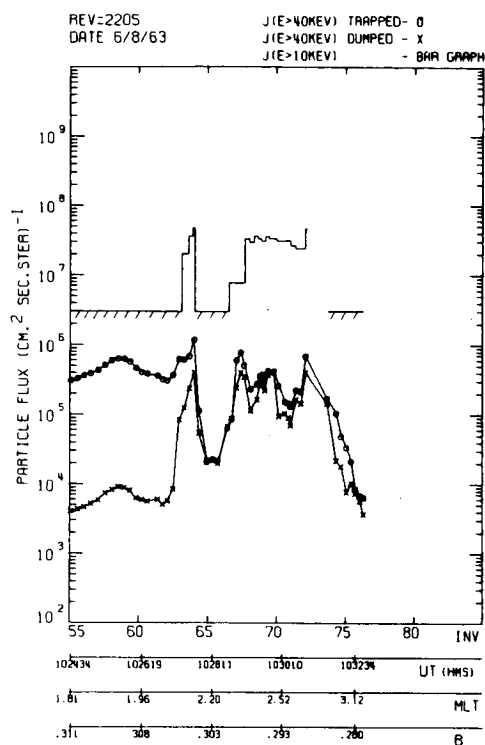


FIGURE 18

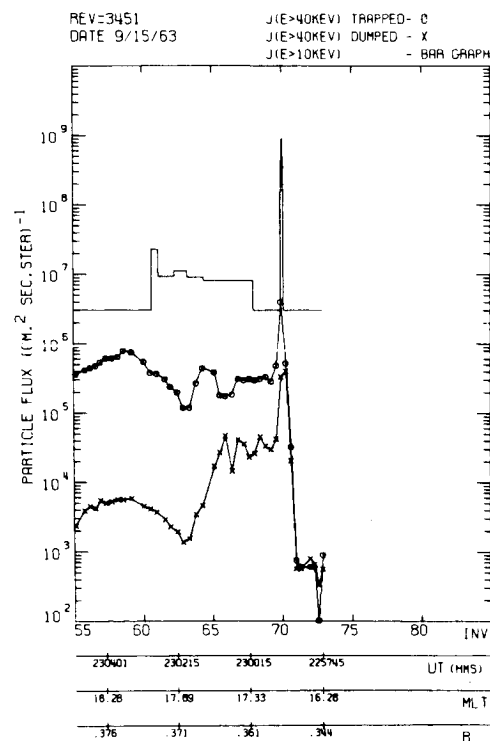
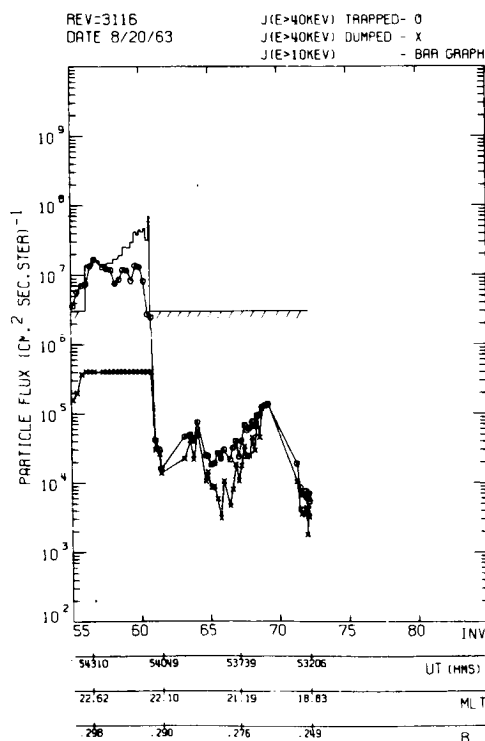
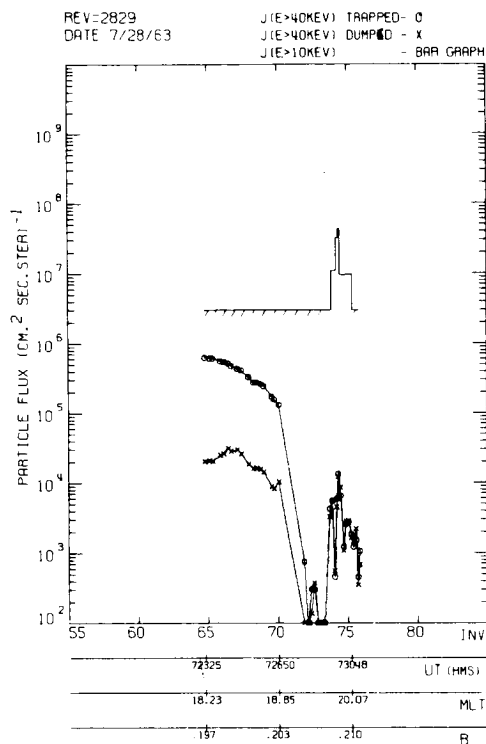
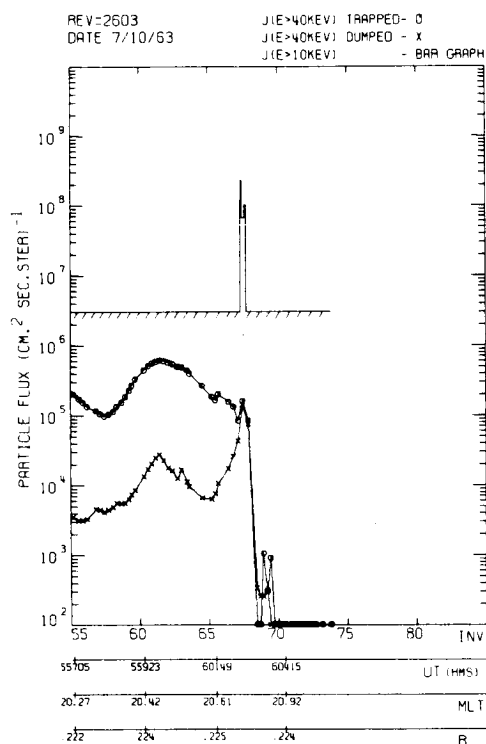


FIGURE 19

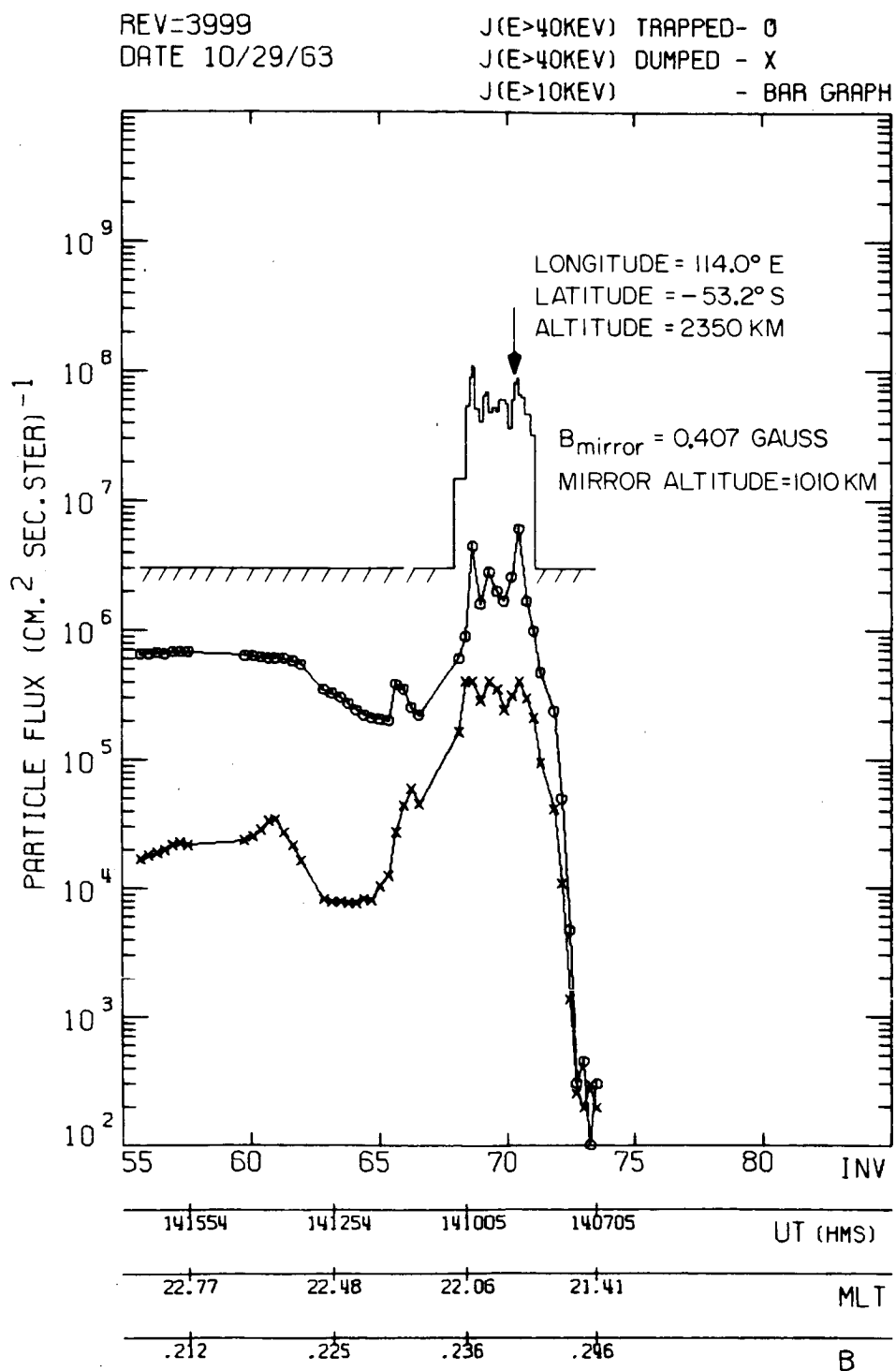


FIGURE 20

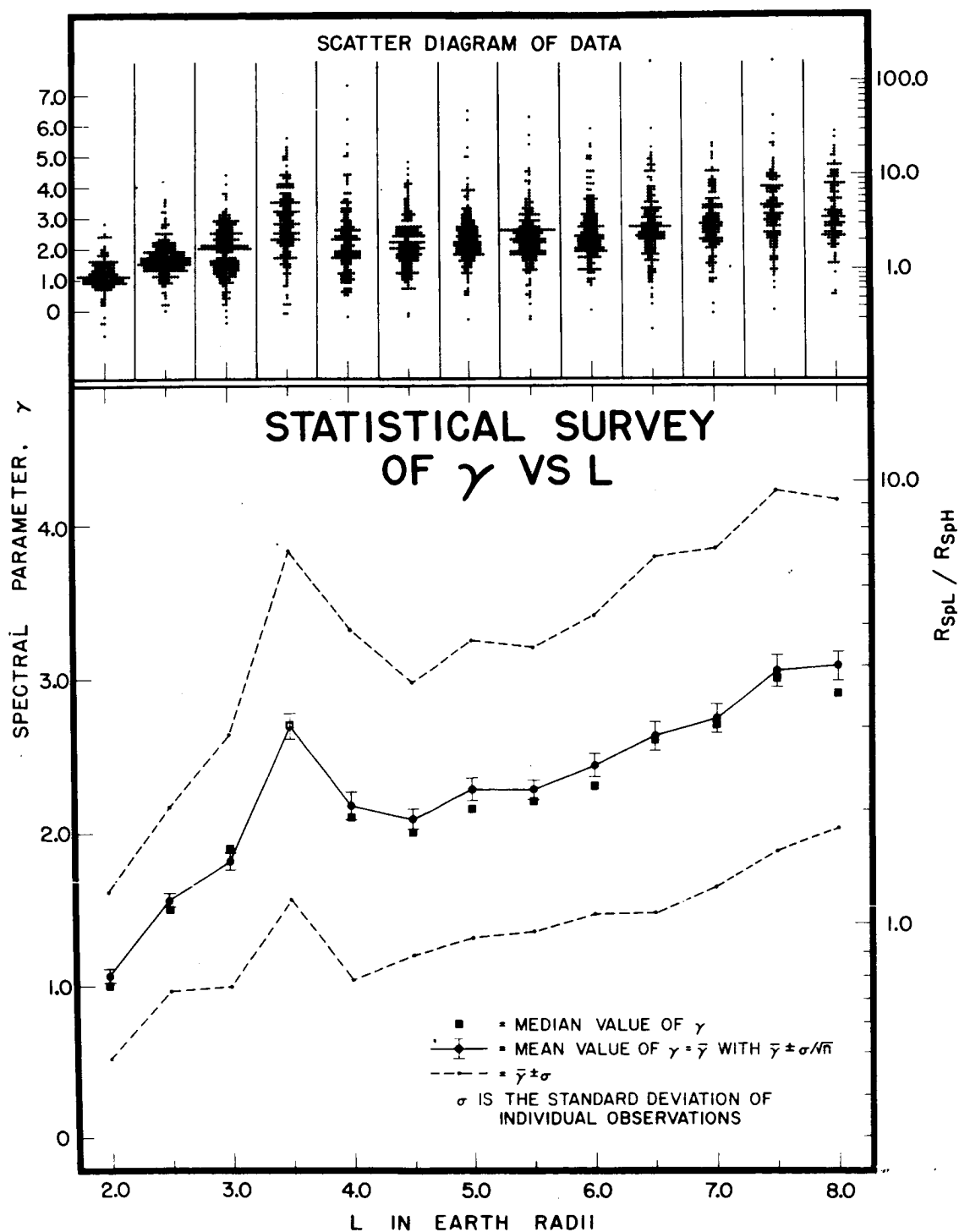


FIGURE 21



THE INJUN 3 SPECTRAL PARAMETER,  $\gamma$ , AS A FUNCTION OF B  
WITH L DEPENDENCE NORMALIZED TO  $\gamma = 2.0$

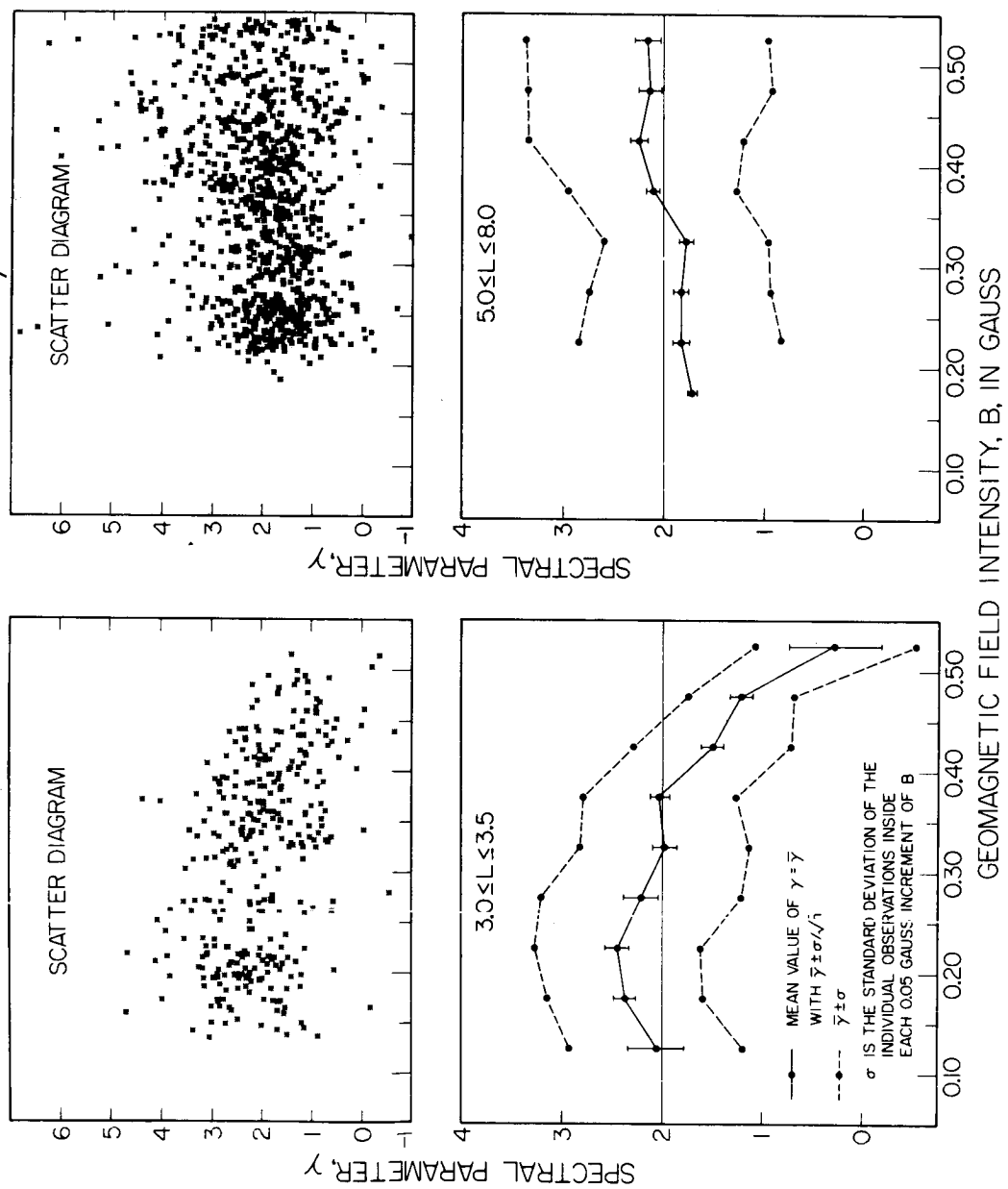


FIGURE 22

G 66-874

# THE INJUN 3 SPECTRAL PARAMETER, $\gamma$ , AS A FUNCTION OF DAILY $K_p$ SUMS WITH THE L DEPENDENCE NORMALIZED TO $\gamma = 2.0$ FOR BOTH PLOTS

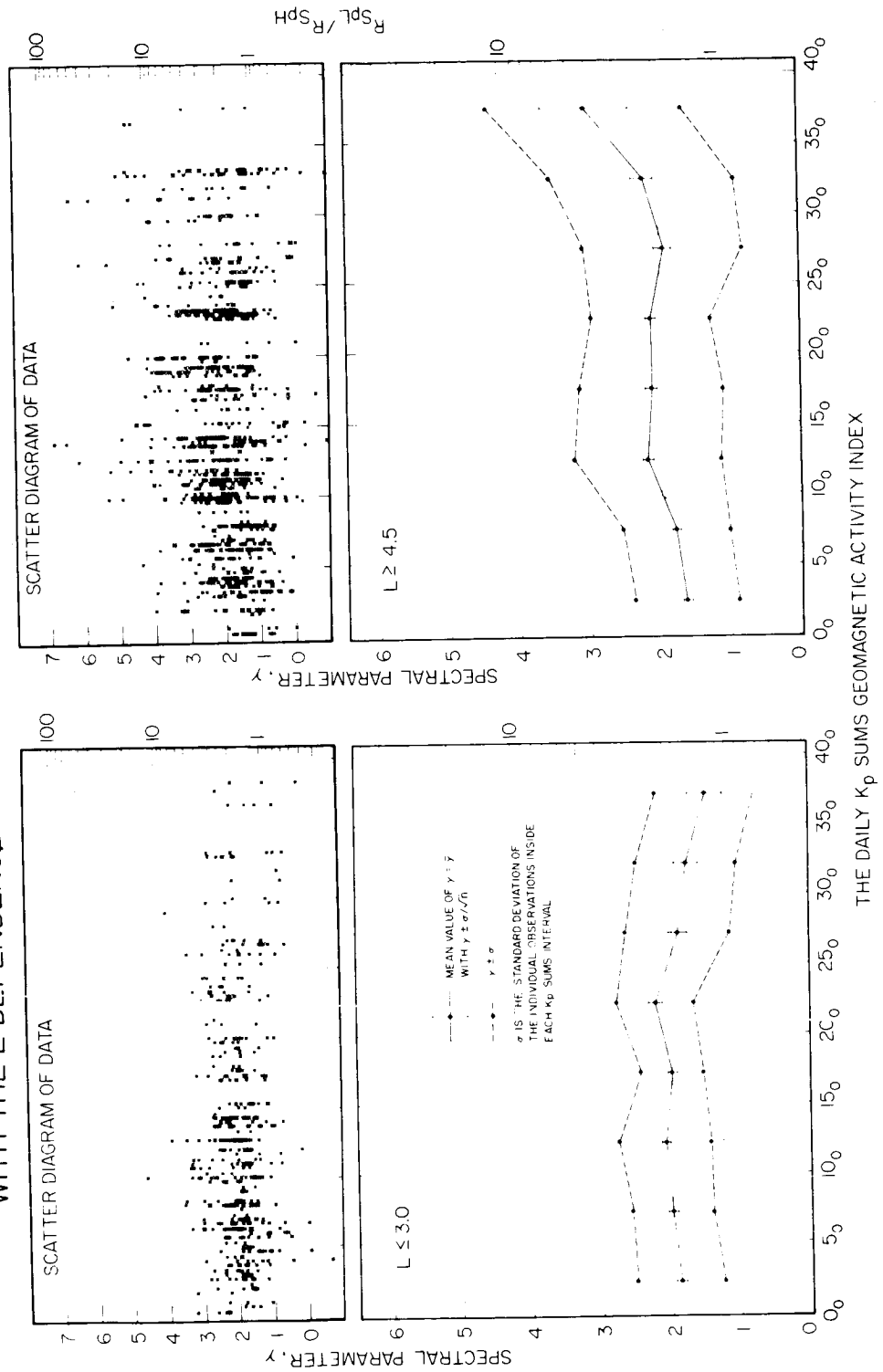


FIGURE 23

THE INJUN 3 SPECTRAL PARAMETER,  $\gamma$ , AS A FUNCTION OF  $j$  ( $E_e \geq 40$  KeV)  
WITH  $L$  DEPENDENCE NORMALIZED TO  $\gamma=2.0$

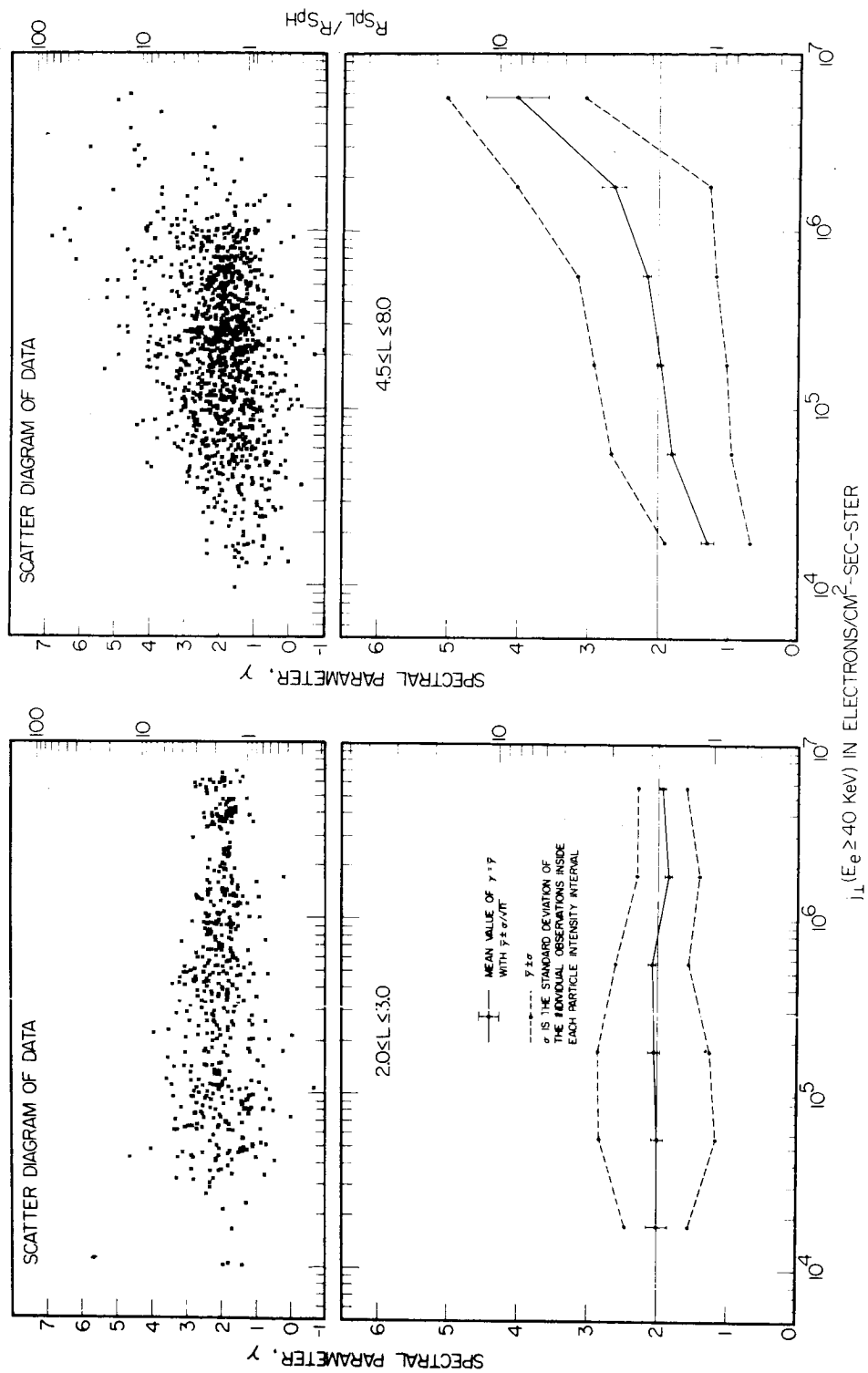


FIGURE 24

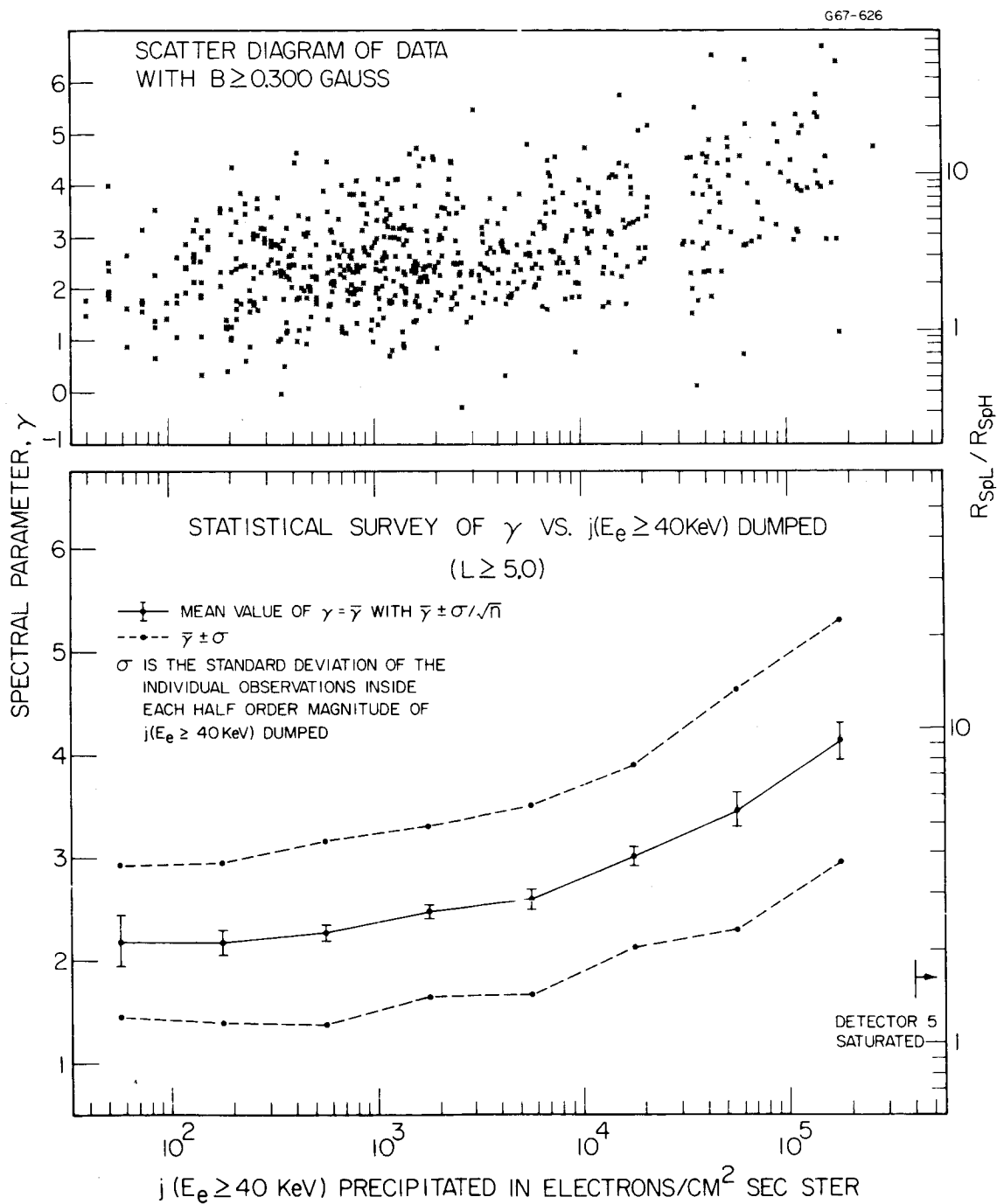


FIGURE 25

G67-627

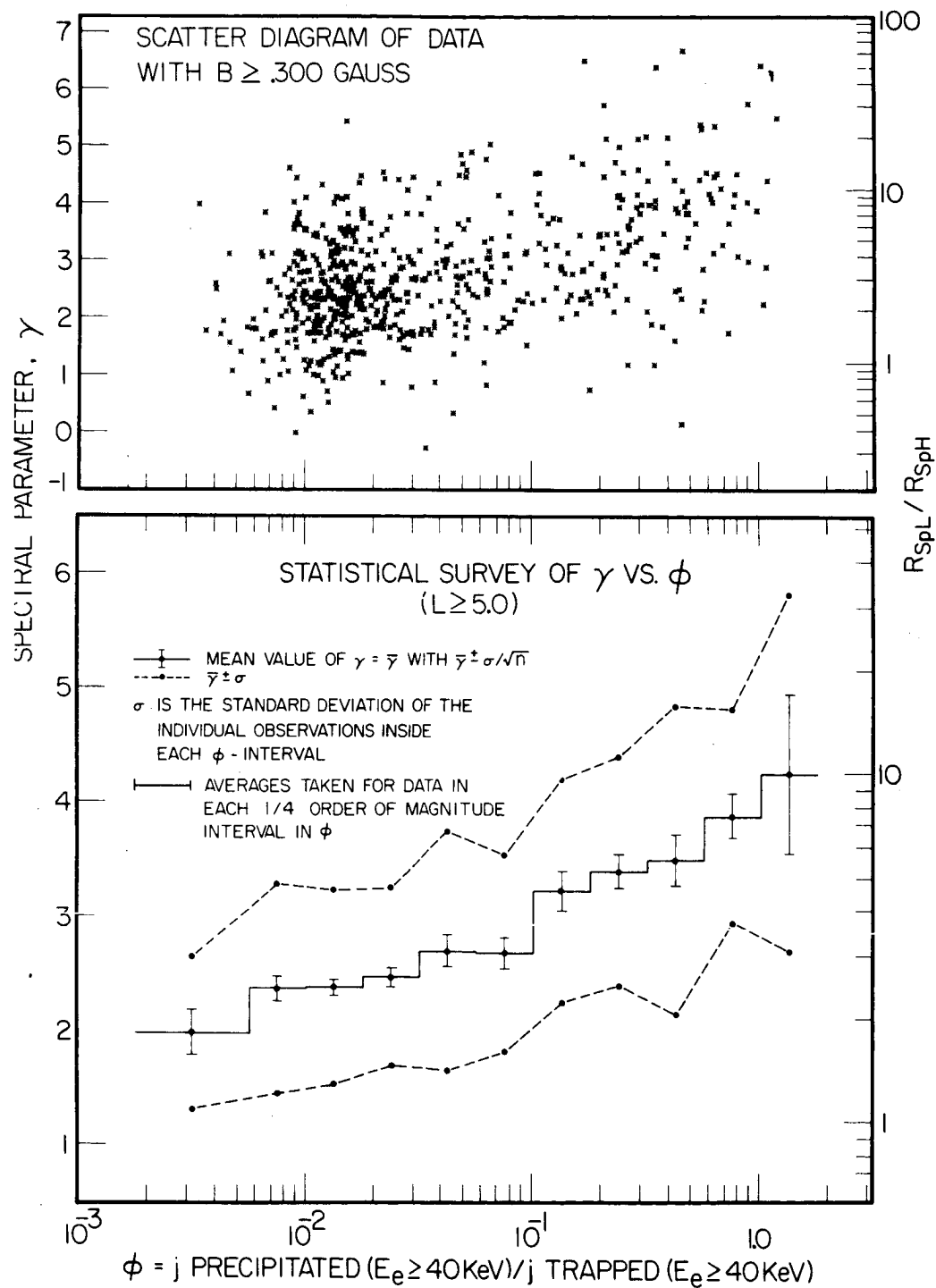


FIGURE 26

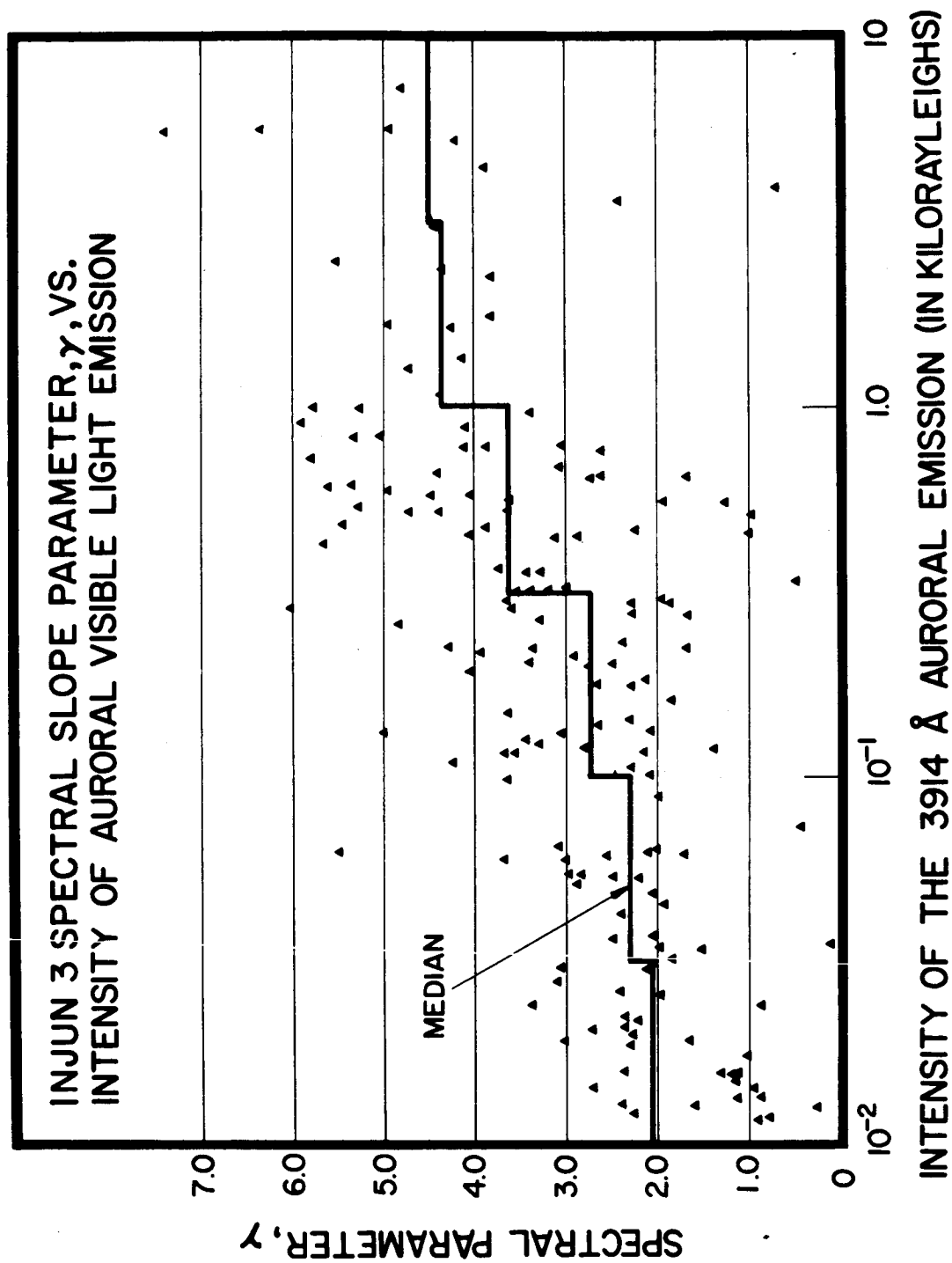


FIGURE 27

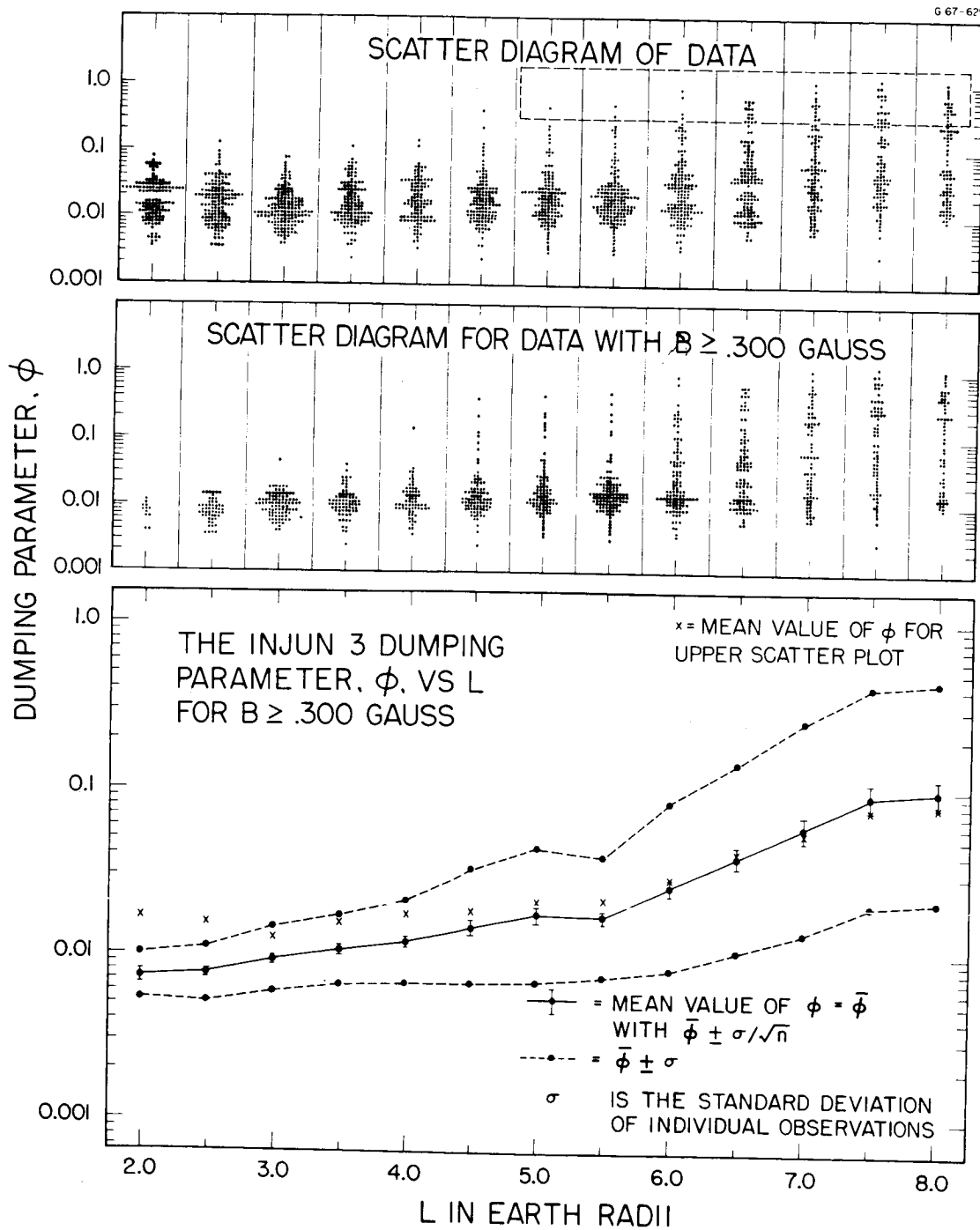


FIGURE 28

G67-23

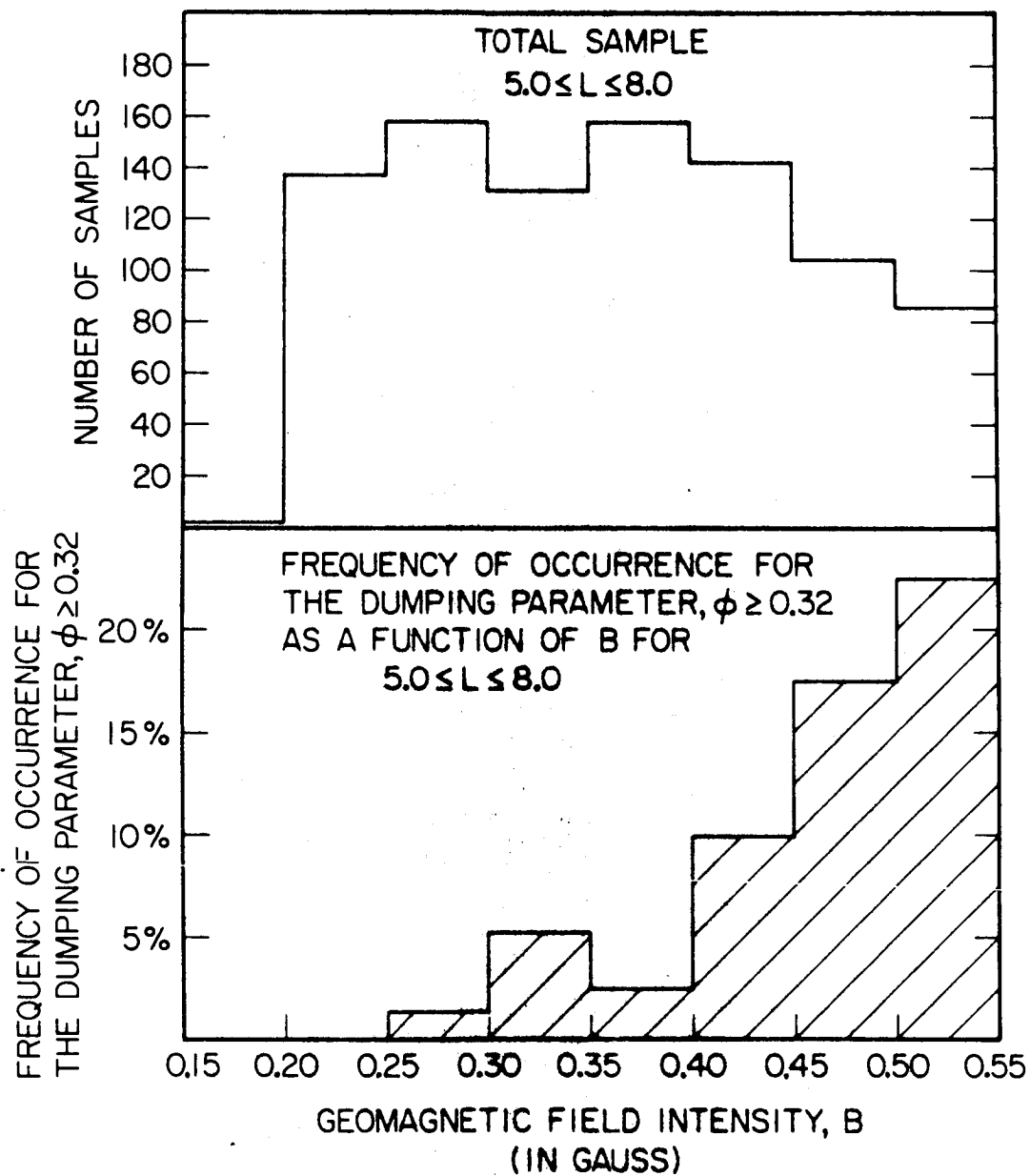


FIGURE 29



G 66-20

# VARIATION OF THE SLOPE OF THE ELECTRON ENERGY SPECTRUM AS A FUNCTION OF INVARIANT LATITUDE

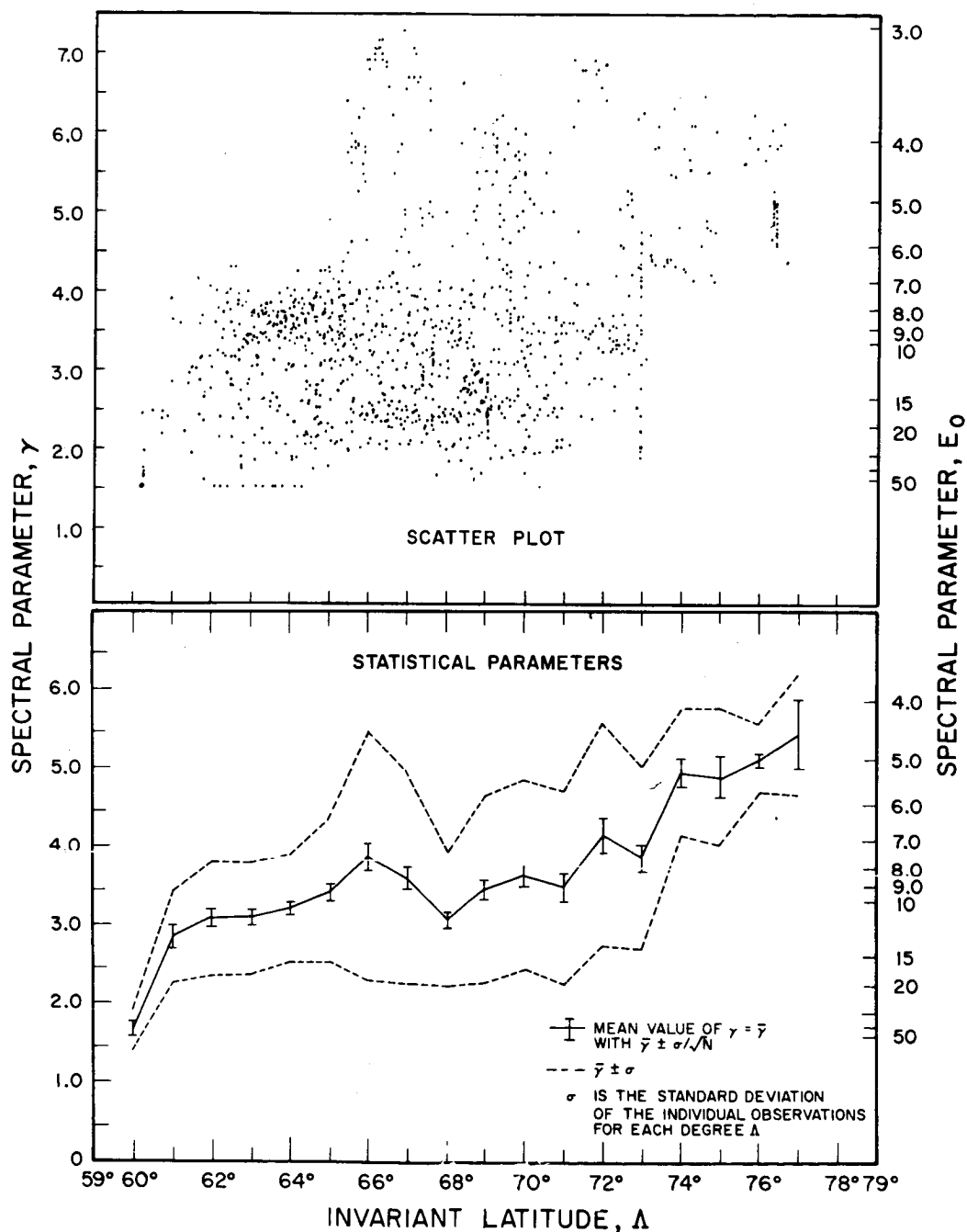


FIGURE 30

G 66-27

# VARIATION OF THE SLOPE OF THE ELECTRON ENERGY SPECTRUM AS A FUNCTION OF MAGNETIC LOCAL TIME

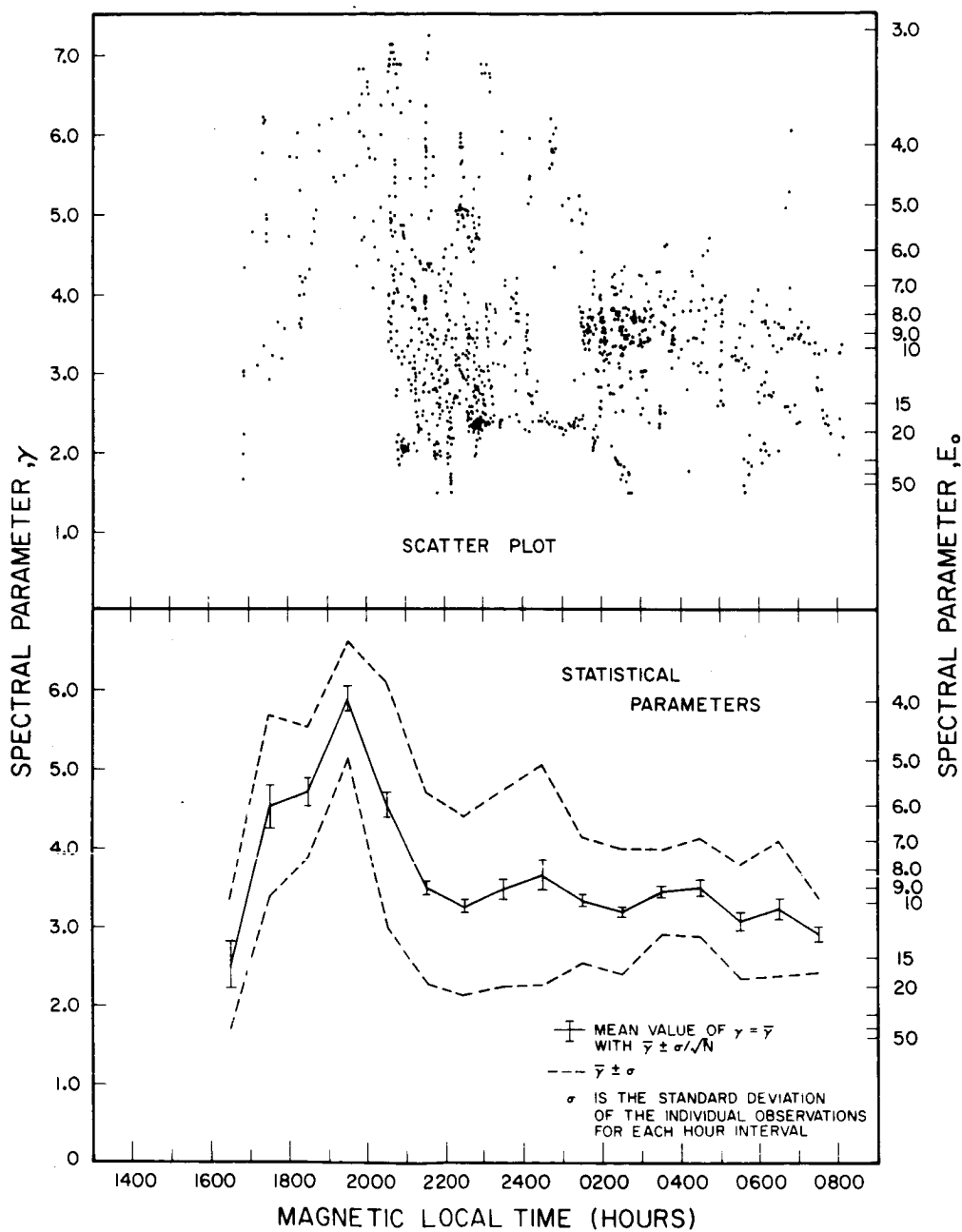


FIGURE 31

G 66-31

VARIATION OF THE SLOPE OF THE ELECTRON  
ENERGY SPECTRUM AS A FUNCTION OF  
 $j(E_e \geq 10 \text{ KeV})$

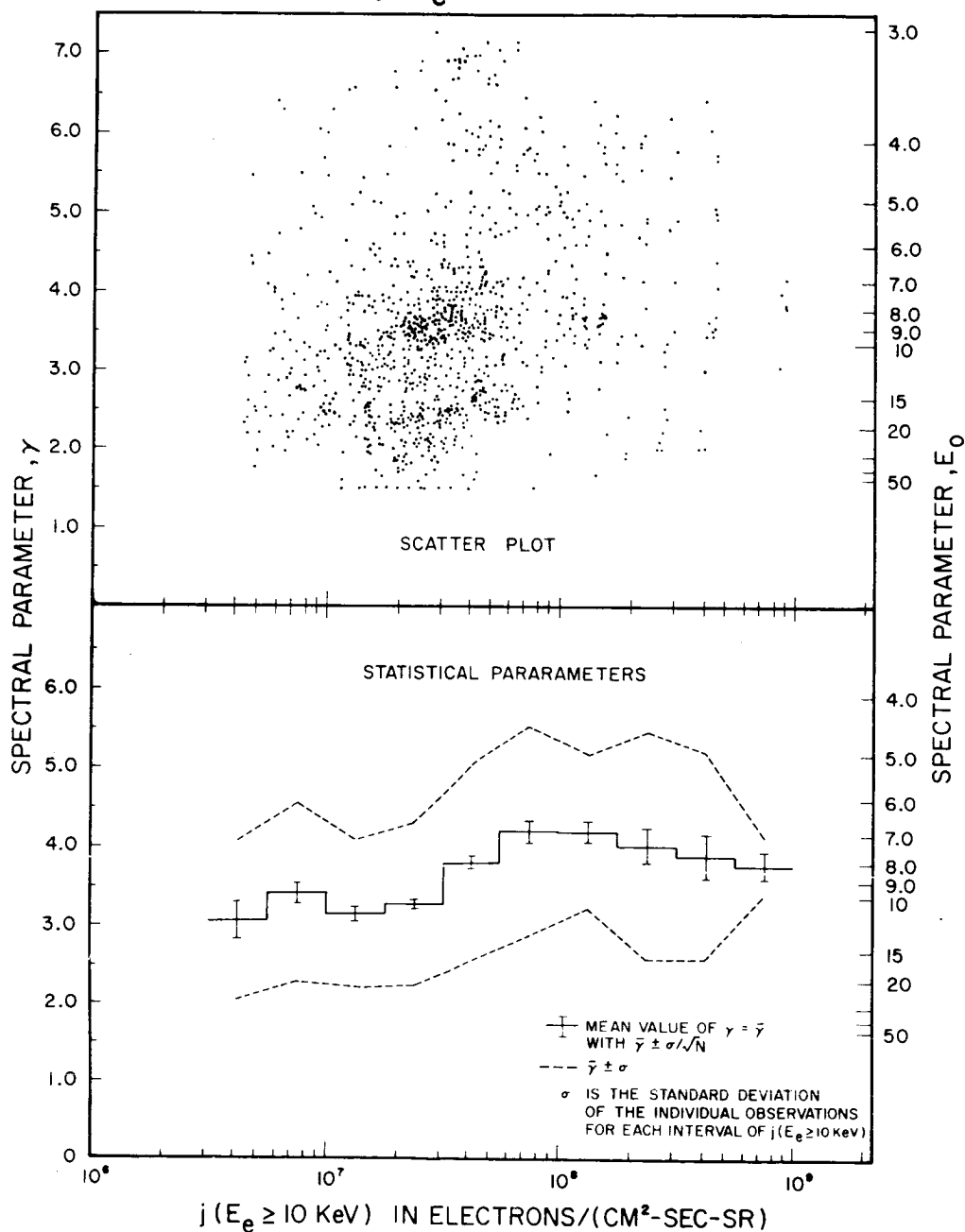


FIGURE 32

G 66 — 32

# VARIATION OF THE SLOPE OF THE ELECTRON ENERGY SPECTRUM AS A FUNCTION OF THE MAGNETIC-ACTIVITY INDEX, $K_p$

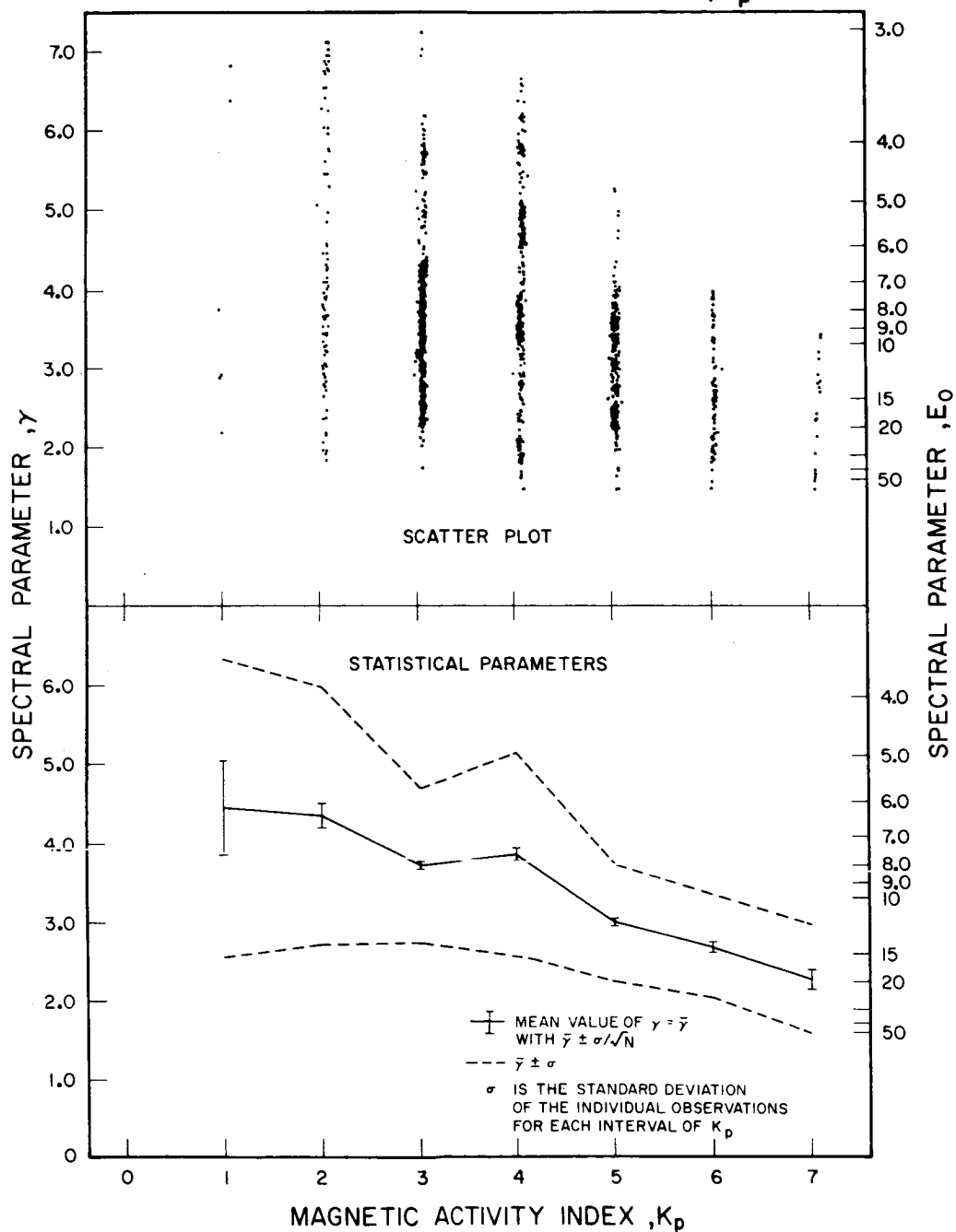


FIGURE 33

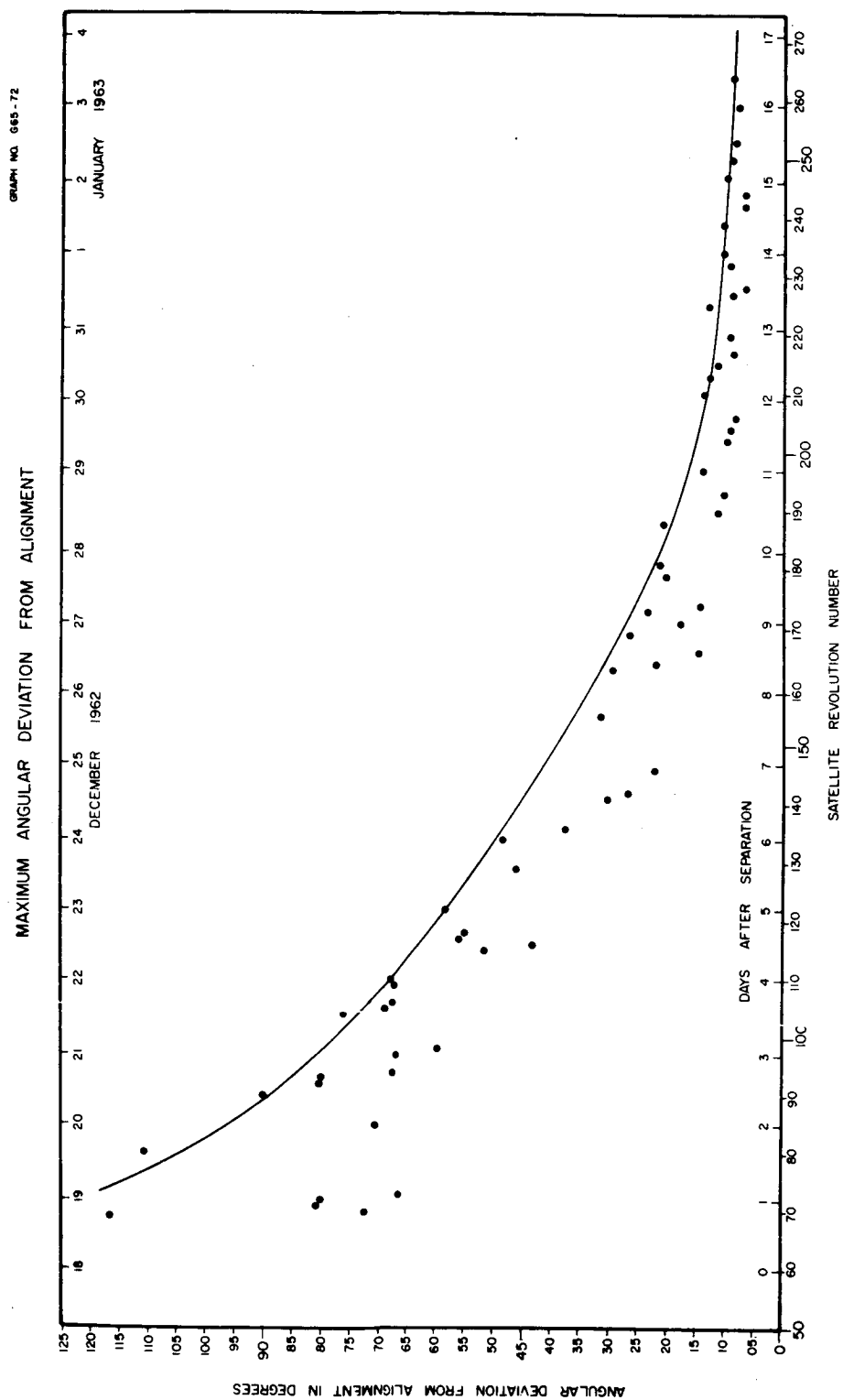


FIGURE 34

G 65-35

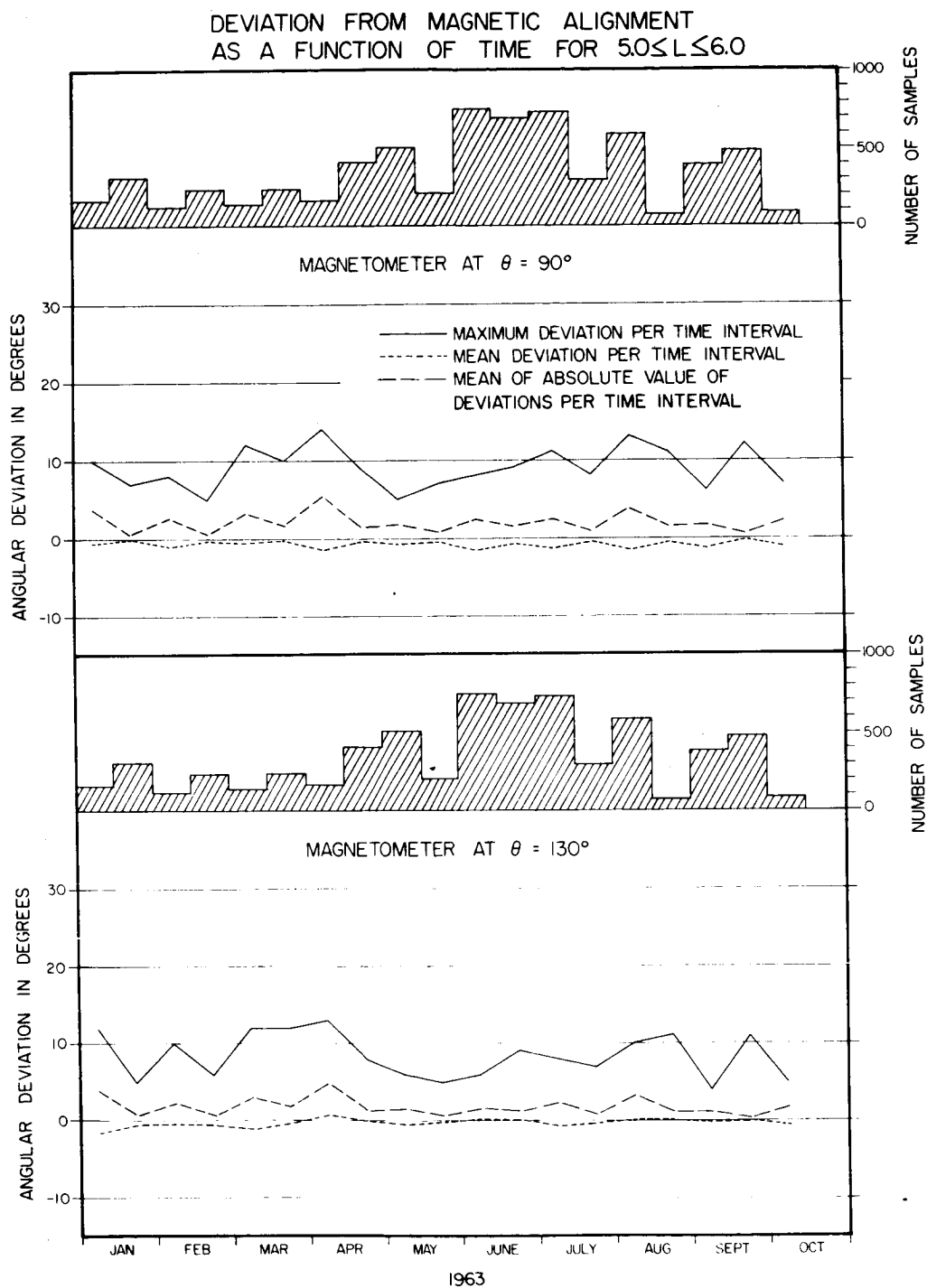


FIGURE 35

667-535

# RMS DEVIATION FROM ALIGNMENT DURING ACTIVE SATELLITE LIFETIME

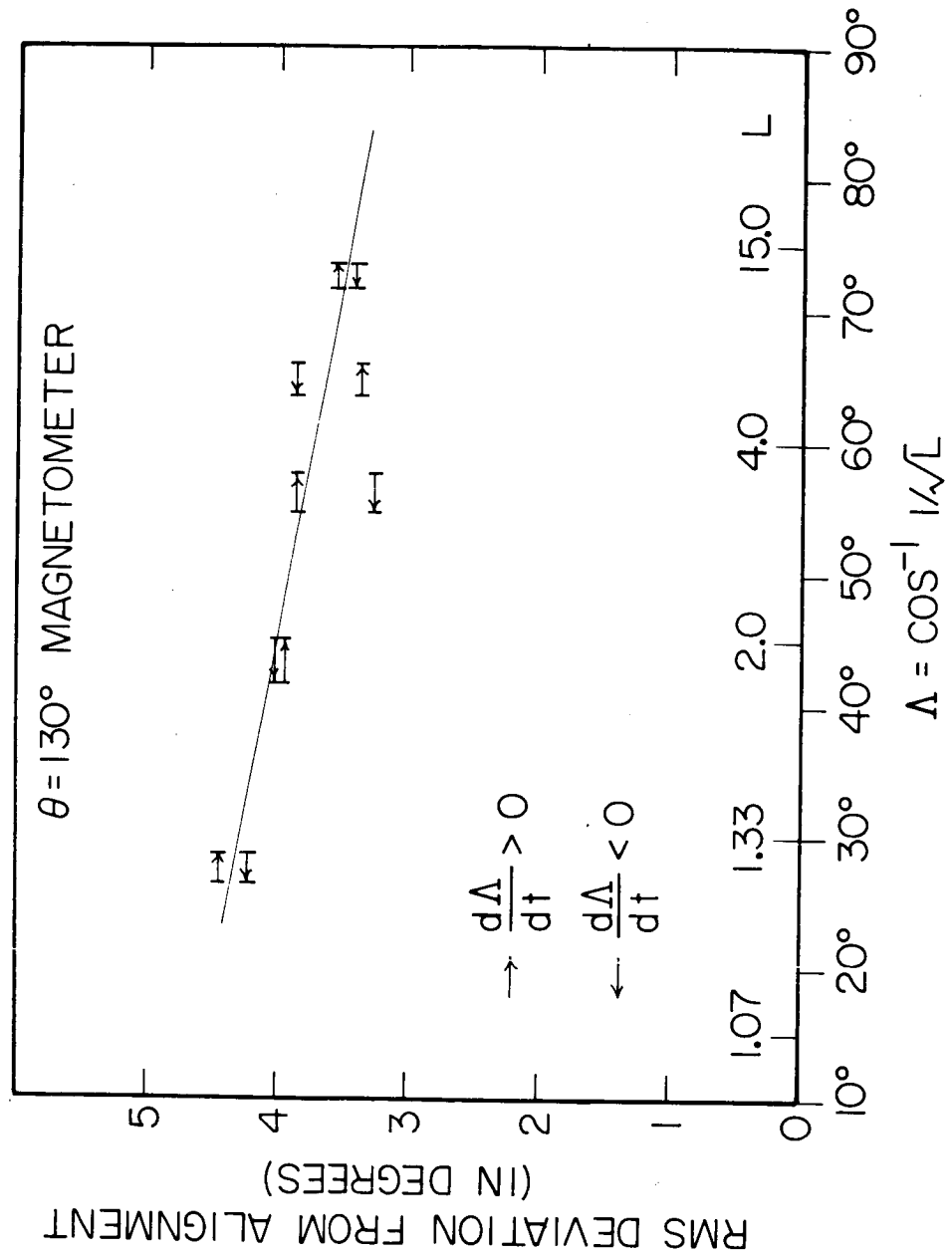


FIGURE 36

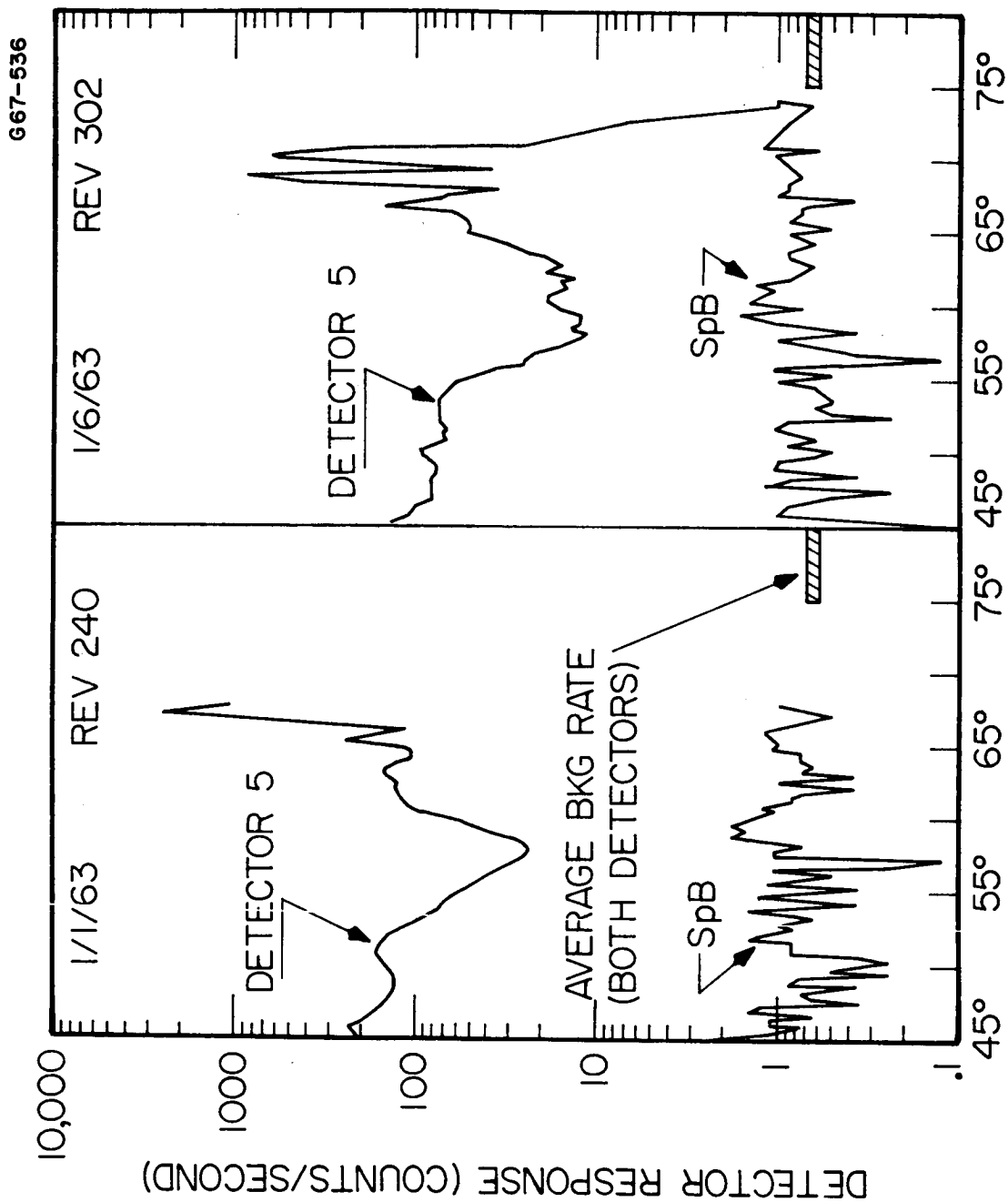


FIGURE 37



G67-537

RATIO  $\frac{j(>40\text{keV}) \text{ DUMPED}}{j(>40\text{keV}) \text{ TRAPPED}}$  AS A FUNCTION OF  $\alpha_D$

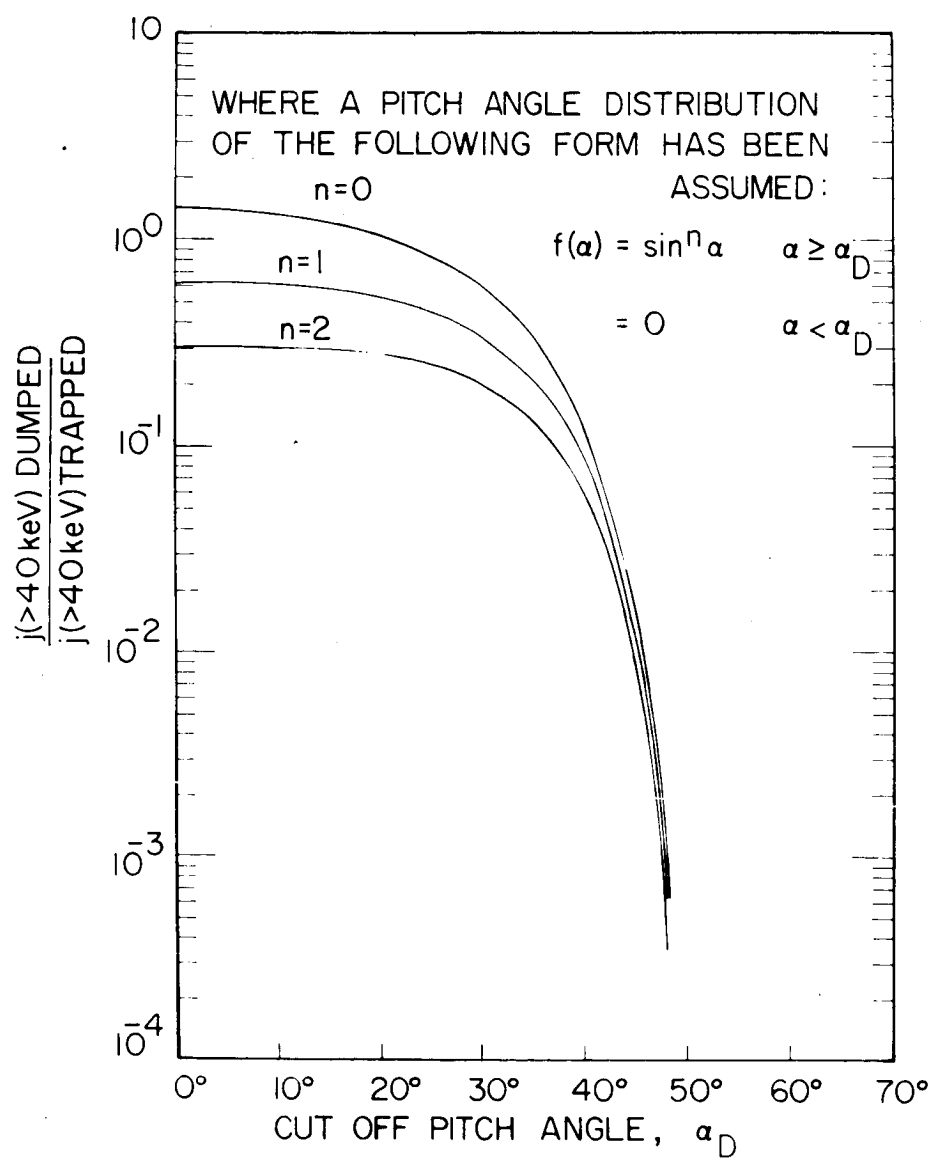


FIGURE 38

14. KEY WORDS	LINK A		LINK B		LINK C	
	ROLE	WT	ROLE	WT	ROLE	WT
Geomagnetically Trapped Radiation						
Radiation Belts						
Aurora						
Outer Zone Electrons						

## INSTRUCTIONS

1. **ORIGINATING ACTIVITY:** Enter the name and address of the contractor, subcontractor, grantee, Department of Defense activity or other organization (*corporate author*) issuing the report.

2a. **REPORT SECURITY CLASSIFICATION:** Enter the overall security classification of the report. Indicate whether "Restricted Data" is included. Marking is to be in accordance with appropriate security regulations.

2b. **GROUP:** Automatic downgrading is specified in DoD Directive 5200.10 and Armed Forces Industrial Manual. Enter the group number. Also, when applicable, show that optional markings have been used for Group 3 and Group 4 as authorized.

3. **REPORT TITLE:** Enter the complete report title in all capital letters. Titles in all cases should be unclassified. If a meaningful title cannot be selected without classification, show title classification in all capitals in parenthesis immediately following the title.

4. **DESCRIPTIVE NOTES:** If appropriate, enter the type of report, e.g., interim, progress, summary, annual, or final. Give the inclusive dates when a specific reporting period is covered.

5. **AUTHOR(S):** Enter the name(s) of author(s) as shown on or in the report. Enter last name, first name, middle initial. If military, show rank and branch of service. The name of the principal author is an absolute minimum requirement.

6. **REPORT DATE:** Enter the date of the report as day, month, year, or month, year. If more than one date appears on the report, use date of publication.

7a. **TOTAL NUMBER OF PAGES:** The total page count should follow normal pagination procedures, i.e., enter the number of pages containing information.

7b. **NUMBER OF REFERENCES:** Enter the total number of references cited in the report.

8a. **CONTRACT OR GRANT NUMBER:** If appropriate, enter the applicable number of the contract or grant under which the report was written.

8b, 8c, & 8d. **PROJECT NUMBER:** Enter the appropriate military department identification, such as project number, subproject number, system numbers, task number, etc.

9a. **ORIGINATOR'S REPORT NUMBER(S):** Enter the official report number by which the document will be identified and controlled by the originating activity. This number must be unique to this report.

9b. **OTHER REPORT NUMBER(S):** If the report has been assigned any other report numbers (*either by the originator or by the sponsor*), also enter this number(s).

10. **AVAILABILITY/LIMITATION NOTICES:** Enter any limitations on further dissemination of the report, other than those

imposed by security classification, using standard statements such as:

- (1) "Qualified requesters may obtain copies of this report from DDC."
- (2) "Foreign announcement and dissemination of this report by DDC is not authorized."
- (3) "U. S. Government agencies may obtain copies of this report directly from DDC. Other qualified DDC users shall request through \_\_\_\_\_."
- (4) "U. S. military agencies may obtain copies of this report directly from DDC. Other qualified users shall request through \_\_\_\_\_."
- (5) "All distribution of this report is controlled. Qualified DDC users shall request through \_\_\_\_\_."

If the report has been furnished to the Office of Technical Services, Department of Commerce, for sale to the public, indicate this fact and enter the price, if known.

11. **SUPPLEMENTARY NOTES:** Use for additional explanatory notes.

12. **SPONSORING MILITARY ACTIVITY:** Enter the name of the departmental project office or laboratory sponsoring (*paying for*) the research and development. Include address.

13. **ABSTRACT:** Enter an abstract giving a brief and factual summary of the document indicative of the report, even though it may also appear elsewhere in the body of the technical report. If additional space is required, a continuation sheet shall be attached.

It is highly desirable that the abstract of classified reports be unclassified. Each paragraph of the abstract shall end with an indication of the military security classification of the information in the paragraph, represented as (TS), (S), (C), or (U).

There is no limitation on the length of the abstract. However, the suggested length is from 150 to 225 words.

14. **KEY WORDS:** Key words are technically meaningful terms or short phrases that characterize a report and may be used as index entries for cataloging the report. Key words must be selected so that no security classification is required. Identifiers, such as equipment model designation, trade name, military project code name, geographic location, may be used as key words but will be followed by an indication of technical context. The assignment of links, roles, and weights is optional.

## DOCUMENT CONTROL DATA - R&amp;D

(Security classification of title, body of abstract and indexing annotation must be entered when the overall report is classified)

1. ORIGINATING ACTIVITY (Corporate author) University of Iowa Department of Physics and Astronomy		2a. REPORT SECURITY CLASSIFICATION UNCLASSIFIED	
		2b. GROUP	
3. REPORT TITLE Spectral, Spatial, and Temporal Variations Observed for Outer Zone Electrons from 10 to 100 keV with Satellite Injun 3			
4. DESCRIPTIVE NOTES (Type of report and inclusive dates) Progress August, 1967			
5. AUTHOR(S) (Last name, first name, initial) FRITZ, Theodore A.			
6. REPORT DATE August 1967		7a. TOTAL NO. OF PAGES 201	7b. NO. OF REFS 61
8a. CONTRACT OR GRANT NO. Nonr 1509(06)		9a. ORIGINATOR'S REPORT NUMBER(S) U. of Iowa 67-42	
b. PROJECT NO.		9b. OTHER REPORT NO(S) (Any other numbers that may be assigned this report)	
c.			
d.			
10. AVAILABILITY/LIMITATION NOTICES Distribution of this document is unlimited.			
11. SUPPLEMENTARY NOTES		12. SPONSORING MILITARY ACTIVITY Office of Naval Research	

## 13. ABSTRACT

Spectral, spatial, and temporal variations of outer zone electrons with energies from 10 keV to 100 keV observed with Injun 3 are presented. Electrons with  $E_e \geq 40$  keV were constantly observed precipitating into the atmosphere for all latitudes,  $\Lambda \geq 45^\circ$ . At latitudes below the high latitude boundary, the flux of  $\geq 40$  keV electrons in the loss cone was observed to always be  $\sim 10^{-2}$  that of the locally mirroring flux. There was usually a spike of precipitating  $\geq 40$  keV electrons observed at the high latitude boundary and the flux of  $\geq 40$  keV electrons was usually observed to approach isotropy over the upper hemisphere at the

(continued)